To the Graduate Council:

I am submitting herewith a dissertation written by Tianniu Chen entitled "Chemistry of High-Oxidation-State Groups V and VI Complexes. Novel Silyl and Imido Complexes and the Reactions of Silyl and Alkyl Alkylidyne Complexes with Oxygen." I have examined the final paper copy of this dissertation for form and content and recommend that it be accepted in partial fulfillment of the requirements for the degree of doctor of Philosophy, with a major in Chemistry.

Ziling (Ben) Xue, Major Professor

We have read this dissertation
and recommend its acceptance:

Jamie L. Adcock

Linda J. Magid

Peter K. Liaw

Accepted for the Council:

Vice Provost and
Dean of Graduate Studies

CHEMISTRY OF HIGH-OXIDATION-STATE GROUPS V AND VI COMPLEXES. NOVEL SILYL AND IMIDO COMPLEXES AND THE REACTIONS OF SILYL AND ALKYL ALKYLIDYNE COMPLEXES WITH OXYGEN

A Dissertation

Presented for the

Doctor of Philosophy Degree

The University of Tennessee, Knoxville

Tianniu Chen

May 2002

DEDICATION

This dissertation is dedicated to

my mother Li Ma, my father Dongping Chen, my wife Dongxiang Zeng,

my mother-in-law Qunxian Wu and in memory of my-father-in-law Bingheng Zeng

ACKNOWLEDGMENTS

There are many people who I would like to thank for their support and friendship during my four and a half years at the University of Tennessee. First, I would like to thank my research advisor, Professor Ziling (Ben) Xue, who has been a mentor and a role model to me while at the University of Tennessee, who has guided me through my academic developments and research projects, and who has set an excellent example for me about the commitment and dedication to research and work.

Secondly, I would like to thank my committee members, Professors Jamie Adcock, Lee Magid, and Peter Liaw for their consideration of my dissertation and constructive comments.

Thirdly, I would like to thank Professors Jamie Adcock, Craig Barnes, Ron Magid, Lee Magid, and Ziling (Ben) Xue for their valuable and interesting courses. Special thanks go out to Dr. Jeff C. Bryan at Oak Ridge National Laboratory, and Professors Craig Barnes and Clifton Woods III for their assistance and support of me as the student operator of the departmental X-ray diffractometer. Special thanks also go to Professor Xinquan Xin at Nanjing University, P. R. China, for being my teacher, mentor and my role model. I cannot thank him enough for all he has done for me.

I would also like to thank Dr. Charmaine Mamantov and Dr. Yihui (Yvette) Yang for their guidance and patience through my teaching period at the University of Tennessee.

The following individuals extended technical support for various aspects of my research at the University of Tennessee, for which I am grateful: Dr. Hongjun Pan for his assistance with NMR; Drs. Yun-Dong Wu and Zheng-Yang Lin at the Hong Kong University of Science and Technology for their theoretical calculations summarized in Chapters 2 and 3; Professor Arnold L. Rheingold at the University of Delaware for his assistance on the crystal structure of **5** in Chapter 3.

I extend thanks as well to the support staff in the chemistry department: Bobby and Darrell Lay, Marilyn Ownby, Art Pratt, Gene French, Bill Gurley, Johnny Jones, Sharon Marshall, Susan Hartzog, Jan McGuire, Maria Motoyama, Rachelle Allen, Kelly Preston, Theresa Turner, and Carol Moulton — you were always kind and willing to help me, and you are the best at what you do.

Of course, I would like to thank all my co-workers and colleagues, both past and present, for putting up with me, for many helpful discussions about my research, and for making the lab a productive and pleasant environment. Special thanks goes to Jaime R. Blanton, who has spent her precious time on proofreading my dissertation and has helped me to improve my spoken English and to get familiar with American culture, to Dr. Zhongzhi (Jim) Wu, who taught me the basics to be an organometallic chemist, to Dr. Jonathan B. Diminnie, who led me to the world of crystallography, to Dr. Hu (Frank) Cai, who kept me busy working on his crystals, to Cheri Clavier and Lynn Rodman, who made the lunch breaks

relaxing and pleasant, to Dr. Hee-Jung Im, who was always reliable when I forgot to turn off something but remembered it at night, to Laurel Morton, who worked with me briefly and is going to continue the research of Groups V and VI complexes, to Andy Canada, whose "Kentucky Blue" theme does not sound too bad, especially during the basketball season, to Xianghua (Bruce) Yu, who worked with me on X-ray diffraction, to Qiu (Steve) He, whose laptop was very beneficial during my interviews. I wish the best for their future careers. I also wish all the best to the rest of my past co-workers, colleagues and friends: Dr. Leonardo Allain, Dr. Mark Burleigh, Chunlan Chen, Dr. Ying Chen, Zhangrong Chen, John Clavier, Gang Dong, Ping Du, Bryan Fagan, Dr. Fang Gao, Xiao Gao, Jian He, Dr. Haifeng Ji, Zhi Lai, Dr. Nansheng Li, Dr. Zhanjiang Li, Dr. Vivian Liu, Dr. Yu Liu, Dr. Hongru Li, Zhibin Li, Dr. Bin Liang, Dr. Lenore McAlexander, Deliang Long, Dr. Jianming Mao, Dr. Jon Morrell, Jason Clark, Dr. Zhongxu Reng, Christy Stine, Guoyi Wei, Karen Welch, Zhigang Wu, Dr. Xiaohe Xu, Qiang Yang, Terry Yost, Dr. Su Yu, Yue Shen, Dr. Xiangrong Ye, Hualei Zhang, Yuanheng Zhang, Dr. Hegen Zheng, Dr.Liming Zheng, Xuejing Zheng, Dr. Sanbao Zhaong, Dr. Shaolian Zhou.

Finally, I am inexpressibly grateful for the love and support of my parents-in-law Bingheng Zeng and Qunxian Wu, my brother-in-law Donghui Zeng for their constant support, encouragement and belief in me. I put my mother, Li Ma, my father Dongping Chen and my wife Dongxiang Zeng, in the last and but certainly not the least place, because it was my parents who taught me to value and love learning for its own sake and to be the best I could be, and the love and support of

ABSTRACT

This dissertation describes the synthesis and characterization of the novel early transition metal (especially group VI metals) complexes free of anionic π-ligands such as cyclopentadienyl (Cp) and studies of their reactions with oxygen and silanes.

Our study of Cp-free tungsten silyl chemistry is reported. A novel d^0 tungsten silyl complex **2** [$(Bu^tCH_2)W(=CHBu^t)_2(SiBu^tPh_2)$ (**2a**) ⇌ $(Bu^tCH_2)_2W(\equiv CBu^t)(SiBu^tPh_2)$ (**2b**)] and an interesting equilibrium between two isomers **2a** and **2b** are described in Chapter 2. The thermodynamics of this equilibrium [ΔH^o = -0.9(0.2) kcal/mol, ΔS^o = -0.6(0.8) eu] was investigated by variable temperature ^1H NMR. The kinetic studies of the α-hydrogen chemical exchange between **2a** and **2b** by 2-D variable temperature EXSY experiments gave kinetic parameters of the exchange: $\Delta H^{\neq}$ = 17.9(1.1) kcal/mol, $\Delta S^{\neq}$ = 1.9(5.7) eu for the forward reaction (**2a** → **2b**) and $\Delta H^{\neq}$ = 18.6 (1.1) kcal/mol, $\Delta S^{\neq}$ = 1.9(5.7) eu for the back reaction (**2b** → **2a**). With the help of the theoretical calculations, we also explained why no such equilibrium existed in $(Bu^tCH_2)_2W(\equiv CBu^t)[Si(SiMe_3)_3]$ (**1**), an analogue of **2**.

The reaction of O_2 with silyl alkylidyne **2b** [$(Bu^tCH_2)W(=CHBu^t)_2(SiBu^tPh_2)$ (**2a**) ⇌ $(Bu^tCH_2)_2W(\equiv CBu^t)(SiBu^tPh_2)$ (**2b**)] is described in Chapter 3. An interesting silyl migration product $(Bu^tCH_2)_2W(=O)[=C(Bu^t)(SiBu^tPh_2)]$ (**5**) from this reaction was isolated and

characterized. A siloxy analog of **2b**, $(Bu^tCH_2)_2W{\equiv}CBu^t(OSiBu^tPh_2)$ (**6**), was prepared and excluded as a possible intermediate in the formation of **5**. *Ab initio* quantum chemical calculations suggested a pathway involving silyl migration in **2b** to give a tungsten (IV) intermediate $(Bu^tCH_2)_2W{=}C(Bu^t)(SiBu^tPh_2)$ (**7**) *prior* to the reaction with O_2. An interesting crystal structure of $(Me_3SiCH_2)_2W(=O)(=CHSiMe_3)(O{=}PMe_3){\bullet}(Me_3SiCH_2)_3W{\equiv}CSiMe_3$ (**12**) was obtained from the reaction of alkyl alkylidyne $(Me_3SiCH_2)_3W{\equiv}CSiMe_3$ with O_2 in the presence of PMe_3. Several structural features were discussed here.

In Chapter 4, preparation and characterization of bis(2,6-diisopropylphenylimido)molybdenum(VI) amide and silyl complexes $(ArN{=})_2Mo(NMe_2)_2$ (**14**, Ar = 2,6-diisopropylphenyl), $(ArN{=})_2Mo(NMe_2)[Si(SiMe_3)_3]$ (**15**), $(ArN{=})_2MoCl[N(SiMe_3)_2]$ (**16**), $(ArN{=})_2Mo(NMe_2)[N(SiMe_3)_2]$ (**17**), and $(ArN{=})_2Mo(NHAr)_2$ (**18**) are reported. In this chapter, new bis(2,6-diisopropylphenylimido)molybdenum(VI) amine adducts $(ArN{=})_2MoCl_2(NHMe_2)$ (**19**), $(ArN{=})_2MoCl_2(NHEt_2)$ (**20**), $(ArN{=})_2MoCl_2(NHMe_2)_2$ (**21**), and $(ArN{=})_2MoCl_2(NHMe_2){\bullet}(ArN{=})_2MoCl_2(DME)$ (**22**, DME = 1,2-dimethoxyethane) and their X-ray structures are reported as well.

Preparation and characterization of Cp-free tantalum(V) amide silyl and amide bis(silyl) complexes have been investigated, as reported in Chapter 5. Thermodynamics of interesting equilibria $(Me_2N)_3Ta[Si(SiMe_3)_3]_2$ (**25**) $\rightleftharpoons$ $(Me_2N)_3Ta(SiBu^tPh_2)[Si(SiMe_3)_3]$ (**27**) $\rightleftharpoons$ $(Me_2N)_3Ta(SiBu^tPh_2)_2$ (**26**) was studied. In the equilibrium **25** + $Li(THF)_3SiBu^tPh_2$ $\rightleftharpoons$ **27** + $Li(THF)_3Si(SiMe_3)_3$, ΔH° =

-0.54(0.17) kcal/mol and $\Delta S°$ = -0.79(0.65) eu, and in the equilibrium **27** + $Li(THF)_3SiBu^tPh_2$ ⇌ **26** + $Li(THF)_3Si(SiMe_3)_3$, $\Delta H°$ = -0.56(0.17) kcal/mol and $\Delta S°$ = -1.52(0.65) eu.

TABLE OF CONTENTS

LIST OF SCHEMES

LIST OF FIGURES

LIST OF TABLES

NUMBERING SCHEME FOR COMPOUNDS IN THE TEXT

1 $(Bu^tCH_2)_2W(\equiv CBu^t)[Si(SiMe_3)_3]$

2 $(Bu^tCH_2)W(=CHBu^t)_2(SiBu^tPh_2)$ (**2a**) $\rightleftharpoons$ $(Bu^tCH_2)_2W(\equiv CBu^t)(SiBu^tPh_2)$ (**2b**)

2b′ $Me_2W(\equiv CCH_3)(SiMe_3)$

3 $(Bu^tCH_2)_2W(\equiv CBu^t)(Cl)$

4 $(Me_3SiCH_2)_2W(\equiv CSiMe_3)(Cl)(PMe_3)$

5 $(Bu^tCH_2)_2W(=O)[=C(Bu^t)(SiBu^tPh_2)]$

5′ $Me_2W(=O)[=C(Me)(SiBu^tPh_2)]$

6 $(Bu^tCH_2)_2W(\equiv CBu^t)(OSiBu^tPh_2)$

7 $(Bu^tCH_2)_2W[=C(Bu^t)(SiBu^tPh_2)]$

7′ $Me_2W[=CMe(SiMe_3)]$

8 $(Bu^tCH_2)_2W(\eta^2\text{-}O_2)[=CBu^t(SiBu^tPh_2)]$

8′ $Me_2W(\eta^2\text{-}O_2)[=CMe(SiMe_3)]$

9 $LiOSiBu^tPh_2$

10 $\{(Bu^tCH_2)_2W[=CBu^t(SiBu^tPh_2)]\}_2(\mu\text{-}O_2)$

10′ $\{(CH_3)_2W[=CMe(SiMe_3)]\}_2(\mu\text{-}O_2)$

11 $(Me_3SiCH_2)_2W(=O)(=CHSiMe_3)(O=PMe_3)$

12 $(Me_3SiCH_2)_2W(=O)(=CHSiMe_3)(O=PMe_3)\bullet(Me_3SiCH_2)_3W\equiv CSiMe_3$

13 $(ArN=)_2MoCl_2(DME)$

14 $(ArN=)_2Mo(NMe_2)_2$

15 $(ArN=)_2Mo(NMe_2)[Si(SiMe_3)_3]$

16 $(ArN=)_2MoCl[N(SiMe_3)_2]$

17 $(ArN=)_2Mo(NMe_2)[N(SiMe_3)_2]$

18 $(ArN=)_2Mo(NHAr)_2$

19 $(ArN=)_2MoCl_2(NHMe_2)$

20 $(ArN=)_2MoCl_2(NHEt_2)$

21 $(ArN=)_2MoCl_2(NHMe_2)_2$

22 $(ArN=)_2MoCl_2(NHMe_2)\bullet(ArN=)_2MoCl_2(DME)$

23 $(Me_2N)_3Ta[Si(SiMe_3)_3)]Cl$

24 $(Me_2N)_3Ta(SiPh_2Bu^t)Cl$

25 $(Me_2N)_3Ta[Si(SiMe_3)_3]_2$

26 $(Me_2N)_3Ta(SiBu^tPh_2)_2$

27 $(Me_2N)_3Ta(SiPh_2Bu^t)[Si(SiMe_3)_3]$

CHAPTER 1

Introduction

1.1. Foreword

Over the past decade, the area of transition-metal silyl chemistry has grown rapidly, particularly since the applications of metal silyl complexes in catalysis and as precursors for the silicon-based microelectronic materials have either been explored or expanded.[1] Chemistry of early-transition-metal silyl complexes free of anionic π-ligands such as η^5-cyclopentadienyl (Cp) or stabilizing ligands such as carbonyls,[2] however, remains a largely unexplored area.

Our research has been focused on two areas:

(a) Fundamental chemistry of Cp-free early transition metal silyl, imido and amido complexes and their reactivities toward silanes.

(b) The use of this chemistry to probe the mechanistic pathways in the preparation of microelectronic materials by the CVD (chemical vapor deposition) process because the mechanistic pathways in many CVD processes are often complicated and unknown. The reactions between the metal amide and imido complexes and silanes could lead to the formation of microelectronic materials such as metal silicides, metal nitrides, M-Si-N or M-Si-O ternary materials. These materials have been used as stable diffusion barriers,[3] new capacitor materials for DRAM (dynamic random access memory) devices,[4] and

the next generation of gate materials in very-large-scale-integration (VLSI) devices.[5]

We are interested in the reactions of O_2 with transition metal complexes as well since they are essential steps in some biological and catalytic processes[6] and the reactions of $Ta(NR_2)_5$ and $(Et_2N)_3Ta{=}N\text{-}Bu^t$ with O_2 are of intense current interest in the preparation of metal oxide (Ta_2O_5) thin films.[5h-l]

1.2. Current dissertation

The preparation and characterization of the novel early transition metal (especially Mo and W) complexes free of anionic π-ligands, the mechanistic pathways in the formation of these compounds, and the studies of their reactions towards O_2 and silanes are the focuses of my Ph.D. studies.

1.2.1. *Chapter 2*

In Chapter 2, our studies of Cp-free tungsten silyl chemistry is reported. A novel d^0 tungsten silyl complex **2** [$(Bu^tCH_2)W(=CHBu^t)_2(SiBu^tPh_2)$ (**2a**) ⇌ $(Bu^tCH_2)_2W(\equiv CBu^t)(SiBu^tPh_2)$ (**2b**)], prepared by the addition of one equiv of $LiSiBu^tPh_2(THF)_3$ to a thermally unstable intermediate $(Bu^tCH_2)_2W{\equiv}CBu^t(Cl)$ (**3**), provided us a unique opportunity to directly observe for the first time an equilibrium **2a** ⇌ **2b** between alkylidene and alkylidyne complexes.[7] The thermodynamics of this equilibrium [ΔH^o = -0.9(0.2) kcal/mol, ΔS^o = -0.6(0.8) eu] was investigated by variable temperature ^1H NMR. The kinetics of α-hydrogen chemical exchange

between **2a** and **2b** by variable temperature 2-D EXSY experiments gave kinetic parameters of the exchange: $\Delta H^{\neq}$ = 17.9(1.1) kcal/mol, $\Delta S^{\neq}$ = 1.9(5.7) eu for **2a** → **2b** and $\Delta H^{\neq}$ = 18.6(1.1) kcal/mol, $\Delta S^{\neq}$ = 1.9(5.7) eu for **2b** → **2a**.

1.2.2. *Chapter 3*

The reaction of silyl alkylidyne complex **2b** [$(Bu^tCH_2)W(=CHBu^t)_2(SiBu^tPh_2)$ (**2a**) ⇌ $(Bu^tCH_2)_2W(\equiv CBu^t)(SiBu^tPh_2)$ (**2b**)] with O_2 was found to give an interesting silyl migration product $(Bu^tCH_2)_2W(=O)[=C(Bu^t)(SiBu^tPh_2)]$ (**5**). The structure of **5** was confirmed by X-ray diffraction. $(Bu^tCH_2)_2W\equiv CBu^t(OSiBu^tPh_2)$ (**6**) was prepared by the addition of one equiv of $LiOSiBu^tPh_2$ (**9**) to $(Bu^tCH_2)_2W(\equiv CBu^t)(Cl)$ (**3**). **6** was ruled out to be an intermediate in the formation of **5** from **2**. A pathway involving silyl migration from W to alkylidyne C *prior* to the reaction with O_2 to give a W(IV) intermediate $(Bu^tCH_2)_2W=C(Bu^t)(SiBu^tPh_2)$ (**7**) was supported by *ab initio* quantum chemical calculations.

The reaction of alkyl alkylidyne complex $(Me_3SiCH_2)_3W\equiv CSiMe_3$ with O_2 was found to yield $(Me_3SiCH_2)_2W(=O)(=CHSiMe_3)(O=PMe_3)$• $(Me_3SiCH_2)_3W\equiv CSiMe_3$ (**12**) in the presence of PMe_3. A conjugation system $Me_3P=O\rightarrow W=O\rightarrow W\equiv C\text{-}SiMe_3$ was revealed in the solid-state structure of **12**.

1.2.3. *Chapter 4*

Bis(2,6-diisopropylphenylimido)molybdenum(VI) amide complexes $(ArN=)_2Mo(NMe_2)_2$ (**14**, Ar = 2,6-diisopropylphenyl), $(ArN=)_2Mo(NMe_2)[Si(SiMe_3)_3]$ (**15**), $(ArN=)_2MoCl[N(SiMe_3)_2]$ (**16**), and $(ArN=)_2Mo(NMe_2)[N(SiMe_3)_2]$ (**17**) were prepared from $(ArN=)_2MoCl_2(DME)$ (**13**) and characterized. The preparation and X-ray crystal structures of these new complexes are presented in Chapter 4. In addition, a series of bis(2,6-diisopropylphenylimido)molybdenum(VI) amine adducts $(ArN=)_2Mo(NHAr)_2$ (**18**), $(ArN=)_2MoCl_2(NHMe_2)$ (**19**), $(ArN=)_2MoCl_2(NHEt_2)$ (**20**), $(ArN=)_2MoCl_2(NHMe_2)_2$ (**21**), and $(ArN=)_2MoCl_2(NHMe_2)\bullet(ArN=)_2MoCl_2(DME)$ (**22**, DME = 1,2-dimethoxyethane) were prepared from $(ArN=)_2MoCl_2(DME)$ (**13**) and characterized by X-ray crystallography. Complexes **13** and **18** gave polymorphic structures. A distorted tetrahedral geometry was observed in complexes **13-17** and **18**. Complexes **19** and **20** are trigonal bipyramidal, and **21** has an octahedral geometry around the metal atom. The imido groups in these complexes are nearly linear. There are intra-molecular hydrogen bonds in **19** and **20**, while no α-agostic interaction between amine hydrogen atoms and the metal center was observed in **19-21**.

1.2.4. *Chapter 5*

The synthesis and characterization of amide silyl and amide bis(silyl) complexes of tantalum(V) free of π-anionic ligands are reported in Chapter 5. The

amide silyl chloride complexes $(Me_2N)_3Ta(SiR_3)Cl$ [SiR_3 = $Si(SiMe_3)_3$ (**23**), $SiPh_2Bu^t$ (**24**)] were prepared from the reactions of $(Me_2N)_3TaCl_2$ with $Li(THF)_3Si(SiMe_3)_3$ and $Li(THF)_3SiPh_2Bu^t$, respectively. The amide bis(silyl) complexes $(Me_2N)_3Ta(SiR_3)_2$ [SiR_3 = $Si(SiMe_3)_3$ (**25**), $SiPh_2Bu^t$ (**26**)] were prepared by the reactions of $(Me_2N)_3TaCl_2$ with 2 equiv of $Li(THF)_3Si(SiMe_3)_3$ and $Li(THF)_3SiPh_2Bu^t$, respectively. The mixed bis(silyl) complex $(Me_2N)_3Ta(SiPh_2Bu^t)[Si(SiMe_3)_3]$ (**27**) was obtained by the reaction of **2** with one equiv of $Li(THF)_3Si(SiMe_3)_3$.

Thermodynamics of the equilibria **25** ⇌ **27** ⇌ **26** were studied by variable temperature ^1H NMR. The equilibrium **25** + $Li(THF)_3SiBu^tPh_2$ ⇌ **27** + $Li(THF)_3Si(SiMe_3)_3$ yielded $\Delta H°$ = -0.54(0.17) kcal/mol and $\Delta S°$ = -0.79(0.65) eu while the equilibrium **27** + $Li(THF)_3SiBu^tPh_2$ ⇌ **26** + $Li(THF)_3Si(SiMe_3)_3$ yielded $\Delta H°$ = -0.56(0.17) kcal/mol and $\Delta S°$ = -1.52(0.65) eu.

1.2.5. *Chapter 6*

Base on the work reported in the current dissertation, some future studies are suggested in this chapter.

CHAPTER 2

Synthesis, Characterization and Dynamic Studies of d^0 Tungsten Silyl Complexes Free of Anionic π-ligands

2.1. Introduction

Our initial interest in early-transition-metal d^0 silyl complexes free of anionic π-ligands originated from our investigation of the reactions between d^0 alkyls $(RCH_2)_4M$ (M = Ti, Zr, Hf),[8] alkylidenes $(RCH_2)_3M{=}CHR$ (M = Ta, Nb),[9] and alkylidynes $(RCH_2)_3M{\equiv}CR$ (M = Mo, W)[10] with SiH_4, which could lead to the formation of metal silicides (Scheme 2.1). Metal silicides are used as low-resistivity contacts and new interconnection metallization in very-large-scale-integration (VLSI) microelectronic circuits to prevent the formation of an unstable interface between metal and silicon wafer (Figure 2.1).[11] $MoSi_2$ is also widely used, *e.g.*, as matrix materials for high temperature structural composites because of its outstanding mechanical properties, high melting point, and excellent oxidation resistance at high temperature.[12] In addition, silicides have been employed as IR detector materials to "see" thermal radiation for night vision and visualization of heat flow.[13]

In our proposed new routes to make metal silicides, alkyl, alkylidene and alkylidyne ligands could leave cleanly as alkanes through two possible pathways to form silicides (MSi_n) (Scheme 2.1). Possible intermediates in the first step of these reactions (Scheme 2.2) may be unstable. We thus proposed the use of model

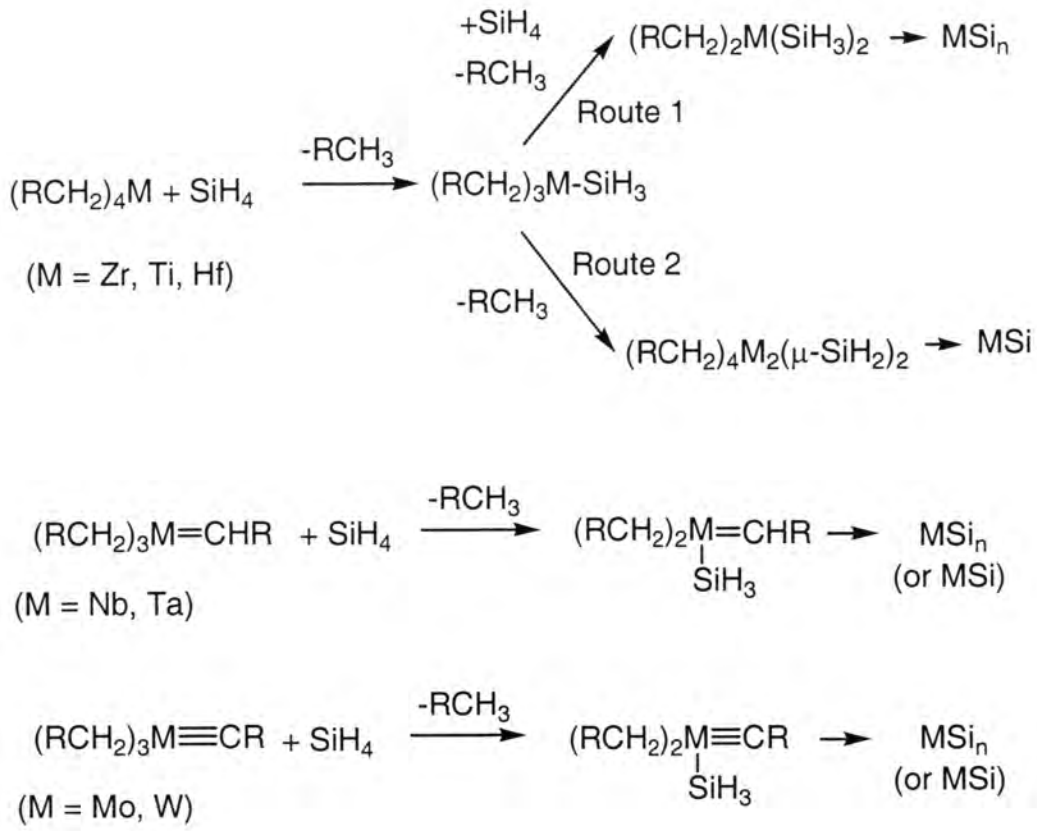

Scheme 2.1. Proposed pathways to form metal silicides.

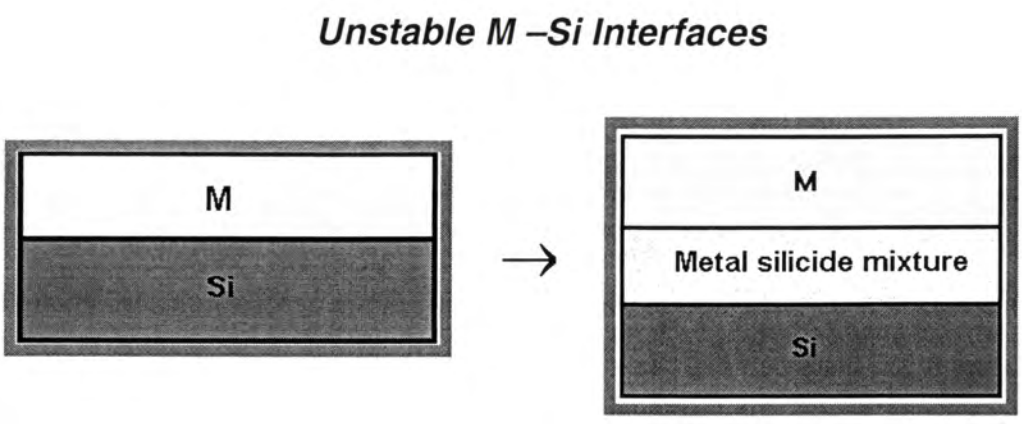

Figure 2.1. Illustrations of the stability of the metal silicides films. MSi_n thin films are more stable on Si wafers.

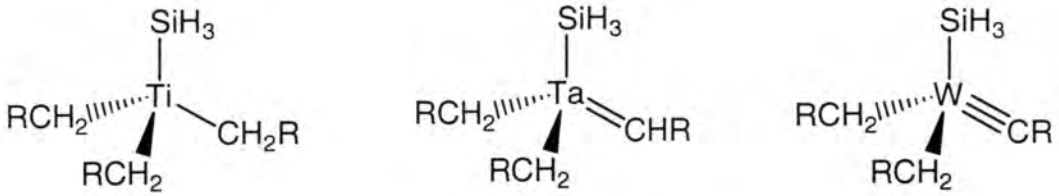

Possible Intermediates

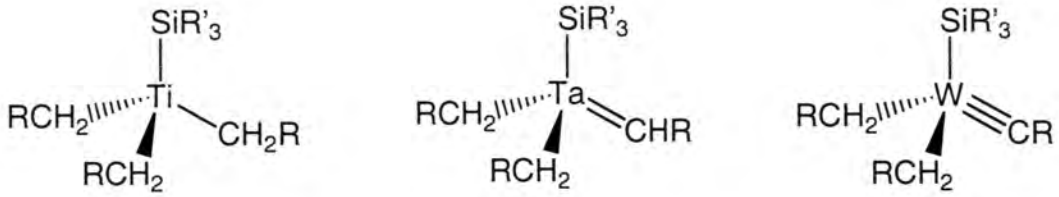

Model Complexes

Scheme 2.2. Proposed intermediates and model complexes for the new routes to metal silicides.

complexes. Besides the potential relevance of these model complexes to the proposed intermediates, we are also interested in their fundamental chemistry. Except for a few known Cp-free early-transition-metal silyl complexes such as $(Bu^tO)_3MSi(SiMe_3)_3$ (M = Zr, Hf),[14a] $V(CO)_6SiH_3$[2a] and $(Me_3P)_3W(H)_2I(SiMe_3)$[14b] with carbonyls, alkoxides or phosphines as ancillary ligands, the chemistry of these electron-deficient early-transition-metal silyl complexes is largely an uncharted area.[1] Most studies in this area have been focused on the complexes supported by cyclopentadienyl (Cp) or analogous anionic π-ligands.[1,15] The presence of such ligands in, *e.g.*, $Cp_2Zr(SiR_3)R'$,[15a] $Cp_2Ta(=CH_2)SiHBu^t_2$,[15b] and $Cp_2W(\eta^2\text{-}Me_2Si{=}SiMe_2)$[15c] is believed to contribute to the enhanced stability of these silyl compounds. Our group has successfully prepared first Cp-free silyl alkyl, alkylidenes complexes $(RCH_2)_3MSi(SiMe_3)_3$ (R = CMe_3, $SiMe_3$; M = Ti, Zr) and $(RCH_2)_2Ta(=CHR)SiR'_3$ [R'_3 = $(SiMe_3)_3$, Bu^tPh_2] (Scheme 2.3).[16]

We are interested as well in the reactivity of α-H atoms in β-H free alkyl (Bu^tCH_2- and Me_3SiCH_2-), alkylidene, and alkylidyne ligands of these complexes. α-Hydrogen atoms in such complexes have been shown to play a pivotal role in the formation of high-oxidation-state alkylidene and alkylidyne complexes.[9,10,17-19] In addition, the α-H atoms in d^0 $(Bu^tCH_2)_3Ta{=}CDBu^t$, $(Bu^tCH_2)_3W{\equiv}^{13}CBu^t$, $(Bu^tCH_2)_3W{\equiv}CSiMe_3$ are known to undergo exchange (scrambling).[9b,20a-c] In $(Bu^tCH_2)_3W{\equiv}CSiMe_3$, deuterium labeling and kinetic studies are consistent with unimolecular and stepwise transfer of two hydrogen atoms in one alkyl ligand to the alkylidyne ligand.[20a] A bis(alkylidene) intermediate

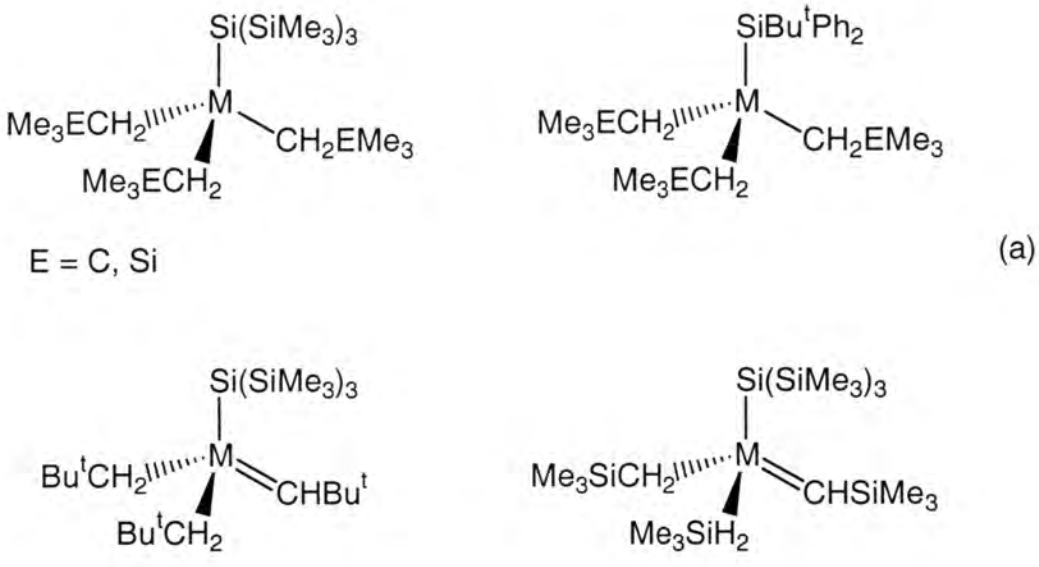

Scheme 2.3. Cp-free silyl compounds prepared in our group:[8b-c,16a] (a) Group 4 silyl alkyl complexes; (b) Group 5 silyl alkylidene complexes.

"$(Bu^tCH_2)_2W(=CHSiMe_3)(=CHBu^t)$" was proposed in the transfer $[(Bu^tCH_2)_3W{\equiv}CSiMe_3 \rightleftharpoons$ "$(Bu^tCH_2)_2W(=CHSiMe_3)(=CHBu^t)$" $\rightleftharpoons$ $(Bu^tCH_2)_2W(CH_2SiMe_3)({\equiv}CBu^t)]$ (Scheme 2.4a).[20a] In a d^2 bis(alkylidene) complex $Os(=CHBu^t)_2(CD_2Bu^t)_2$, hydrogen/deuterium atoms were found to scramble among the α-carbon atoms at 273 K (Scheme 2.4c).[20d-e] This exchange is believed to occur through an alkylidyne intermediate "$(Bu^tCH_2)_3Os{\equiv}CBu^t$" $[Os(=CHBu^t)_2(CH_2Bu^t)_2 \rightleftharpoons$ "$(Bu^tCH_2)_3Os{\equiv}CBu^t$"]. Although the exchange of α-H atoms is a fundamental dynamic process in these archetypical alkylidene and alkylidyne complexes, there has been no report of a direct observation of such an exchange between alkylidene and alkylidyne complexes.[20,22]

Our group reported earlier the preparation of the first Cp-free tungsten d^0 silyl $(Bu^tCH_2)_2W({\equiv}CBu^t)[Si(SiMe_3)_3]$ (**1**).[8c,16a] We report here the preparation of a new silyl alkylidyne complex $(Bu^tCH_2)_2W({\equiv}CBu^t)(SiBu^tPh_2)$ (**2b**),[16a,17] direct observation of the exchange $(Bu^tCH_2)W(=CHBu^t)_2(SiBu^tPh_2)$ (**2a**) $\rightleftharpoons$ $(Bu^tCH_2)_2W({\equiv}CBu^t)(SiBu^tPh_2)$ (**2b**), and our studies of this unusual exchange.[17] **2a** is also one of the rare known d^0 bis(neopentylidene) complexes; only tantalum and niobium d^0 bis(neopentylidene) complexes have been reported.[16e-f,20d,21]

2.2. Results and Discussion

2.2.1. *Synthesis of Cp-free tungsten d^0 silyl complexes 2a and 2b*

We reported earlier the preparation of **1** from $(Bu^tCH_2)_2W({\equiv}CBu^t)Cl$ (**3**)[8c,16a] and $Li(THF)_3Si(SiMe_3)_3$ (Scheme 2.5).[24a] **2** was prepared in a procedure similar to

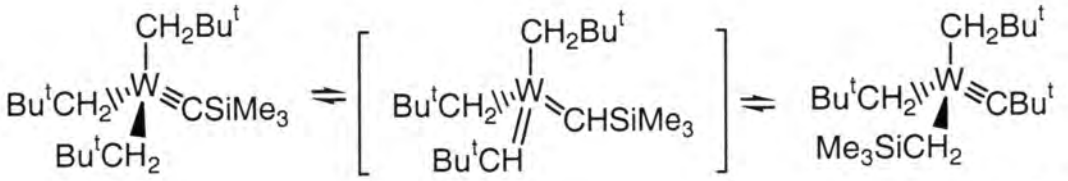

(a)[20a-b]

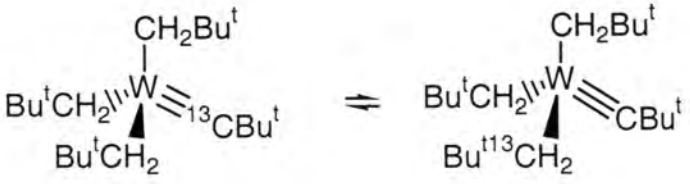

(b)[20c]

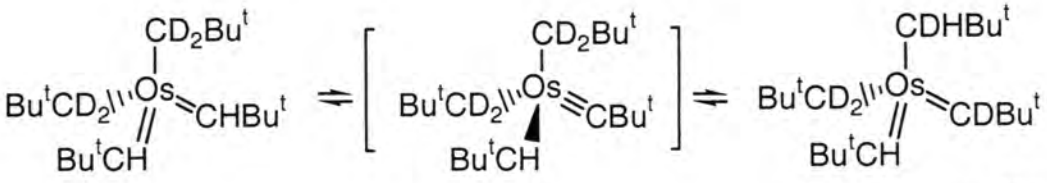

(c)[20d-e]

Scheme 2.4. Reported α-hydrogen exchange processes.

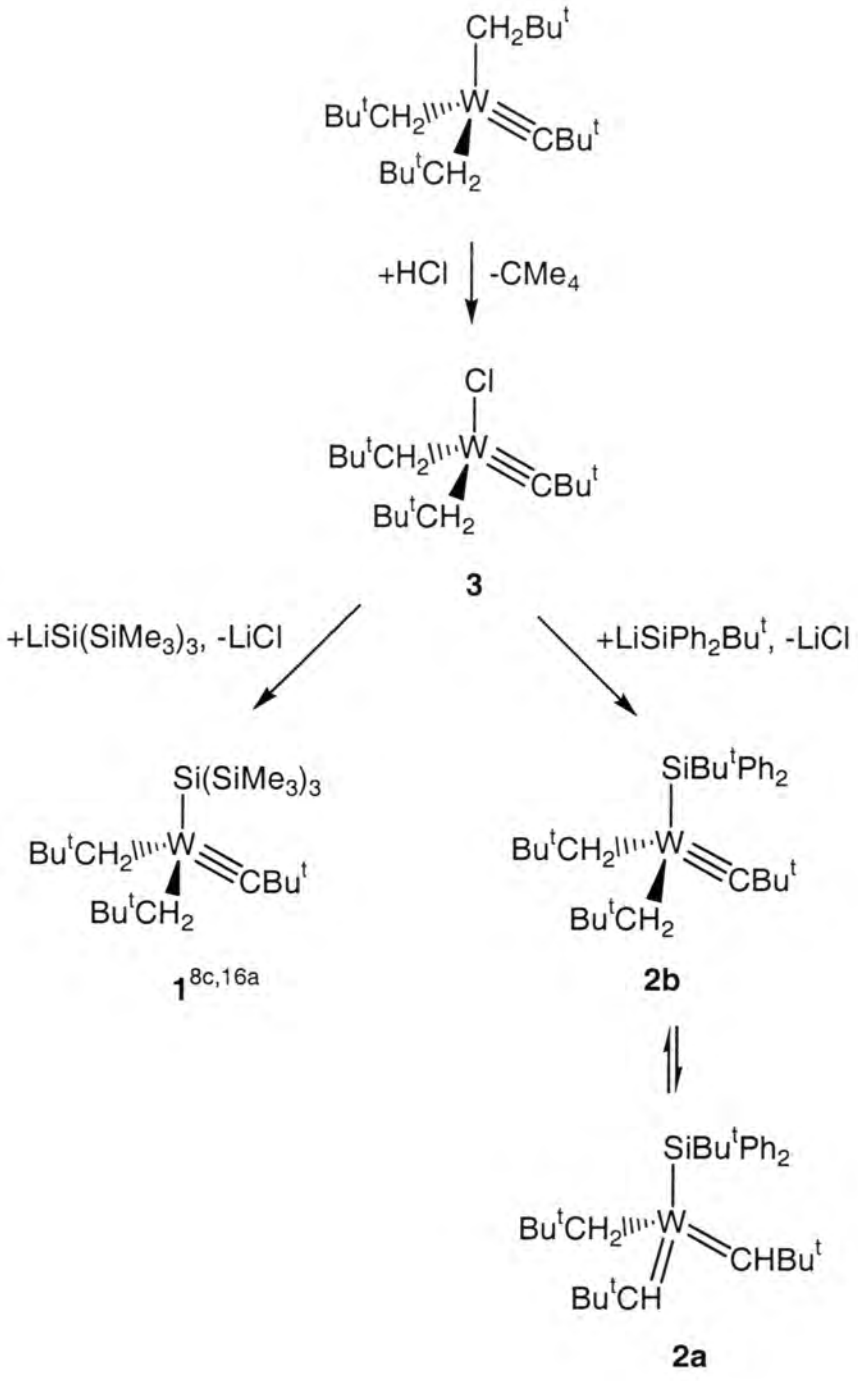

Scheme 2.5. Synthetic pathways to Cp-free tungsten d^0 silyl alkylidyne complexes.

that in the preparation of **1** (Scheme 2.5).[8c,16a] The addition of 1 equiv of HCl to $(Bu^tCH_2)_3W{\equiv}CBu^t$ [23] led to the formation of thermally unstable alkylidyne $(Bu^tCH_2)_2W{\equiv}CBu^t(Cl)$ (**3**).[8c,16a] The reaction of **3** with 1 equiv of $LiSiBu^tPh_2(THF)_3$ [24b] at -40 °C (Scheme 2.5), followed by workup of the product at -10 °C and crystallization at -30 °C, yielded crystalline **2** in 58% yield. Spectroscopic properties [^1H, $^{13}C\{^1H\}$, ^1H-gated-decoupled ^{13}C, ^1H-^{13}C heteronuclear correlation (HETCOR), and $^{29}Si\{^1H\}$ NMR] of **2a** and **2b** were consistent with the structure assignments and the existence of the two isomers in solution. The resonances of the alkylidene ligand in **2a** and alkylidyne ligand in **2b** appeared as a doublet at 272.30 ppm and a singlet at 318.38 ppm, respectively, in the ^1H-gated-decoupled ^{13}C spectra. There was one ^1H NMR resonance at 6.03 ppm ($=CH^tBu$) for the two alkylidene ligands in **2a** between -20 °C and 20 °C. It is thus unlikely that these two ligands are involved in a fast rotation about the W=C bonds.

If a fast rotation existed, one would expect to observe three alkylidene-hydrogen resonances for the *anti, anti* and *syn, anti* rotamers (Scheme 2.6) in the

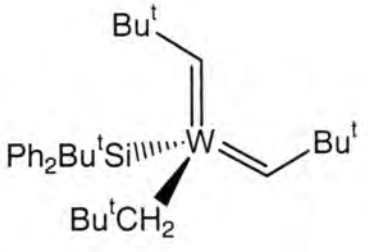

***syn, anti*-2a**

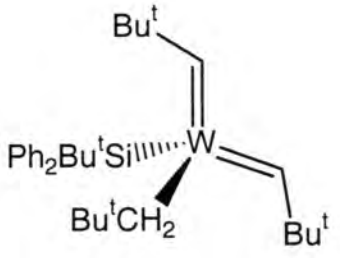

***anti, anti*-2a**

Scheme 2.6. Two possible rotamers of complex **2a**.

low-temperature ^{1}H NMR spectrum. The presence of a single =C*H*Bu^t resonance in the ^{1}H NMR spectrum thus suggests that the two alkylidene ligands adopt an *anti*, *anti*-configuration. Such configuration has been observed in *anti*, *anti*-Os(=CHBu^t)$_2$(CH$_2$Bu^t)$_2$.[20d] The prochiral tungsten atom in **2b** gives rise to diastereotopic methylene (CH_aH_bBu^t) protons with chemical shifts of 2.08 and -0.77 ppm ($^2J_{H_a\text{-}H_b}$ = 11.9 Hz). The mixture of **2a** and **2b** is stable as a solid, but slowly decomposes in solution at room temperature, forming HSiBu^{t}Ph$_2$ and unknown species.

In the solid-state CPMAS (cross-polarization magic angle spinning) ^{13}C{^{1}H} NMR spectrum of crystalline **2** (Figure 2.2), both **2a** and **2b** were observed, indicating that both isomers are present even in the crystalline solids.

2.2.2. *Thermodynamics of the exchange 2a ⇌ 2b*

Variable-temperature NMR spectra of the isomerization **2a** ⇌ **2b** were studied, and the equilibrium constants, K_{eq} = [**2b**]/[**2a**], measured between 237 and 287 K are listed in Table 1. A plot of lnK_{eq} vs 1/T (Figure 2.3) gave a linear fit and yielded $\Delta H°$ = -0.9(0.2) kcal/mol and $\Delta S°$ = -0.6(0.8) eu by Eq. 2.1.[25]

$$-RT \ln K_{eq} = \Delta H° - T\Delta S° \qquad \text{(Eq. 2.1)}$$

The equilibrium constants K_{eq} range from 4.590(0.006) at 237 K to 3.34(0.05) at 287 K, indicating that the alkylidyne isomer **2b** is favored, and

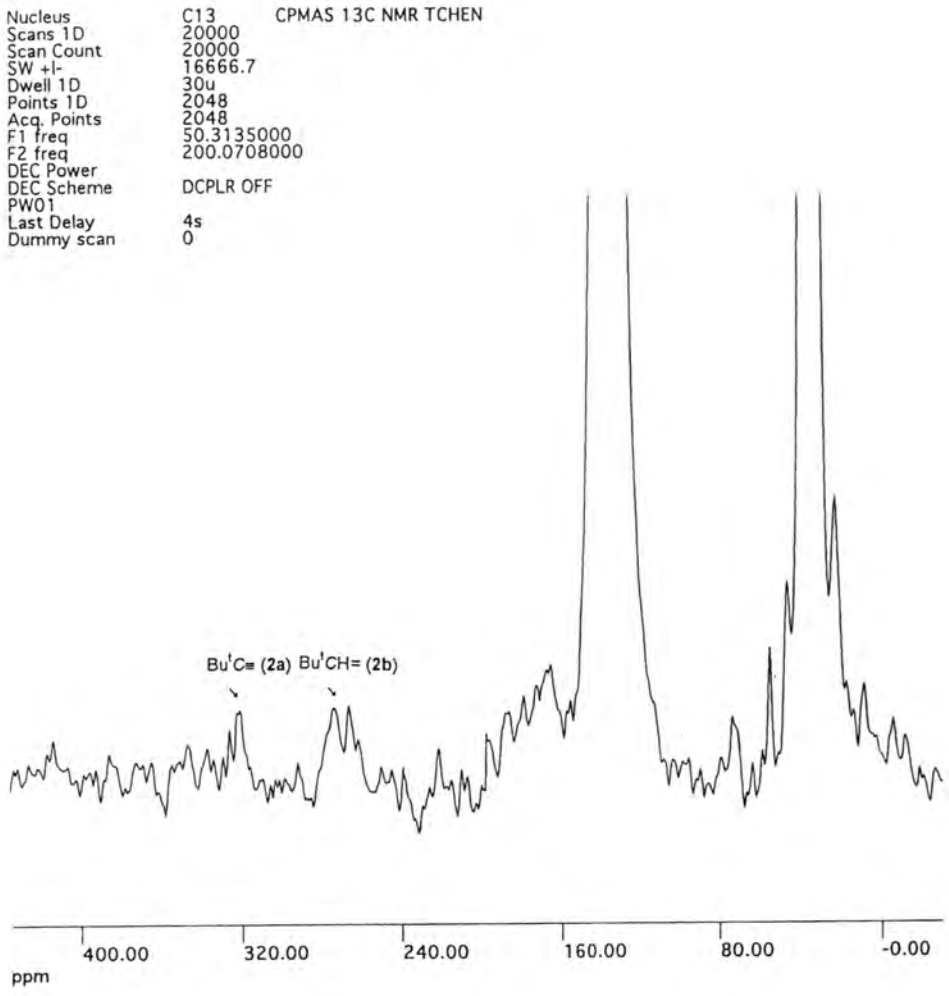

Figure 2.2. Partial solid-state CPMAS (cross-polarization magic angle spinning) $^{13}C\{^{1}H\}$ NMR of **2**.

Table 2.1. Equilibrium Constants (K_{eq}) for **2a** ⇌ **2b**

T (K)	$K_{eq} \pm \delta K_{eq(ran)}$ [a]
287 ± 1	3.34 ± 0.05
282 ± 1	3.45 ± 0.04
277 ± 1	3.520 ± 0.005
272 ± 1	3.620 ± 0.015
267 ± 1	3.760 ± 0.004
262 ± 1	3.860 ± 0.001
257 ± 1	3.990 ± 0.016
252 ± 1	4.130 ± 0.011
247 ± 1	4.260 ± 0.004
242 ± 1	4.450 ± 0.002
237 ± 1	4.590 ± 0.006

[a] The largest random uncertainty is $\sigma K_{eq(ran)}/K_{eq} = 0.05/3.34 = 1.5\%$. The total uncertainty $\sigma K_{eq}/K_{eq}$ of 5.2% was calculated from $\sigma K_{eq(ran)}/K_{eq} = 1.5\%$ and the estimated systematic uncertainty $\sigma K_{eq(sys)}/K_{eq} = 5\%$ by $\sigma K_{eq}/K_{eq} = [(\sigma K_{eq(ran)}/K_{eq})^2 + (\sigma K_{eq(sys)}/K_{eq})^2]^{1/2}$.

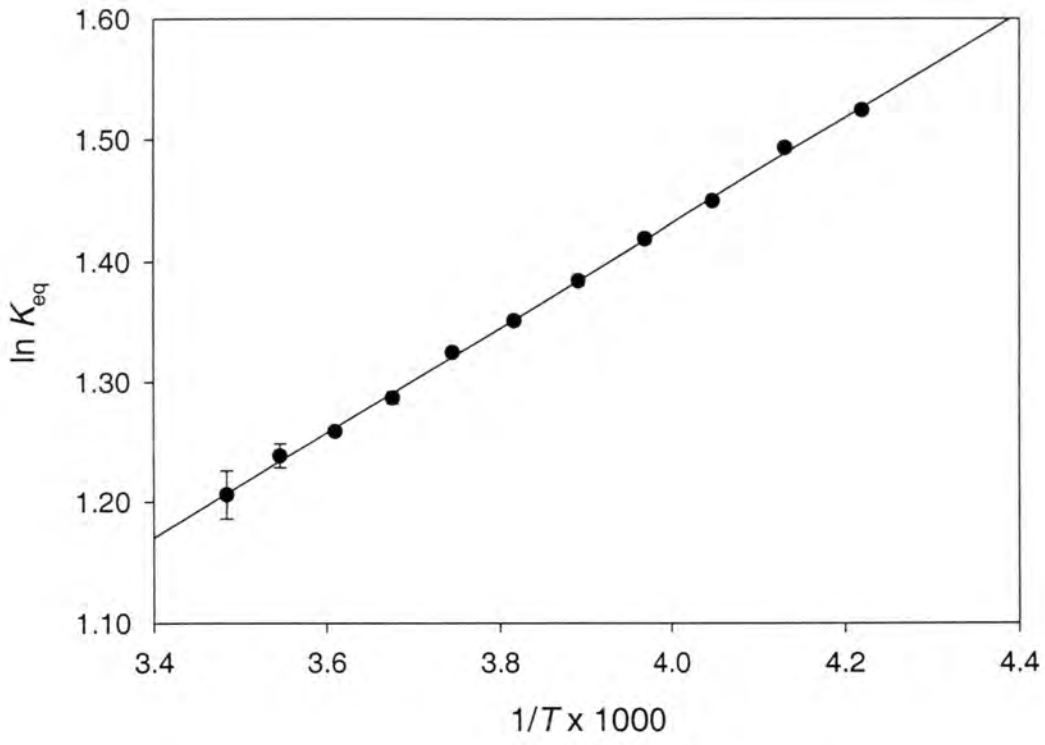

Figure 2.3. A plot of $\ln K_{eq}$ vs $1/T$ of the equilibrium **2a** ⇌ **2b**.

increasing the temperature shifts the equilibrium towards **2a**. The process **2a** ⇌ **2b** is slightly exothermic with $\Delta H°$ = -0.9(0.2) kcal/mol.

This enthalpy change outweighs the entropy change [$\Delta S°$ = -0.6(0.8) eu] in the isomerization **2a** ⇌ **2b** to give $\Delta G°$ = -0.7(0.4) kcal/mol at 287(1) K in favor of **2b**. It is interesting to note that the d^0 alkylidyne complex **2b** is thermodynamically close in energy to its bis(alkylidene) isomer **2a**, although **2b** is slightly more stable. In the α-H exchange in $(Bu^tCH_2)_3W{\equiv}CSiMe_3$ ⇌ $(Bu^tCH_2)_2W(CH_2SiMe_3)(\equiv CBu^t)$, the proposed bis(alkylidene) intermediate "$(Bu^tCH_2)_2W(=CHSiMe_3)(=CHBu^t)$" is so much higher in energy than the ground state alkylidyne structure that this intermediate is not observed.[20a-c]

In the 2D-NOESY spectra of **2a** and **2b** at 296 K (t_{mix} = 3 s), strong *positive* cross peaks were observed between the methylene ($CH_aH_bBu^t$) protons in **2b** and the alkylidene ($=CHBu^t$) and methylene (CH_2Bu^t) protons in **2a**, consistent with a chemical exchange process between **2a** and **2b** at this temperature (Scheme 2.7).

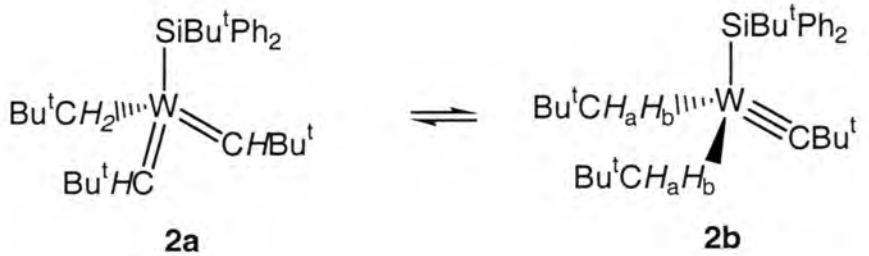

Scheme 2.7. α-H exchange between **2a** and **2b**.

2.2.3. *Kinetics of the exchange 2a ⇌ 2b*

The extension of NMR methodology from one- to two-frequency regimes has been of great benefit to the investigations of molecular stereodynamics. Specifically, the 2D-exchange spectroscopy (2D EXSY) technique based on the 2D-NOESY pulse sequence has become well established as a powerful structural determination method.[26-29] As compared with 1D NMR bandshape analysis for determining exchange rates, 2D EXSY experiments have the following advantages: First, in the region of slow exchange, it is difficult for one-dimensional method to distinguish between broadening caused by exchange and by numerous other factors contributing to natural linewidths; Secondly, in complex multisite exchanging systems, where the bandshape is a function of several independent rate constants, it is often impossible to find a unique solution to the problem. Multidimensional methods, particularly 2D EXSY can largely overcome these hurdles. The common pulse sequence for 2D EXSY experiments is shown in Figure 2.4.

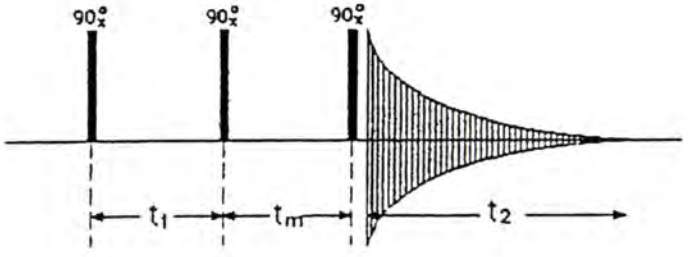

Figure 2.4. Pulse sequence for two-dimensional NOESY or EXSY experiments.[29]

In a two-spin system of spins A and B mutually interacting through exchange or cross-relaxation, after the first $90°_x$ pulse the magnetization vectors will evolve in the $x'y'$ plane in the usual manner of free induction decay (FID) for a period t_1 (evolution time). At this point a second $90°_x$ pulse, the mixing pulse, is applied, tipping the magnetization vectors into the –z direction. During the mixing period t_m, an exchange (or cross-relaxation) takes place between nuclei A and B, which changes the longitudinal magnetization of B, $M_{BZ}(t_1)$, by an amount $C_k M_{AZ}(t_1)$, where C_k is a constant depending on the exchange rate. A third $90°_x$ pulse, the detection pulse, converts this term into transverse magnetization of B, where it is detected as a part of the familiar FID during the detection period t_2. The amplitude of the detected magnetization of B is thus modulated with frequency ν_A as a function of t_1. A two-dimensional Fourier transformation then results in a spectrum with cross-peaks at (ν_A, ν_B), provided that exchange took place during the mixing time t_m. Correlations arising from any other cause, *e.g.*, through scalar coupling, may be eliminated by phase cycling and a random variation of the mixing period t_m. To obtain quantitative exchange rates from this 2D EXSY experiment, some care has to be taken in the choice of the mixing time lengths. If this is too short, the resulting cross-peaks are weak and subject to large experimental errors. If t_m is too long then the intensities of cross-peaks may approach those of the diagonal peaks and become rather insensitive to the exchange rates. It should also be remembered that spins relax during the mixing period with a time constant of T_1, and if $t_m > 1/T_1$, no magnetization may remain to be detected. In practice, one has to

optimize t_m to minimize the error in the rate constant. For multisite systems the situation is more complex. In general there can be no optimum t_m for all magnitudes of rate constants, and so it may be necessary to repeat the experiment for several magnitudes of mixing times. To extract accurate rate information, it is necessary to perform reliable measurements of peak intensities, usually by volume integration. It should also be stressed that the effects of cross-relaxation (Nuclear Overhauser Effects) and chemical exchange on the final 2D spectrum are analogous. NOE effect leads to cross-peaks between nuclei that are spatially close in the molecule, and it is necessary to separate these NOESY contributions from chemical exchange effects. Fortunately, this is usually easily achieved, because exchange rates are strongly temperature-dependent whereas cross-relaxation rates are not. Also, in phase-sensitive 2D EXSY chemical exchange and cross-relaxation cross-peaks may be distinguished by their opposite phases. Another undesirable feature in 2D EXSY spectra are so called $T1$ ridges, *i.e.*, signals appearing as ridges parallel to the $F1$ frequency axis. These ridgescans contribute to false cross-peak intensities after symmetrization. Proper phase cycling minimizes this artifact.

The exchange among α-H atoms in **2a** and **2b** was investigated between 267 K and 297 K by 2-D exchange spectroscopy. Representative phase-sensitive ^{1}H EXSY spectra of (**2a/2b**) are shown in Figures 2.5 and 2.6. At temperatures ≤267 K, cross-peaks between C*H*= (**2a**)/CH_aH_b (**2b**) and between CH_2 (**2a**)/CH_aH_b (**2b**) (Figure 2.5) were too weak to be detected, indicating that the exchange was nearly frozen at these temperatures. As the temperature was increased, the intensities of

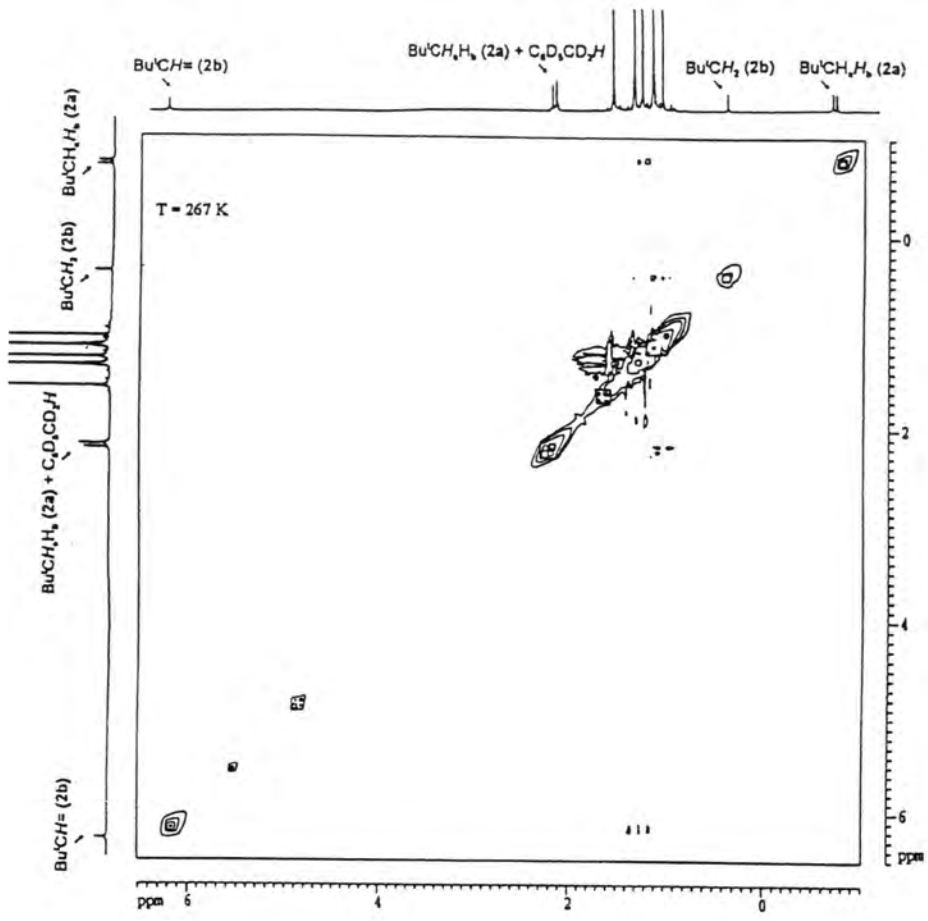

Figure 2.5. 2D EXSY spectrum of the exchange between **2a** and **2b** at 267 K in toluene-d_8.

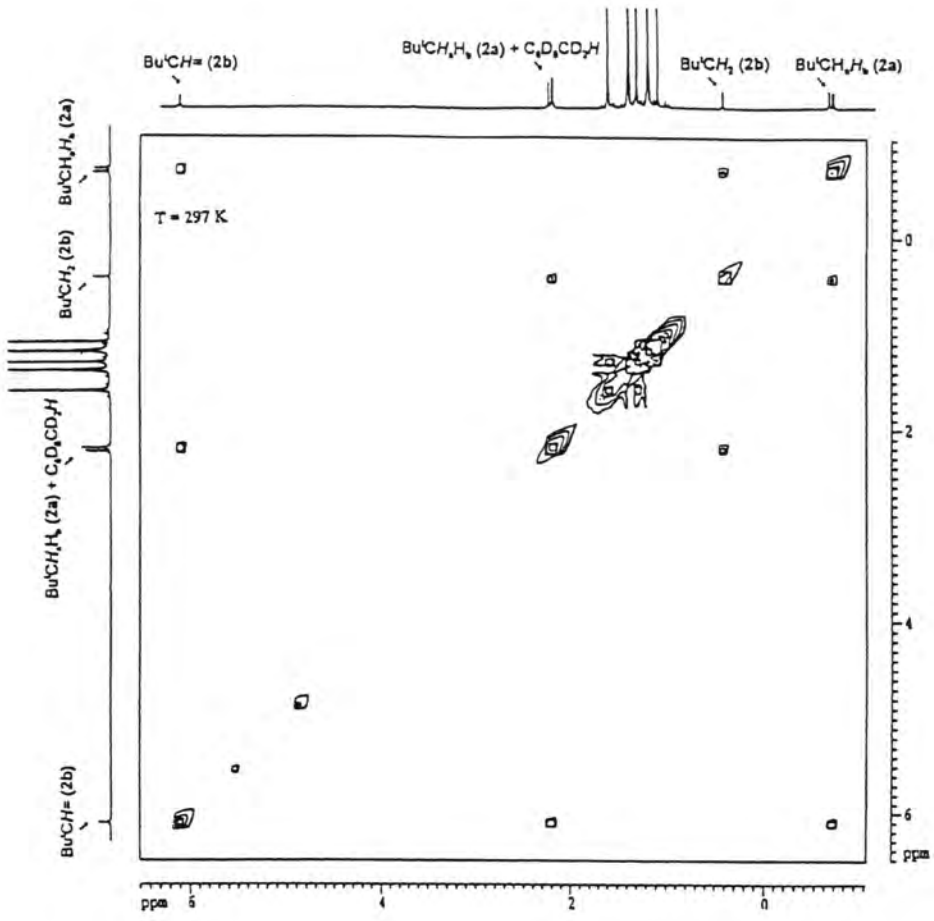

Figure 2.6. 2D EXSY spectrum of the exchange between **2a** and **2b** at 297 K in toluene-d_8.

the exchange cross-peaks increased. Between 277 K and 297 K, the spectra (Figure 2.6) displayed high-intensity cross-peaks for C*H*= (**2a**)/CH_aH_b (**2b**) and between CH_2 (**2a**)/CH_aH_b (**2b**) (Scheme 2.7) as expected for the exchange process. The 2D EXSY data were treated quantitatively using the methods summarized by Perrin and Dwyer.[28] Each of the sets of diagonal and cross-peak intensities was processed, assuming a two-site exchange system according to Eqs. 2.2 and 2.3, in which k' is the sum of the forward and reverse rate constants, t_m is the mixing time, X denotes the mole fractions of the two sites, which is a variable and calculated from K_{eq} in aforementioned variable-temperature 1-D NMR, I_{2a2a} and I_{2b2b} are the diagonal peak intensities of **2a** and **2b**, respectively, and I_{2a2b} and I_{2b2a} are the cross-peak intensities.

$$k' = (1/t_m) \times \ln[(r + 1)/(r - 1)] \qquad \text{(Eq. 2.2)}$$

$$r = \{4X_{2a}X_{2b}(I_{2a2a} + I_{2b2b})/(I_{2a2b} + I_{2b2a})\} - (X_{2a} - X_{2b})^2 \qquad \text{(Eq. 2.3)}$$

Considering that the forward and reverse rates ($R_{2a\rightarrow2b}$, $R_{2b\rightarrow2a}$) at equilibrium **2a** $\rightleftharpoons$ **2b** are equal (Eq. 2.4), the rate constants for the conversions **2a** $\rightarrow$ **2b** and **2b** $\rightarrow$ **2a** are given in Eq. 2.5.

$$R_{2a\rightarrow2b} = X_{2a}k_{2a\rightarrow2b} = X_{2b}k_{2b\rightarrow2a} = R_{2b\rightarrow2a} \qquad \text{(Eq. 2.4)}$$

$$k_{2a\rightarrow 2b} = k'/(1 + X_{2a}/X_{2b}) \text{ and } k_{2b\rightarrow 2a} = k'/(1 + X_{2b}/X_{2a}) \qquad \text{(Eq. 2.5)}$$

Two separate experiments were performed at each temperature. Within each experiment, two independent values of r_1 and r_2 were obtained from the intensities of C*H*= (**2a**)/CH_aH_b (**2b**) and CH_2 (**2a**)/CH_aH_b (**2b**) peaks, respectively. The averages of r_1 and r_2 from the two experiments $r_{1\text{-ave}}$ and $r_{2\text{-ave}}$ are listed in Table 2.2. The values of $k'_{1\text{-ave}}$ and $k'_{2\text{-ave}}$ were calculated from $r_{1\text{-ave}}$ and $r_{2\text{-ave}}$, and were used to yield $k_{2a\rightarrow 2b}$ and $k_{2b\rightarrow 2a}$, which are the first-order rate constants for the conversions **2a** → **2b** and **2b** → **2a**, respectively. $k_{2a\rightarrow 2b}$ and $k_{2b\rightarrow 2a}$ were then used in a least-squares Eyring analysis (Eqs. 2.6 and 2.7) to give the activation parameters for conversions **2a** → **2b** and **2b** → **2a** (Figures 2.7 and 2.8).

$$\ln(k_{2a\rightarrow 2b}/T) = -\Delta H^{\neq}_{2a\rightarrow 2b}/(RT) + (\Delta S^{\neq}_{2a\rightarrow 2b}/R) + \ln(k_b/h) \qquad \text{(Eq. 2.6)}$$

$$\ln(k_{2b\rightarrow 2a}/T) = -\Delta H^{\neq}_{2b\rightarrow 2a}/(RT) + (\Delta S^{\neq}_{2b\rightarrow 2a}/R) + \ln(k_b/h) \qquad \text{(Eq. 2.7)}$$

(k_B = Boltzmann constant, 1.38×10^{-23} JK^{-1}; $h = 6.62608 \times 10^{-34}$ Js)

2.2.4. *Studies of solid-state structures of complexes 1 and 2*

Crystals of **2** were found to be severely disordered, and attempts to fully refine the structure of **2** (**2b/2a**, Figure 2.9) were unsuccessful. Disorders were also observed in the crystals of $(Bu^tCH_2)_2W(\equiv CBu^t)[Si(SiMe_3)_3]$ (**1,** Figure 2.10), although both unit cells looked reasonable. For **2**, the unit cell after initial matrix

Table 2.2. Exchange Rate Constants Derived from the 2D ^{1}H EXSY Spectra of **2a** $\rightleftharpoons$ **2b**[b]

T[a] (K)	X_{2a}/X_{2b}	t_m (s)	$r_{1\text{-ave}}$[b]	$k'_{1\text{-ave}}$[c] (s^{-1})	$r_{2\text{-ave}}$[b]	$k'_{2\text{-ave}}$[c] (s^{-1})	$k_{2a\rightarrow2b}$[d] (s^{-1})	$k_{2b\rightarrow2a}$[d] (s^{-1})
297	0.341(5)	0.3	4.832(3)	1.402(4)	4.578(4)	1.478(3)	1.10(4)	0.35(1)
292	0.307(6)	0.4	3.141(2)	0.832(2)	5.619(3)	0.901(4)	0.66(4)	0.20(1)
287	0.299(5)	0.5	9.772(3)	0.411(4)	8.547(4)	0.472(2)	0.34(3)	0.10(1)
282	0.289(4)	0.6	15.925(5)	0.213(2)	12.364(2)	0.269(3)	0.19(3)	0.054(8)
277	0.284(5)	0.7	22.053(4)	0.131(2)	15.925(5)	0.179(3)	0.12(3)	0.035(8)
272	0.276(2)	0.8	35.483(4)	0.071(4)	31.303(3)	0.079(2)	0.059(6)	0.016(1)
267	0.266(4)	1.0	55.054(6)	0.036(6)	42.667(8)	0.047(5)	0.033(6)	0.009(1)

[a] The estimated uncertainty in temperature measurement was 1 K.

[b] r_1 and r_2 were calculated from the intensities of the C*H*= (**2a**)/CH_aH$_b$ (**2b**) and CH_2 (**2a**)/CH$_a$$H_b$ (**2b**) peaks, respectively, according to Eq. 2.3. Their averages $r_{1\text{-ave}}$ and $r_{2\text{-ave}}$ are given here.

[c] $k'_{1\text{-ave}}$ and $k'_{2\text{-ave}}$ were calculated from $r_{1\text{-ave}}$ and $r_{2\text{-ave}}$ according to Eq. 2.2. The total uncertainties $\delta k/k$ in k'_1 and k'_2 were calculated from $\delta k_{(ran)}/k$ and the estimated systematic uncertainty $\delta k_{(sys)}/k = 5\%$ by $\delta k/k = [(\delta k_{(ran)}/k)^2 + (\delta k_{(sys)}/k)^2]^{1/2}$.

[d] $k_{2a\rightarrow2b}$ and $k_{2b\rightarrow2a}$ were calculated from $k'_{1\text{-ave}}$ and $k'_{2\text{-ave}}$ according to Eq. 2.5.

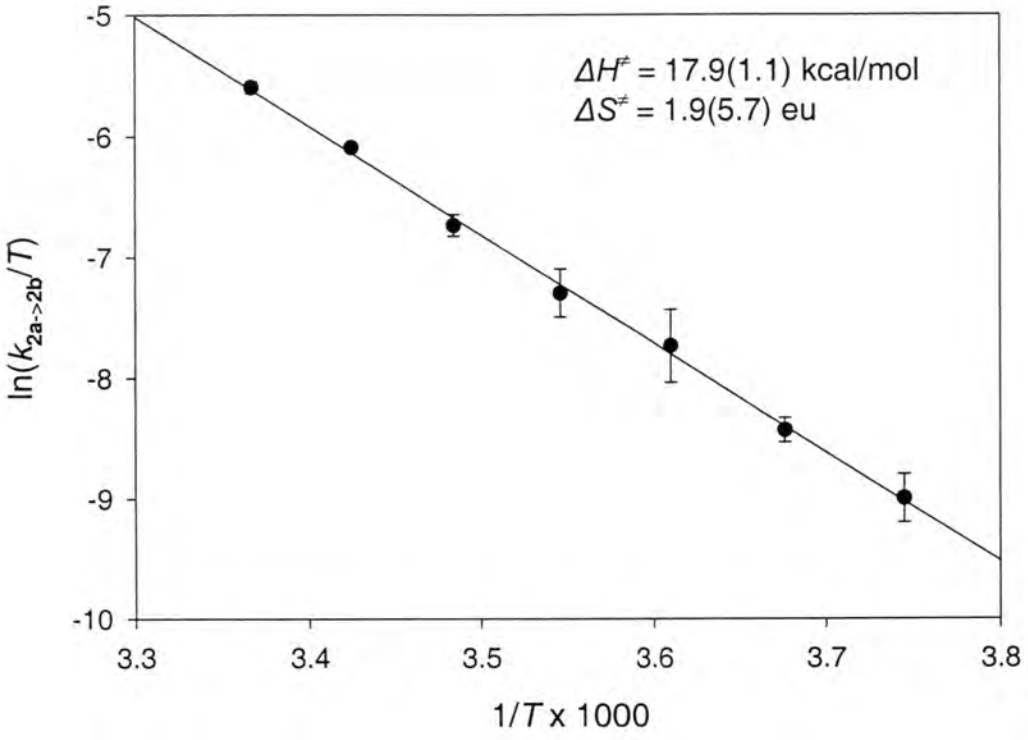

Figure 2.7. Eyring plot for the conversion **2a** → **2b**.

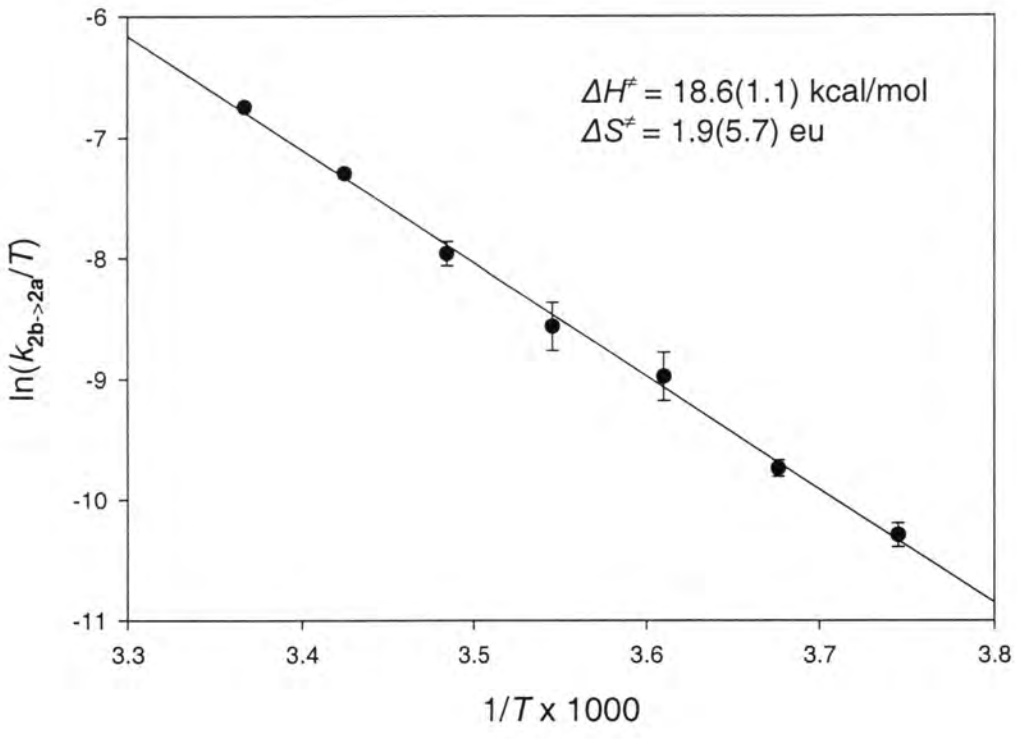

Figure 2.8. Eyring plot for the conversion **2b** → **2a**.

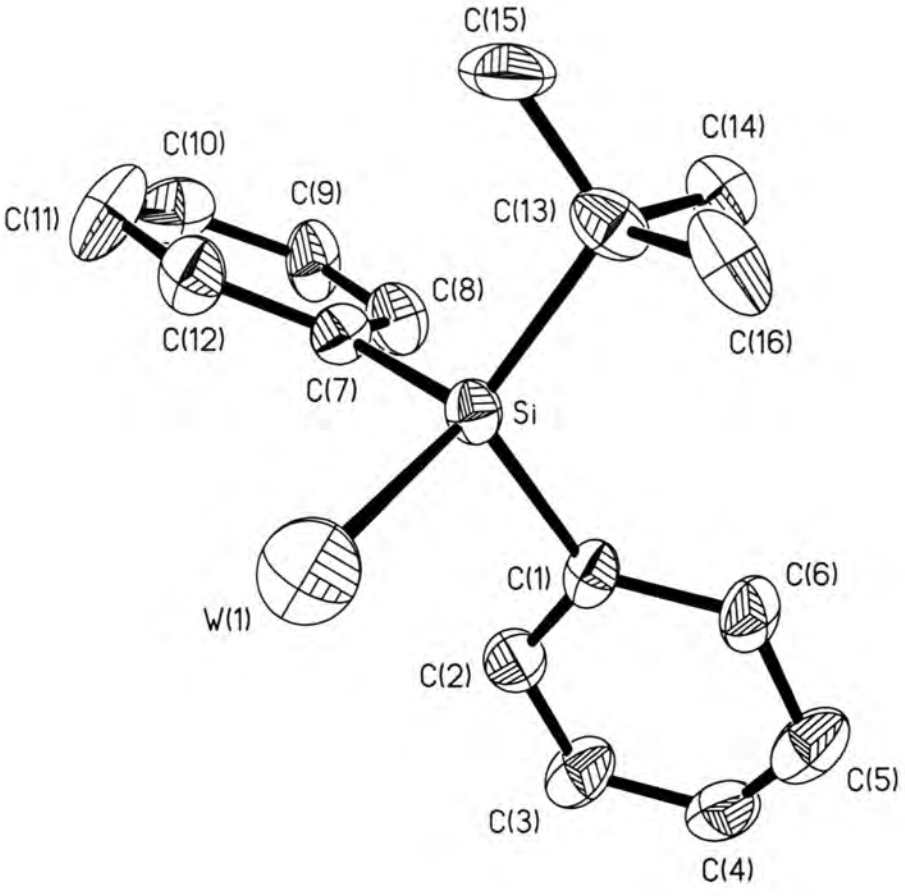

Figure 2.9. Partial ORTEP of **2** (**2a/2b**) showing 25% probability thermal ellipsoids.

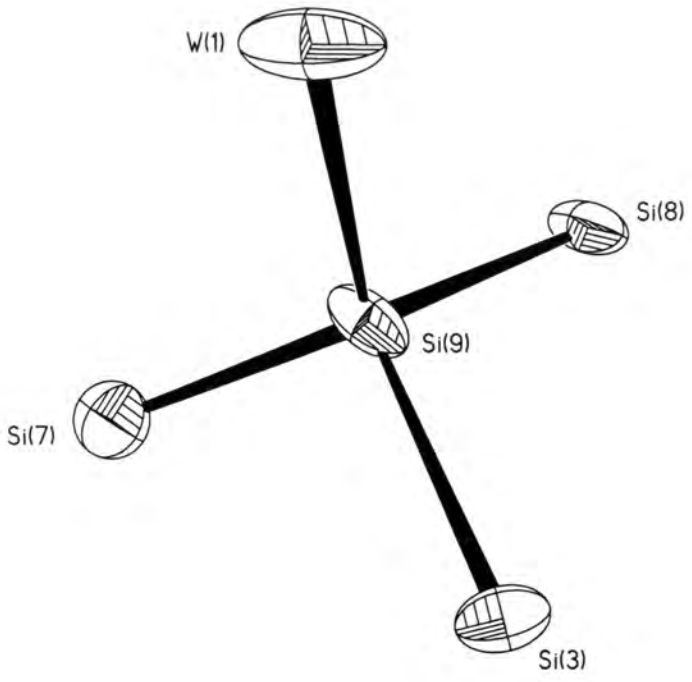

Figure 2.10. Partial ORTEP of **1**, showing 25% probability thermal ellipsoids.

determination was: *P*2(1), a = 9.1352(4) Å, b = 10.0788(5) Å, c = 17.3642(8) Å, α = 90°, β = 98.709(1)°, γ = 90°, Z = 2; and the unit cell for **1** is: *P*-3, a = 28.08(1) Å, b = 28.08(1) Å, c = 11.300(7) Å, α = 90°, β = 90°, γ = 120°, Z = 12. Only the cores of the two structures, silyl ligands W-SiBu^{t}Ph$_2$ and W-Si(SiMe$_3$)$_3$, could be located from the electron density difference maps. All alkyl groups remain uncertain due to disorder. Final R_1 = 0.1516 was obtained for the W-SiBu^{t}Ph$_2$ group in the structure of **2**. The final R_1 = 0.4822 for the W-Si(SiMe$_3$)$_3$ group in **1** indicated much more severe disorder. The W(1)-Si bond distances are 2.537(10) Å in **2** and 2.498(10) Å in **1**, respectively. They are relatively shorter than other reported W-Si single bond distances {2.614(2) Å in [PPN][W(CO)$_5$SiMe$_3$],[2c] PPN = bis(triphenylphosphine)nitrogen; 2.652(4) Å in [NEt$_4$][(CO)$_5$WSi(SnMe$_3$)$_3$];[2i] 2.599(1) Å and 2.644 Å in Cp$_2$W(SiMe$_3$)[Si(Bu^t)$_2$CH];[30a] 2.591(3) Å in Cp$_2$W(SiMe$_3$)(GeMe$_2$Cl);[30b] 2.602(1) Å and 2.594(1) Å in Cp$_2$W(SiMe$_3$)[Si(Pr^i)$_2$Cl];[30c] 2.670(2) Å in [Li(DIME)$_2$][W(CO)$_5$Si$_6$Me$_{11}$] (Si$_6$Me$_{11}$ = cyclohexasilyl),[30c] DIME = diethylene glycol dimethyl ether}. Of particular interest was the W-Si bond distance in **2**, which is close to the reported W=Si distance [2.481(3) Å] in Cp(CO)$_2$W(=SiMe$_2$HMPA)(SiMe$_3$) [HMPA = (Me$_2$N)$_3$P=O].[30d]

The presence of three-fold rotational axis through the W-Si bond in the crystal structure of (Bu^{t}CH$_2$)$_2$(Bu^{t}C≡)W-Si(SiMe$_3$)$_3$ (**1,** space group: *P*-3) may reflect the disorder between the two Bu^{t}CH$_2$ and the Bu^{t}C≡ groups. Although such three-fold symmetry does not exit in the structure of **2** [**2a/2b**, space group: *P*2(1)],

the presence of both **2a** and **2b** as well as their α-H exchange in the solid state, as observed in the ^{13}C SSNMR of **2** (**2a/2b**, Figure 2.2), may lead to the disorder in the structure of **2**.

2.2.5. *Theoretical studies of the exchange 2a ⇌ 2b*[31]

The theoretical studies were mainly conducted by Professor Zhen-Yang Lin and coworkers and are summarized here. Thermodynamically, the d^0 alkylidyne complex $(Bu^tCH_2)_2W(\equiv CBu^t)(SiBu^tPh_2)$ (**2b**) and its bis(alkylidene) tautomer $(Bu^tCH_2)W(=CHBu^t)_2(SiBu^tPh_2)$ (**2a**, Scheme 2.5) were found close in energy, and the alkylidyne tautomer **2b** is slightly more stable. It is surprising that such an equilibrium is only observed for complexes with a $-SiBu^tPh_2$ substituent, but not for alkyl, chloro, or even the $-Si(SiMe_3)_3$ substituents.[16a] In comparison, d^2 bis(alkylidene) complex $Os(=CHBu^t)_2(CD_2Bu^t)_2$ is more stable than its alkylidyne tautomer intermediate "$(Bu^tCH_2)_3Os\equiv CBu^t$," as only the former was observed in the H/D scrambling process (Scheme 2.4b).[20d] These observations are examples of d electrons and substituted ligands with different electronic properties having an influence on the relative stabilities of a tautomeric pair. Density functional molecular orbital calculations at the B3LYP level were performed to investigate the relative stabilities of the tautomeric pairs of transition metal alkylidyne $(CH_3)_2M(\equiv CH)(X)$ and bis(alkylidene) $(CH_3)M(=CH_2)_2(X)$ complexes (M = W, Mo, Os, and Ru; X = Cl, CH_3, CF_3, SiH_3, and SiF_3). Calculation results indicate that the relative stabilities of the bis(alkylidene) tautomers increase with the increasing π-

accepting ability of X for the W and Mo complexes. When X is a silyl ligand, it is found that the tautomeric pair for W or Mo have similar stabilities. These results have been explained in terms of π interaction between ligand X and the electron density in the metal-alkylidyne/alkylidene bonds. For the Os and Ru complexes, the bis(alkylidene) tautomers are found more stable no matter what X is. The stabilities of the bis(alkylidene) tautomers for these d^2 metal complexes have been related to the bonding characteristic of the orbital that accommodates the two metal d electrons.

2.3. Conclusions

The preparation of a novel d^0 tungsten silyl complex **2** and an unusual equilibrium between **2a** and **2b** are reported. The thermodynamics of this equilibrium was investigated to give ΔH° = -0.9(0.2) kcal/mol, ΔS° = -0.6(0.8) eu. The kinetic studies of the α-H exchange between **2a** and **2b** by 2-D EXSY experiments gave kinetic parameters of the exchange: $\Delta H^{\neq}$ = 17.9(1.1) kcal/mol, $\Delta S^{\neq}$ = 1.9(5.7) eu for the forward reaction (**2a** → **2b**), and $\Delta H^{\neq}$ = 18.6 (1.1) kcal/mol, $\Delta S^{\neq}$ = 1.9(5.7) eu for the back reaction (**2b** → **2a**).

2.4. Experiment Section

2.4.1. *General procedures*

All manipulations, unless otherwise noted, were performed under a dry nitrogen atmosphere with the use of either a drybox or standard Schlenk techniques.

All solvents were purified by distillation from potassium/benzophenone ketyl. Benzene-d_6 and toluene-d_8 were dried over activated molecular sieves and stored under N_2. One-dimensional ^1H and ^{13}C NMR spectra, unless noted, were recorded at 23 °C on a Bruker AC-250 or AMX-400 Fourier transform (FT) spectrometer and referenced to solvents (residual protons in the ^1H spectra). ^1H -^{13}C heteronuclear correlation (HETCOR) and $^{29}Si\{^1H\}$ (DEPT) NMR experiments were conducted at 23 °C on a Bruker AMX-400 FT spectrometer. The $^{29}Si\{^1H\}$ (DEPT) NMR spectra were referenced to $SiMe_4$. 2D NOESY spectra were recorded at 23 °C on a Varian Mercury 300 FT spectrometer (ns = 32, t_{mix} = 3 s, increments = 128). 2D EXSY spectra (297 K to 267 K) were recorded on an updated Bruker AMX-400 FT spectrometer. $Li(THF)_3SiBu^tPh_2$,[24b] $(Me_3SiCH_2)_3W{\equiv}CSiMe_3$,[32] $(Bu^tCH_2)_3W{\equiv}CBu^t$,[23] and **1**[16a] were prepared by the literature procedures. HCl in Et_2O (1.0 M, Aldrich) was used as received. Elemental analyses were performed by Complete Analysis Laboratories Inc., E&R Microanalytical Division, Parsippany, New Jersey 07054-4909.

2.4.2. *NMR experiments*

For the thermodynamic studies, the equilibrium constants K_{eq} were obtained from at least two separate experiments at a given temperature, and their averages are listed (Table 2.1). The *maximum* random uncertainty in the equilibrium constants was combined with the estimated systematic uncertainty, ca. 5%. The total uncertainties in the equilibrium constants were used in the $\ln K_{eq}$ vs. $1/T$ plot in

Figure 2.3 and error propagation calculations. The estimated uncertainty in the temperature measurements for an NMR probe was 1 K. The enthalpy ($\Delta H°$) and entropy ($\Delta S°$) changes were calculated from an unweighted nonlinear least-squares procedure contained in the SigmaPlot Scientific Graph System, which is available from Jandel Corporation. The uncertainties in $\Delta H°$ and $\Delta S°$ were computed from the following error propagation formulas (Eqs. 2.8 and 2.9), which were derived from $-RT \ln K_{eq} = \Delta H° - T\Delta S°$ (Eq. 2.1).

$$(\sigma\Delta H°)^2 = (\Delta T/T)^2 R^2 (T_{max}^2 T_{min}^4 + T_{min}^2 T_{max}^4)[\ln(K_{eq(max)}/K_{eq(min)})]^2/\Delta T^4 + 2R^2 T_{max}^2 T_{min}^2 (\sigma K_{eq}/K_{eq})^2/\Delta T^2 \quad \text{(Eq. 2.8)}$$

$$(\sigma\Delta S°)^2 = 2R^2 T_{min}^2 T_{max}^2 [\ln(K_{eq(max)}/K_{eq(min)})]^2 (\Delta T/T)^2/\Delta T^4 + R^2 (T_{max}^2 + T_{min}^2)(\sigma K_{eq}/K_{eq})^2/\Delta T^2 \quad \text{(Eq. 2.9)}$$

where $\Delta T = (T_{max} - T_{min})$.[7]

The pulse sequence for 2D EXSY was $D1$-90°-$D0$-90°-$D9$-90°-FID. The initial relaxation delay time $D1$ was typically 3 s ($> 4T_1$, vide infra), the initial $D0$ was 3 μs, and the mixing time $D8$ (t_m) was varied according to the experimental temperature (vide infra). The pulse sequence was repeated for 128 values of $D0$, that is, the F_1 dimension contained 2048 points. The number of scans per experiment was 32, giving a total experiment time of ~270 min. The optimal mixing time $t_{m,opt}$ was chosen on the basis of Eq. 2.10 to minimize the relative error

in the rate constant.[27] The activation parameters determined from the Eyring analysis (Figures 2.7 and 2.8), were obtained by using the average rate constants $k_{2a\rightarrow 2b}$ and $k_{2b\rightarrow 2a}$ for the temperature range from 267 K to 297 K. The activation enthalpies ($\Delta H^{\neq}$) and entropies ($\Delta S^{\neq}$) were calculated from an unweighted nonlinear least-squares procedure contained in the SigmaPlot Scientific Graph System. Spin-lattice relaxation times T_1 were measured by using the standard inversion-recovery method. T_1 values for the hydrogen atoms of **2a** and **2b** measured at 287 K and 267 K are listed in Table 2.3.

$$t_{m,opt} \sim 1/(T_1^{-1} + k_{2a\rightarrow 2b} + k_{2b\rightarrow 2a}) \qquad \text{(Eq. 2.10)}$$

Control experiments established that rate constants determined by EXSY are not significantly affected by a ±50% variation in $t_{m,opt}$. Uncertainties in rate constant values were estimated assuming ±1% uncertainty in the finite *s/N* ratios of the computed spectra, and ±2% uncertainty in 2D signal integrations. At least two separate experiments performed for all temperatures gave the uncertainty. The

Table 2.3. T_1 (s) values for the α-H atoms of **2a** and **2b** at 287 K and 267 K

T (K)	CH= (**2a**)	CH_2 (**2a**)	CH_aH_b (**2b**)	CH_aH_b (**2b**)
287	1.35	0.86	0.67	0.63
267	1.19	0.55	0.33	0.33

maximum random uncertainty in the equilibrium constants was combined with the estimated systematic uncertainty, ca. 5%. The total uncertainties in the rate constants were used in the Eyring plots in Figures 2.7 and 2.8 and error propagation calculations. The estimated uncertainty in the temperature measurements for an NMR probe was 1 K. The uncertainties in $\Delta H^{\neq}$ and $\Delta S^{\neq}$ were computed from the following error propagation formulas, which were derived from $R\ln(kh/k_bT) = -\Delta H^{\neq}/T + \Delta S^{\neq}$ (Eqs. 2.6 and 2.7).[33]

$$(\sigma\Delta H^{\neq})^2 = R^2T_{max}^2T_{min}^2/\Delta T^2\{(\sigma T/T)^2[(1 + T_{min}\Delta L/\Delta T)^2 + (1 + T_{max}\Delta L/\Delta T)^2] + 2(\sigma k/k)^2\} \quad \text{(Eq. 2.11)}$$

$$(\sigma\Delta S^{\neq})^2 = R^2/\Delta T^2\{(\sigma T/T)^2[T_{max}^2(1 + T_{min}\Delta L/\Delta T)^2 + T_{min}^2(1 + T_{max}\Delta L/\Delta T)^2] + (\sigma k/k)^2(T_{max}^2 + T_{min}^2)\} \quad \text{(Eq. 2.12)}$$

where $\Delta L = [\ln(k_{max}/T_{max}) - \ln(k_{min}/T_{min})]$ and $\Delta T = (T_{max} - T_{min})$.

2.4.3. *Preparation of 2 [(Bu^tCH_2)W(=CHBu^t)$_2$($SiBu^tPh_2$) (2b) ⇌ (Bu^tCH_2)$_2$W(≡CBu^t)($SiBu^tPh_2$) (2a)]*

HCl (0.54 mmol, 1.0 M in Et_2O) was added dropwise to a vigorously stirred solution of $(Bu^tCH_2)_3W{\equiv}CBu^t$ (0.25 g, 0.54 mmol) in Et_2O (30 mL) at -78 °C. The color of the solution changed slowly from dark yellow to green yellow when the solution was allowed to gradually warm to -40 °C in 3 h. All the volatiles were removed under vacuum at -40 °C. $LiSiBu^tPh_2(THF)_3$ (0.25 g, 0.54 mmol) in Et_2O

was added dropwise to the solid at -40 °C, and the solution was warmed slowly to -10 °C. Removal of volatiles *in vacuo*, followed by extraction with pentane, filtration, and crystallization at -30 °C gave 0.20 g of **2** (0.32 mmol, 58% yield). Data for **2**: Anal. Calcd for $C_{31}H_{50}SiW$: C, 58.67; H, 7.94. Found: C, 58.30; H, 8.31. Data for **2a**: ^{1}H NMR (benzene-d_6, 250.1 MHz) δ 7.79-7.75, 7.24-7.15 (m, 10H, C_6H_5), 2.08 (d, 2H, $CH_aH_bCMe_3$, $^2J_{H\text{-}H}$ = 11.9 Hz), 1.53 (s, 9H, ≡CCMe_3), 1.28 (s, 9H, SiCMe_3Ph_2), 1.06 (s, 18H, CH_2CMe_3), -0.77 (d, 2H, $CH_aH_bCMe_3$); $^{13}C\{^1H\}$ (benzene-d_6, 62.9 MHz) δ 318.38 (≡CCMe$_3$), 143.81, 137.90, 128.59, 127.91 (C_6H_5), 134.52 (CH_2CMe_3), 53.87 (≡CCMe$_3$), 37.66 (CH_2CMe_3), 34.14 (CH_2CMe_3), 32.29 (≡CCMe_3), 30.60 (SiCMe$_3$), 21.63 (SiCMe_3); $^{29}Si\{^1H\}$ NMR (benzene-d_6, 79.5 MHz) δ 73.74 (SiBu^{t}Ph$_2$). Data for **2b**: ^{1}H NMR (benzene-d_6, 250.1 MHz) δ 7.86-7.84, 7.24-7.15 (m, 10H, C_6H_5), 6.03 (s, 2H, =CHCMe$_3$), 1.29 (s, 9H, SiCMe_3Ph_2), 1.19 (s, 18H, =CHCMe_3), 0.96 (s, 9H, CH_2CMe_3), 0.35 (s, 2H, CH_2CMe_3); $^{13}C\{^1H\}$ (benzene-d_6, 62.9 MHz) δ 272.32 (=CHCMe$_3$, $^1J_{C\text{-}H}$ = 104.1 Hz), 144.31, 137.69, 128.18, 127.61 (C_6H_5), 131.21 (CH_2CMe_3), 45.49 (=CHCMe$_3$), 37.31 (CH_2CMe_3), 35.01 (CH_2CMe_3), 32.04 (=CHCMe_3), 30.30 (SiCMe$_3$), 20.69 (SiCMe_3); $^{29}Si\{^1H\}$ NMR (benzene-d_6, 79.5 MHz) δ 62.11 (SiBu^{t}Ph$_2$).

2.4.4. *Preparation of $(Me_3SiCH_2)_2W(\equiv CSiMe_3)(Cl)(PMe_3)$ (4)*

4 was prepared by a method developed by our former group member Liting Li.[8c] New NMR spectra at a lower temperature and its elemental analysis were obtained in the current studies. ^{1}H NMR (toluene-d_8, 400.1 MHz, -35 °C) δ 1.09 (d,

2H, CH_aH$_b$CSiMe$_3$, $^2J_{H-H}$ = 13.7 Hz), 1.05 (d, 2H, CH$_a$$H_b$CSiMe$_3$), 0.99 (d, 9H, P$Me_3$, $^2J_{P-H}$ = 8.6 Hz), 0.38 (s, 18H, CH$_2$SiMe_3, $^2J_{Si-H}$ = 6.6 Hz), 0.18 (s, 9H, ≡CSiMe_3, $^2J_{Si-H}$ = 6.6 Hz); ^{13}C{^{1}H} NMR (toluene-d_8, 100.6 MHz, -35 °C) δ 368.75 (d, ≡CSiMe$_3$, $^2J_{P-C}$ = 20.3 Hz), 48.24 (CH$_2$SiMe$_3$, $^1J_{C-H}$ = 114.3 Hz), 48.13 (CH$_2$SiMe_3, $^1J_{C-H}$ = 114.3 Hz), 18.66 (d, PMe_3, $^1J_{C-H}$ = 128.9 Hz, $^1J_{P-C}$ = 32.2 Hz), 2.74 (CH$_2$SiMe_3, $^1J_{C-H}$ = 118.7 Hz, $^1J_{Si-C}$ = 50.3 Hz), 1.92 (≡CSiMe_3, $^1J_{C-H}$ = 119.1 Hz, $^1J_{Si-C}$ = 51.3 Hz). Data for **4** Anal. Calcd for $C_{15}H_{40}PClSi_3W$: C, 32.46; H, 7.26. Found: C, 32.18; H, 7.09.

2.4.5. *X-ray crystal structure determination for 1 and 2*

The crystal structures of **1** and **2** were determined on a Bruker AXS Smart 1000 X-ray diffractometer equipped with a CCD area detector and a graphite-monochromated Mo source (K_α radiation, 0.71073 Å) and fitted with an upgraded Nicolet LT-2 low temperature device. Suitable crystals were coated with paratone oil (Exxon) and mounted on a glass fiber under a stream of nitrogen at 173(2) K. The structure of **2** was partially solved by direct methods while automatic Patterson interpretation was applied to the structure of **1**. Among non-hydrogen atoms, only tungsten, silicon and the carbon atoms that were found were anistropically refined. Empirical absorption corrections for **1** and **2** were performed with SADABS.[35a] Global refinements for the unit cells and data reductions of structures **1-2** were performed using the Saint program (Version 6.02). All calculations were performed using the SHELXTL (Version 5.1) proprietary software package.[35b]

CHAPTER 3

Reactions of d^0 Tungsten Silyl and Alkyl Alkylidyne Complexes with Oxygen

3.1. Introduction

More than a billion years of life on earth under reducing conditions produced metal sulfides, iron(II), iron, and residual saturated hydrocarbons that could not be oxidized in the absence of dioxygen. The mutation that gave rise to the blue-green algae about three billion years ago permitted photosynthesis, which produced dioxygen as a by-product. This changed the world forever. The iron, iron(II), and the hydrocarbons were oxidized as was the hydrogen sulfide. Living organisms developed enzymes to activate O_2, and thereby let far more complicated compounds evolve. Under reducing conditions, membranes used triterpenoids derived from squalene. With O_2, sequalene epoxide could be formed and cyclized to oxygenated triterpenoids such as lanosterol – from which cholesterol, the hormones of the adrenal cortex, the sex hormones, and vitamin D could be produced. Dioxygen also permitted respiration, which produced more energy to be expended per unit of weight and of time.[6]

Much work has been done on the chemistry and biochemistry of O_2 activation and reactivity. A large interdisciplinary effort has been mounted to understand oxygenase enzymes of all kinds by isolating and studying the pure enzymes, and by developing model systems.[6d-e] There has also been intense

industrial interest in oxygen chemistry. Here economics takes a dominant role. At least dioxygen (as air) is free and, in principle, could be used to convert a saturated hydrocarbon directly to a ketone and water. In addition, industrial processes are not confined to copper and iron, two elements most commonly associated with O_2 activation in biological systems. Other elements or combinations of elements may be used in industrial O_2 activation.

Recently the selective oxidation of organic substrates by oxygen plays a crucial role in a variety of industrial and biological processes.[36] A control of these oxidations is achieved by catalysts in which the active sites are metal centers, and as a consequence, the reactivity of metal complexes toward O_2 is of fundamental importance. Furthermore, stoichiometric reactions of O_2 with organometallic derivatives have provided useful synthetic methods for the formation of alkyl hydroperoxides and alcohols.[37] In order to control such metal based oxidation processes using O_2, it is essential to understand the factors that influence the reactivity of O_2 with metal-alkyl derivatives.

Reactions of O_2 with transition-metal alkyl complexes have been actively investigated, and these studies have focused on d^n metal complexes.[38] Early transition metals are oxophilic, and their complexes are often O_2-sensitive. However the nature of the reactions of these complexes with O_2 is largely unknown. Few studies have been conducted of the reactions of O_2 with d^0 high-oxidation-state transition metal complexes. Schwartz,[39a-b] Gibson,[39c] and coworkers reported oxygen insertion into the Zr-R bond in the reaction of Cp_2ZrRCl with O_2. Similar reactions between Cp_2ZrR_2 and O_2 were shown by Brindley and Scotton to give

$Cp_2Zr(OR)_2$.[39d] Bercaw and coworkers studied the conversion of $Cp^*_2Hf(R)(OOBu^t)$ to $Cp^*_2Hf(OR)(OBu^t)$.[39e-f] In Cp-free complexes, Wolczanski, Rothwell, Gibson and their coworkers reported reactions of O_2 with $(RO)_2TiMe_2$,[39g] $(ArO)_2TaMe_3$,[39h] and $(ArN=)_2MoMe_2$ [39i] to yield $(RO)_2Ti(OMe)_2$, $(ArO)_2Ta(OMe)_3$, and $[(ArN=)_2MoMe(\mu\text{-}OMe)]_2$, respectively. Autoxidation of $M(CH_2R)_4$ by O_2 was found to be rapid.[39j] Yoo and his coworkers found that reactions of O_2 with chelating diamides (N~N)TiMeX (X = Me, Cl; N~N = silacyclo-alkane or –alkene bridge) gave $[(N\sim N)Ti(\mu\text{-}OMe)X]_2$.[36k] In contrast, the reaction of alkyl-free $(N\sim N)TiCl_2$ with O_2 led to diamide ligand oxidation.[39l] Schaverien and Orpen reported that $LY(\mu\text{-}Me)_2AlMe_2$ (L = porphyrin) activates O_2 to give $LY(\mu\text{-}OMe)_2AlMe_2$.[39m] Other studies of reactions of O_2 with d^0 complexes are summarized in references 39n-r.

Insertion of oxygen into metal carbon bonds also offers an interesting alternative route[40] (Scheme 3.1) to the preparation of thermally and chemically stable alkoxides, which are widely used to give high-tech ceramics such as microelectronic, superconducting, and ionic conducting materials.

$$MR_n \xrightarrow{n/2\ O_2} M(OR)_n$$

(M = B, Al)

Scheme 3.1. An alternative synthetic route to alkoxides.[40]

We recently observed some unusual reactions of O_2 with d^0 W alkylidyne complexes. The reaction of a *silyl* alkylidyne complex $(Bu^tCH_2)_2W(\equiv CBu^t)(SiBu^tPh_2)$ [**(2b)** as an equilibrium mixture $(Bu^tCH_2)W(=CHBu^t)_2(SiBu^tPh_2)$ **(2a)** $\rightleftharpoons$ **2b**] with O_2 led to a silyl migration to the alkylidyne ligand to give $(Bu^tCH_2)_2W(=O)[=C(Bu^t)(SiBu^tPh_2)]$ (**5**). In contrast, the reaction of an *alkyl* alkylidyne complex $(Me_3SiCH_2)_3W\equiv CSiMe_3$ with O_2 in the presence of PMe_3 yielded $(Me_3SiCH_2)_2W(=O)(=CHSiMe_3)(O=PMe_3)\bullet (Me_3SiCH_2)_3W(\equiv CSiMe_3)$ (**12**), which contains two independent molecules in the crystal lattice $(Me_3SiCH_2)_2W(=O)(=CHSiMe_3)(O=PMe_3)$ (**11**) and $(Me_3SiCH_2)_3W\equiv CSiMe_3$. Our studies of reactions of O_2 with these d^0 W alkylidyne complexes are reported here.

3.2. Results and Discussion

3.2.1. *Reaction of a d^0 silyl alkylidyne complex with O_2. Synthesis and characterization of a tungsten oxo alkylidene complex $(Bu^tCH_2)_2W(=O)[=C(Bu^t)(SiBu^tPh_2)]$ (5)*

When a yellow-orange solution of **2** in benzene-d_6 was exposed to 1 equiv of gaseous O_2 at room temperature, a rapid reaction occurred and the color of the solution turned red. We were surprised to find the formation of an oxo alkylidene complex $(Bu^tCH_2)_2W(=O)[=C(Bu^t)(SiBu^tPh_2)]$ (**5**) in this reaction in 32% yield by NMR (Scheme 3.2).[7] Formally the silyl ligand in $(Bu^tCH_2)_2W(\equiv CBu^t)(SiBu^tPh_2)$ (**2b**) migrated to the alkylidyne ligand in this reaction to give an alkylidene ligand

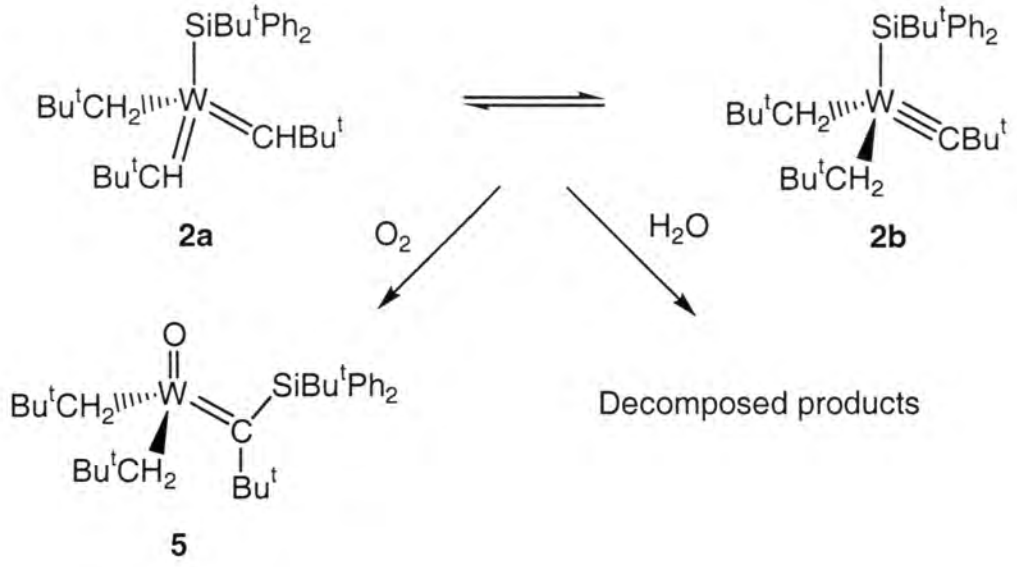

Scheme 3.2. Reactions of an equilibrium mixture **2a** ⇌ **2b** with O_2 and H_2O.

=C(Bu^t)(SiBu^{t}Ph$_2$) in **5**. To our knowledge, this observation is the first of such a silyl ligand migration. Ahn and Mayr have reported a formal insertion of an alkylidyne group into a W-N bond and the elimination of HBr in the reaction of TpW(=CHPh)(=X)Br [Tp = tris(pyrazolyl)borate; X = NR, O] with Br_2.[41] The formation of **5** through the reaction of **2b** with H_2O was excluded.

Spectroscopic properties of **5** are consistent with the structure assignment.[7] The alkylidene resonance of **5** at 269.65 ppm appears as a singlet in the ^{1}H-gated-decoupled ^{13}C NMR spectrum. The molecular structure of **5** has been determined by X-ray crystallography, and is shown in Figure 3.1.[7] Crystallographic data are given in Tables 3.1-3.2. Complex **5** exhibits distorted tetrahedral geometry around

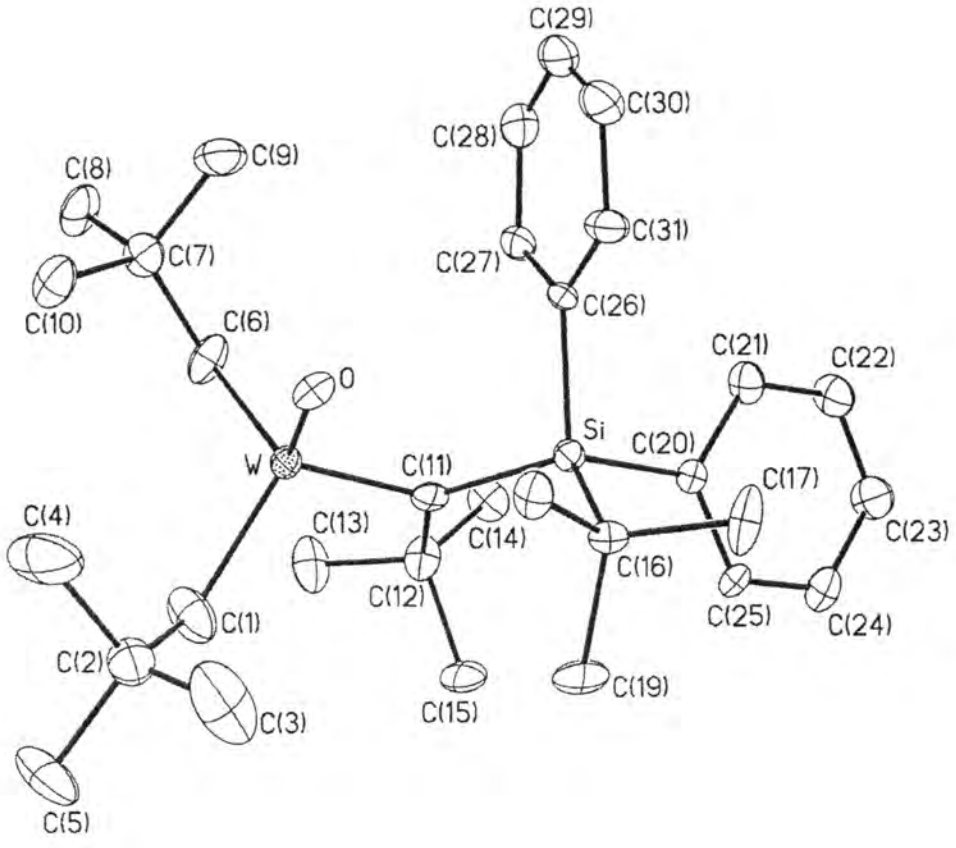

Figure 3.1. ORTEP of **5** showing 50% probability of thermal ellipsoids.

Table 3.1. Crystal data and structure refinement for **5**

Identification code	**5**	
Empirical formula	$C_{31}H_{50}OSiW$	
Formula weight	650.65	
Temperature	223(2) K	
Wavelength	0.71073 Å	
Crystal system	Orthorhombic	
Space group	$Pna2_1$	
Unit cell dimensions	a = 21.8650(5) Å	$\alpha = 90°$
	b = 17.2786(2) Å	$\beta = 90°$
	c = 8.31220(10) Å	$\gamma = 90°$
Volume	3140.32(9) $Å^3$	
Z	4	
Density (calculated)	1.376 Mg/m^2	
Absorption coefficient	3.736 mm^{-1}	
$F(000)$	1328	
Crystal size	0.20 × 0.20 × 0.16 mm^3	
Theta range for data collection	1.50 to 28.26°	
Index ranges	$-28 \le h \le 28$, $-19 \le k \le 13$, $-11 \le l \le 4$	
Reflections collected	9837	
Independent reflections	3931 [R(int) = 0.0334]	

Table 3.1. Continued

Completeness to $\theta = 23.32°$	99.8%
Absorption correction	Semi-empirical from equivalents
Refinement method	Full-matrix least-squares on F^2
Data / restraints / parameters	3930 / 1 / 307
Goodness-of-fit on F^2	1.035
Final R indices $[I > 2\sigma(I)]$[a]	$R1$ = 0.0291, w$R2$ = 0.0544
R indices (all data)[a]	$R1$ = 0.0529, w$R2$ = 0.0638
Largest difference peak and hole	0.638 and –1.313 e.Å^{-3}
Absolute structure parameter	0.015(13)

[a] $wR2 = [\sum w(F_o^2 - F_c^2)^2 / \sum w(F_o^2)^2]^{1/2}$; $R = \sum \left| |F_o| - |F_c| \right| / \sum |F_o|$;

$w = 1 / [\sigma^2(F_o^2) + (aP)^2 + bP]$; $P = [2F_c^2 + \mathrm{Max}(F_o^2, 0)] / 3$

Table 3.2. Selected bond lengths (Å) and angles (°) for **5**

W-O	1.686(5)	W-C(11)	1.920(7)
W-C(1)	2.112(9)	W-C(6)	2.118(9)
O-W-C(11)	104.1(3)	O-W-C(1)	111.8(3)
C(11)-W-C(1)	109.7(3)	O-W-C(6)	109.5(3)
C(11)-W-C(6)	109.0(3)	C(1)-W-C(6)	112.4(4)
C(11)-Si-C(26)	105.8(3)	C(11)-Si-C(20)	114.8(3)
C(26)-Si-C(20)	103.4(3)	C(11)-Si-C(16)	114.8(3)
C(2)-C(1)-W	125.6(5)	C(7)-C(6)-W	120.6(5)
C(9)-C(7)-C(8)	107.6(8)	C(9)-C(7)-C(10)	109.3(8)
C(8)-C(7)-C(10)	107.4(7)	C(9)-C(7)-C(6)	112.3(7)
C(12)-C(11)-Si	124.8(5)	C(12)-C(11)-W	114.4(5)
Si-C(11)-W	120.8(4)	C(18)-C(16)-Si	114.0(6)
C(17)-C(16)-Si	110.4(6)	C(21)-C(20)-Si	120.5(6)
C(19)-C(16)-Si	110.3(5)	C(25)-C(20)-Si	123.6(6)

the tungsten center with interligand angles in the range of 104.1(3)° to 114.8(3)°. The W=C bond distance of 1.920(7) Å is similar to those observed in other d^0 tungsten alkylidene complexes.[42] The W=O bond distance of 1.686(5) Å is also similar to those observed in tungsten oxo complexes.[42a] Complex **5**, which is thermally stable at room temperature, reacts further with excess O_2 to give unknown species.

3.2.2. *Synthesis and characterization of $(Bu^tCH_2)_2W{\equiv}CBu^t(OSiBu^tPh_2)$ (6) and studies of the mechanistic pathway in the formation of $(Bu^tCH_2)_2W(=O)[=C(Bu^t)(SiBu^tPh_2)]$ (5)*

The interesting silyl migration reaction to give **5** likely proceeds through one of two possible pathways (Scheme 3.3). In Pathway **A**, one oxygen atom inserts into the W-Si bond in $(Bu^tCH_2)_2W(\equiv CBu^t)(SiBu^tPh_2)$ (**2b**) to give an intermediate $(Bu^tCH_2)_2W(\equiv CBu^t)(OSiBu^tPh_2)$ (**6**). This insertion is followed by $-SiBu^tPh_2$ migration to the alkylidyne ligand to give **5**. In Pathway **B**, $-SiBu^tPh_2$ migration yields a d^2 W(IV) alkylidene complex **7** *prior* to silyl migration. The reaction of 7 with O_2 gives **8**, and then **5**. **8** may form a peroxo-bridged dimer **10** before the formation of **5**.

We conducted studies to elucidate the mechanistic pathway. First we prepared $(Bu^tCH_2)_2W(\equiv CBu^t)(OSiBu^tPh_2)$ (**6**), a proposed intermediate in Pathway **A**, to see if it converted to **5**. Our initial attempts to prepare **5** are shown in Scheme 3.4. A reported procedure was used to yield silanol $HOSiBu^tPh_2$.[43] The silanol was

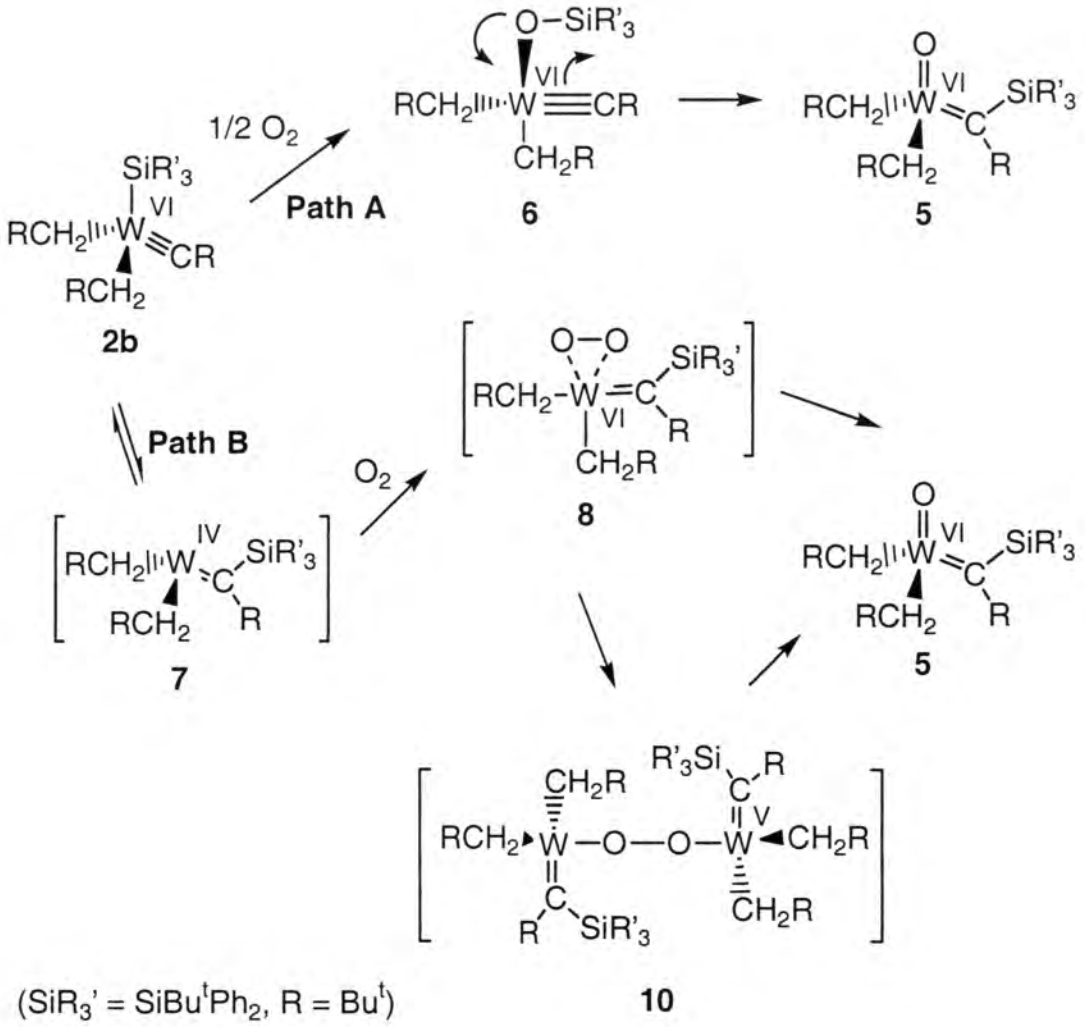

Scheme 3.3. Proposed pathways in the formation of **5**.

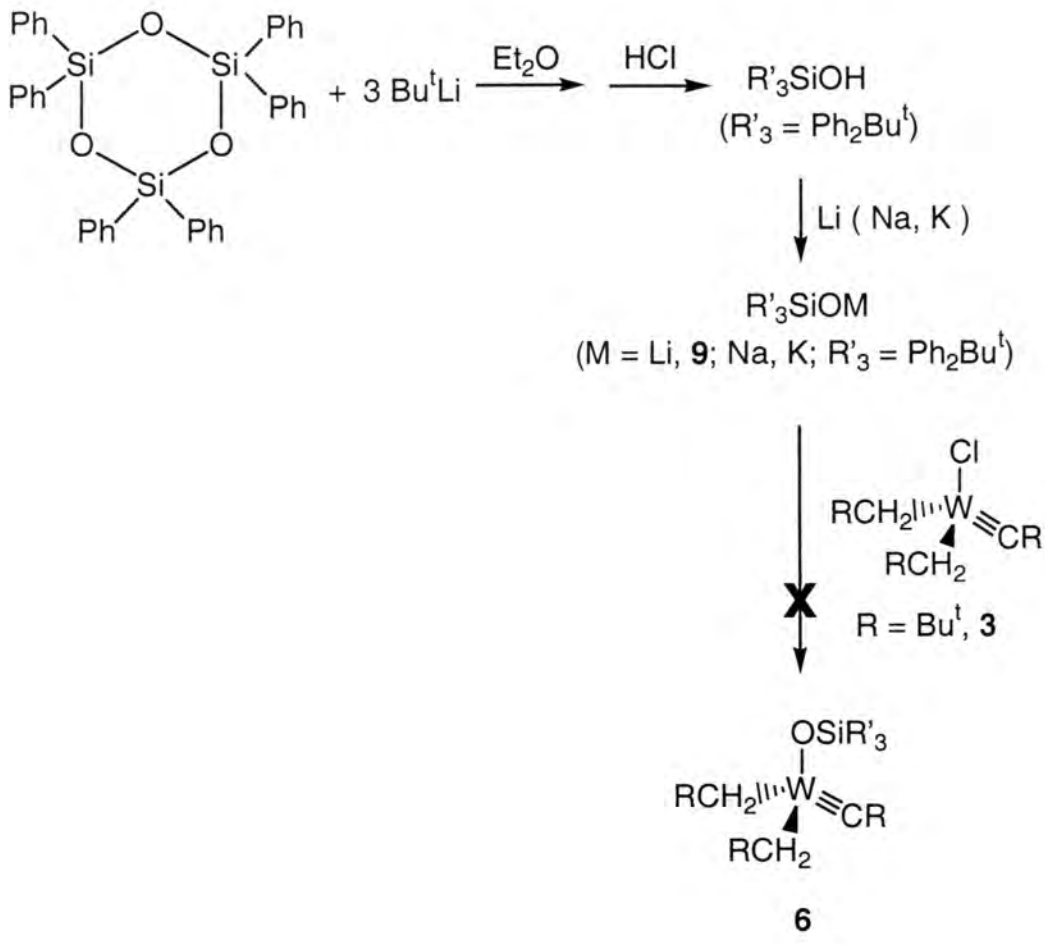

Scheme 3.4. Unsuccessful attempts to prepare **6**.

then reacted with alkali metals to give new complexes $MOSiBu^tPh_2$ (M = Li, **9**; Na, K) (Scheme 3.4). The NMR spectra of these complexes showed that they were relatively pure compounds. However their reactions with $(Bu^tCH_2)_2W(\equiv CBu^t)Cl$ (**3**) did not yield **6**. Perhaps the reactions between alkali metals and the silanol $HOSiBu^tPh_2$ were not complete. $(Bu^tCH_2)_2W(\equiv CBu^t)Cl$ (**3**), a highly sensitive and thermally unstable complex, may react with the residual silanol.

We subsequently used a different route to make silanolate $LiOSiBu^tPh_2$ (**9**). In the first step in Scheme 3.5, Bu^tLi reacted with $(Ph_2SiO)_3$ to yield **9** in 89.5% yield. Rather than hydrolyzing it, followed by the reaction with Li to make **9**, we used this silanolate directly in the reaction with **3** to give **6** (Scheme 3.5).

NMR studies of complex **6** showed that it was stable in both solution and solid state. No isomerization from $(Bu^tCH_2)_2W\equiv CBu^t(OSiBu^tPh_2)$ (**6**) to $(Bu^tCH_2)_2W(=O)[=C(Bu^t)(SiBu^tPh_2)]$ (**5**) was observed over a period of a week at room temperature. Thus Pathway **A** to **5** in Scheme 3.3 is thus unlikely.

Ab initio quantum chemical calculations were conducted to study Pathway **B** in Scheme 3.3 by Professor Yun-Dong Wu's group at the Hong Kong University of Science and Technology. These studies support Pathway **B**, and are summarized here (Scheme 3.6).[44] The migration of silyl ligand to the alkylidyne ligand in the d^0 model complex $Me_2W(\equiv CMe)SiMe_3$ (**2b′**) to give d^2 triplet $Me_2W[=CMe(SiMe_3)]$ (**7′**) is highly endothermic (ΔE = 13.6 kcal/mol). There exists an equilibrium **2b′** ⇌ **7′**, although the equilibrium is shifted to **2b′**. The addition of triplet O_2 to triplet **7′** to give $Me_2(\eta^2\text{-}O_2)W[=CMe(SiMe_3)]$ (**8′**), however, is highly exothermic (ΔE =

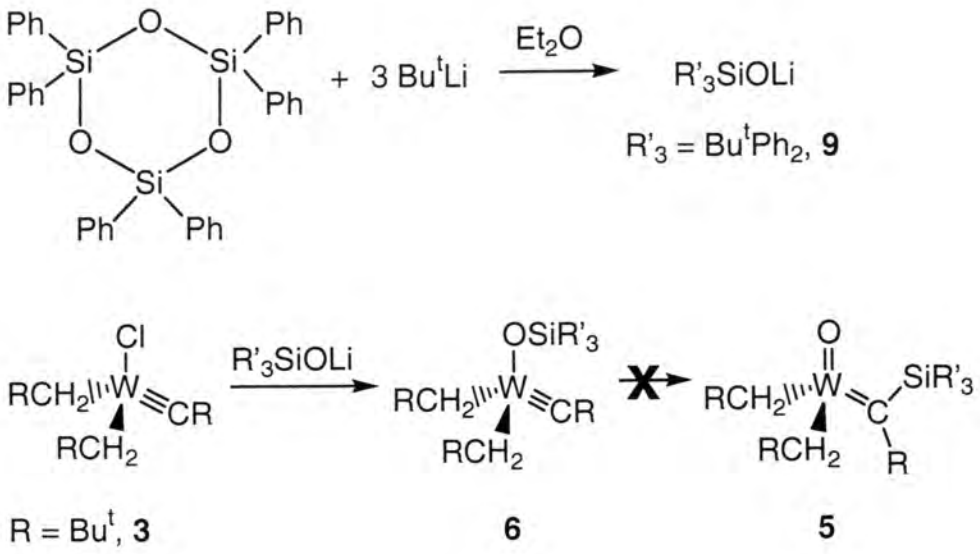

Scheme 3.5. A new route to silonate **9** and **6**.

Pathway B

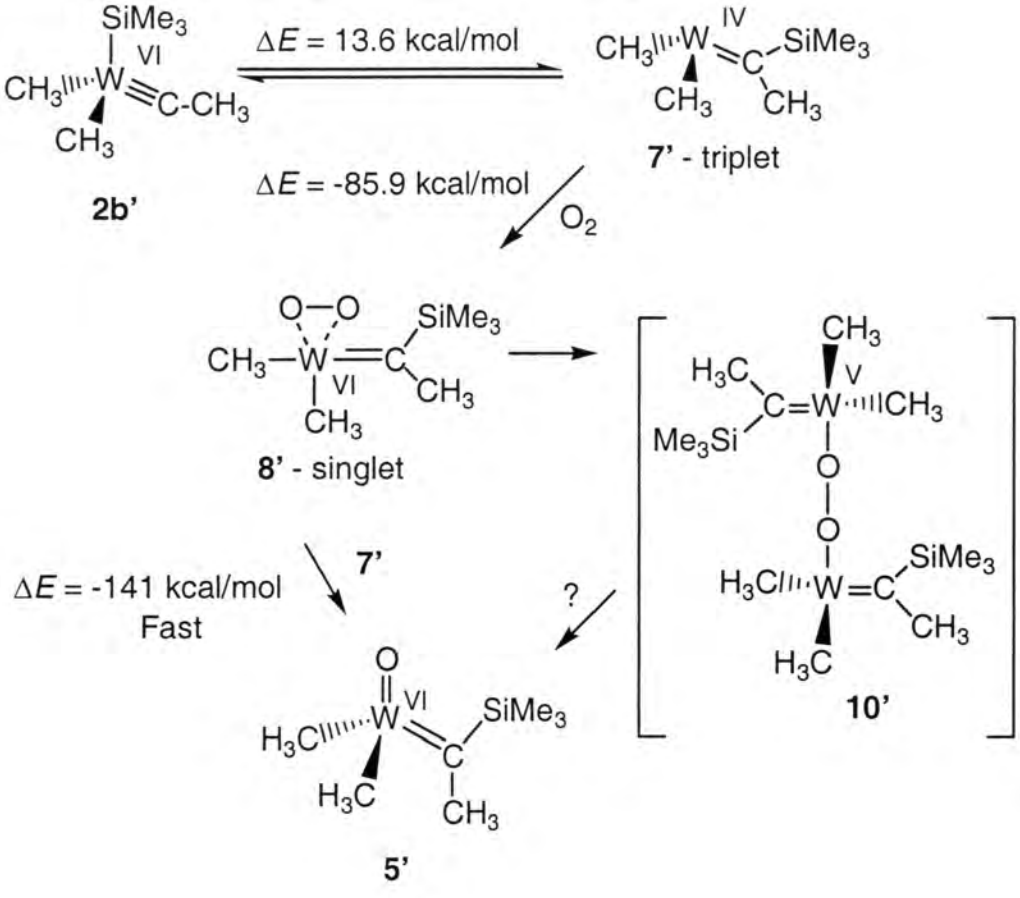

Scheme 3.6. *Ab initio* quantum chemical studies of Pathway **B** in Scheme 3.3.

-85.9 kcal/mol). **7′** is thus trapped by O_2. Subsequent reactions of **8′** lead to the formation of $Me_2(O=)W[=CMe(SiMe_3)]$ (**5′**), *perhaps* through a peroxo dimeric intermediate **10′**. The conversion of **8′** to **5′** was highly exothermic (ΔE = -141 kcal/mol) and fast, and the *ab inito* quantum chemical calculations did not show **10′**.

Rothwell and coworkers reported unusual reactions of a d^2 W complex with O_2 and azobenzenes (Scheme 3.7).[45] We reasoned that (1) that nitrosobenzene PhN=O and azobenzene (PhN=NPh) may show similar reactivities toward **2**; (b) if silyl migration in $(Bu^tCH_2)_2W(\equiv CBu^t)(SiBu^tPh_2)$ (**2b**) occurs prior to its reaction with O_2 (Pathway **B**, Scheme 3.4), we may be able to trap the intermediate $(Bu^tCH_2)_2W[=CBu^t(SiBu^tPh_2)]$ (**7**) by alkenes or alkynes. Girolami and coworkers used $Me_3SiC\equiv CSiMe_3$ to successfully trap a titanium alkylidene intermediate

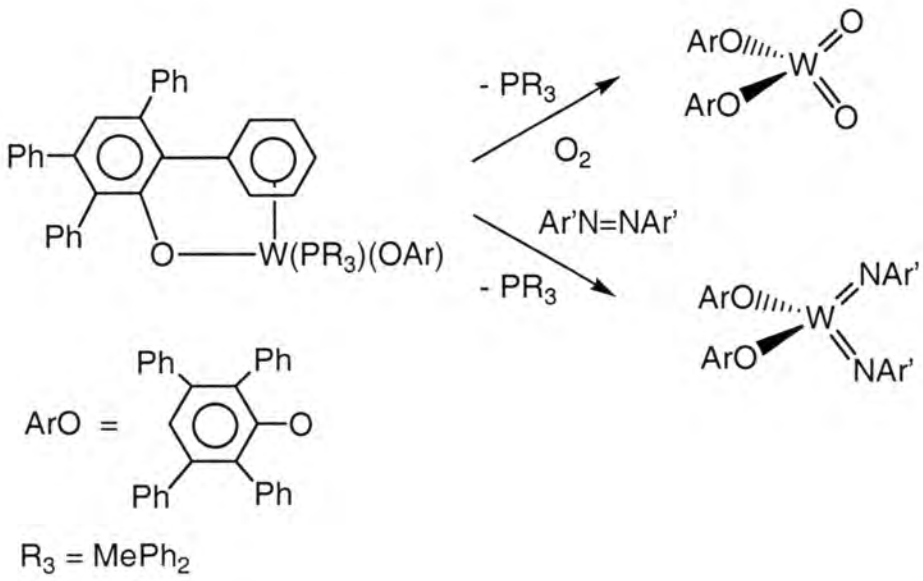

Scheme 3.7. Approaches by Rothwell *et al.* to break O=O and N=N bonds.[45]

"$(Bu^tCH_2)_2Ti{=}CHBu^t$" in the thermal decomposition of $(Bu^tCH_2)_4Ti$ (Scheme 3.8).[46] We thus conducted a series of reactions of **2** with PhN=O, PhN=NPh, and pyridine oxide (Scheme 3.9) as well as with PhC≡CPh, $Me_3SiC{\equiv}CSiMe_3$, PhC≡CH, and $Me_3SiC{\equiv}CH$ (Scheme 3.10).

Reactions of **2** with PhN=O and pyridine oxide were slow at room temperature. However no products could be isolated or identified. No reactions of **2** with PhN=NPh, PhC≡CPh, $Me_3SiC{\equiv}CSiMe_3$, or $Me_3SiC{\equiv}CH$ were observed at room temperature. In the reaction of PhC≡CH with **2** as monitored by ^1H NMR, a slow disappearance of PhC≡CH occurred. We however were not able to identify the products. **2** (**2a** ⇌ **2b**) is not thermally stable at 23 °C, and slowly decomposes to unidentified species. When these reactions were conducted at higher temperatures, the decomposition of **2** seemed to proceed at a faster pace than its reactions with the organic compounds.

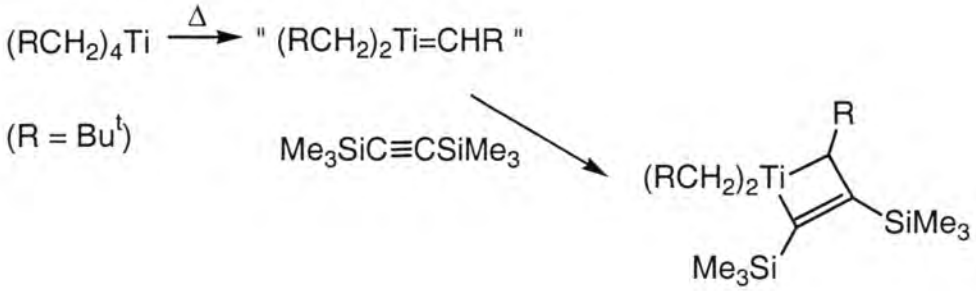

Scheme 3.8. "$(Bu^tCH_2)_2Ti{=}CHBu^t$" trapped by $Me_3SiC{\equiv}CSiMe_3$ in the thermal decomposition of $(Bu^tCH_2)_4Ti$.[46]

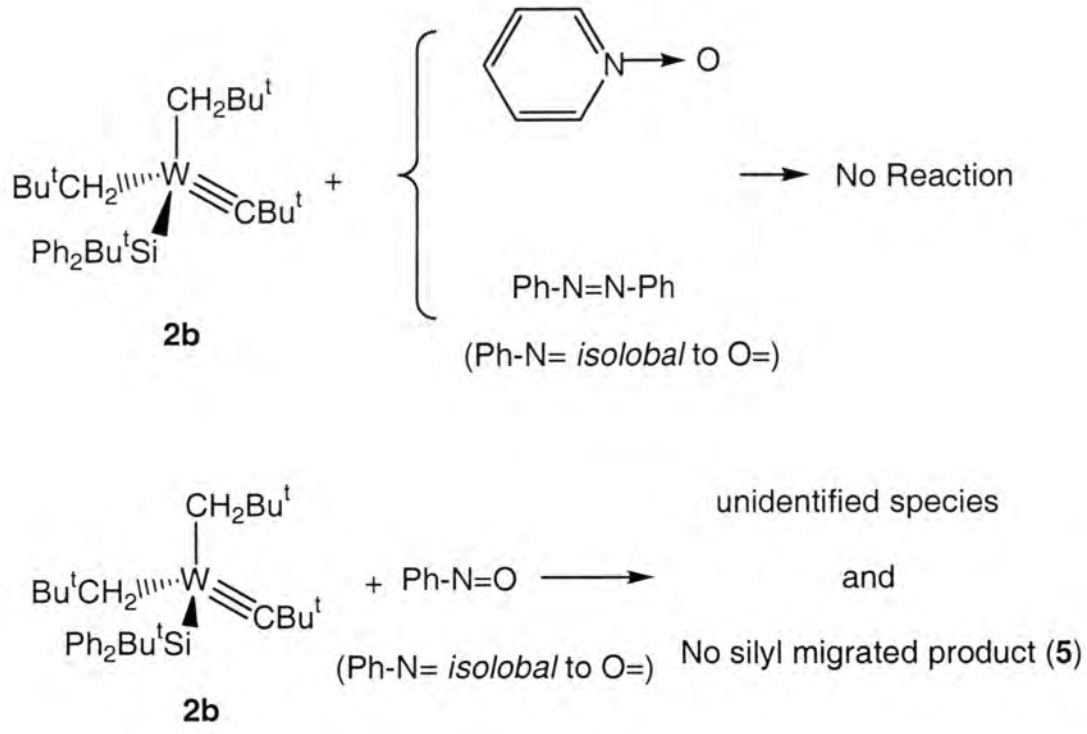

Scheme 3.9. Attempted studies of the reactivities of **2** toward various oxygen donors.

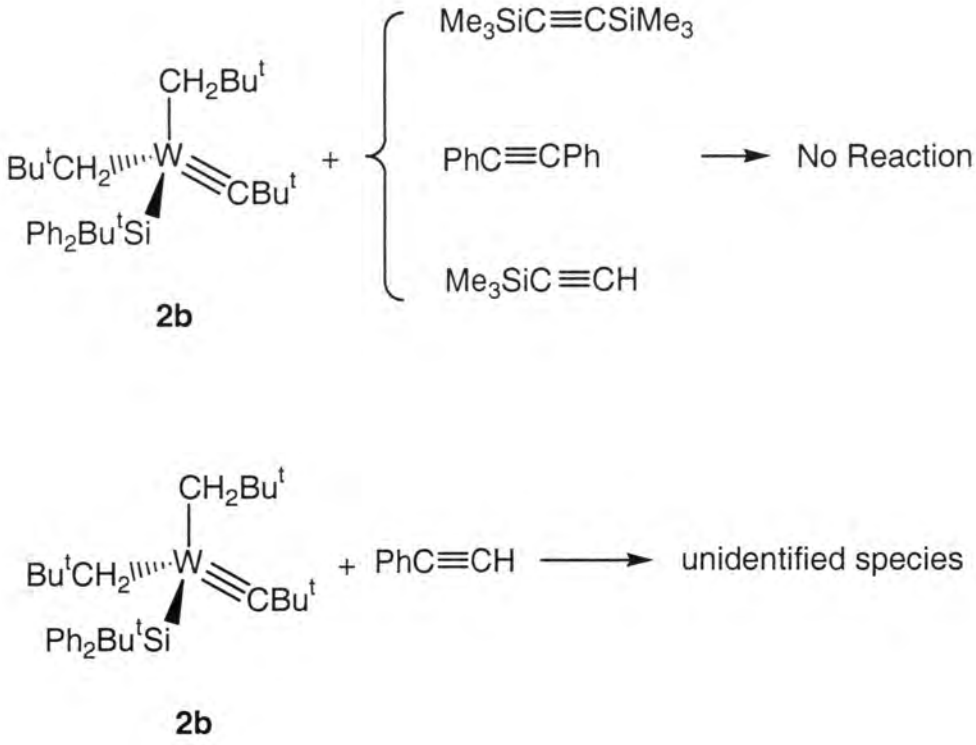

Scheme 3.10. Attempted studies of the reactivities of **2** toward alkynes.

3.2.3. *Reaction of a d^0 alkyl alkylidyne complex with O_2. Synthesis and characterization of unusual d^0 tungsten oxo alkylidene complex $(Me_3SiCH_2)_2W(=O)(=CHSiMe_3)(O=PMe_3)$ (11)*

Clark and Schrock have reported that reactions of $(Bu^tCH_2)_3W{\equiv}CBu^t$ with PMe_3 or $Me_2PCH_2CH_2PMe_2$ give $W(\equiv CBu^t)(=CHBu^t)(CH_2Bu^t)(PMe_3)_2$ and $W(\equiv CBu^t)(=CHBu^t)(CH_2Bu^t)(Me_2PCH_2CH_2PMe_2)$, respectively (Scheme 3.11).[47] These are unusual complexes containing alkyl, alkylidene and alkylidyne ligands in one compound.

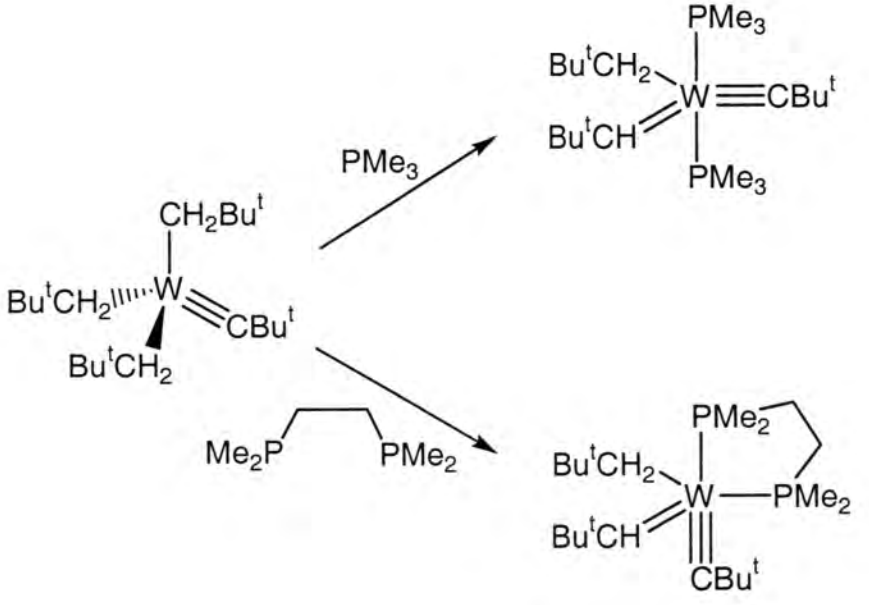

Scheme 3.11. Preparation of $W(\equiv CBu^t)(=CHBu^t)(CH_2Bu^t)(PMe_3)_2$ and $W(\equiv CBu^t)(=CHBu^t)(CH_2Bu^t)(Me_2PCH_2CH_2PMe_2)$.[47]

We were originally interested in the trimethylsilyl-methylidene ($Me_3SiCH=$) and -methylidyne ($Me_3SiC\equiv$) analogs of these complexes. We reported earlier unusual reactions of d^0 Ta bis(alkylidene) complexes such as $(Me_3SiCH_2)Ta(=CHSiMe_3)_2(PMe_3)_2$ with silanes.[16f,16h] The reactivities of the d^0 W complexes with $Me_3SiCH=$ and $Me_3SiC\equiv$ ligands toward silanes were of interest to us. However, in our numerous tests, no reaction was observed when a mixture of $(Me_3SiCH_2)_3W\equiv CSiMe_3$ [33] and liquid PMe_3 was heated at 70 °C in a closed system overnight.

We soon found through an accident that, in the presence of O_2 at room temperature, this mixture of alkyl alkylidyne $(Me_3SiCH_2)_3W\equiv CSiMe_3$ and liquid PMe_3 gave an unusual alkylidene oxo complex $(Me_3SiCH_2)_2W(=O)(=CHSiMe_3)(O=PMe_3)$ (**11**, Scheme 3.12). After $(Me_3SiCH_2)_3W\equiv CSiMe_3$ in excess PMe_3 at –60 °C was exposed to 1.5 equiv of dry O_2, the mixture was warmed to 23 °C. After 20 min, the volatiles were removed *in vacuo*. NMR showed the mixture contained 28% of **11** and 72% unreacted $(Me_3SiCH_2)_3W\equiv CSiMe_3$. Crystallization in pentane at –30 °C gave a solid of a 1:1 adduct of $(Me_3SiCH_2)_2W(=O)(=CHSiMe_3)(O=PMe_3)$ (**11**) and $(Me_3SiCH_2)_3W\equiv CSiMe_3$. As discussed below, the X-ray structure of this solid, $(Me_3SiCH_2)_2W(=O)(=CHSiMe_3)(O=PMe_3)\bullet(Me_3SiCH_2)_3W\equiv CSiMe_3$ (**12**), revealed that **11** and $(Me_3SiCH_2)_3W\equiv CSiMe_3$ formed an adduct through a weak $W=O\rightarrow W$ bridge. A control experiment involving $(Me_3SiCH_2)_3W\equiv CSiMe_3$, PMe_3, and H_2O did not yield **11** or **12**.

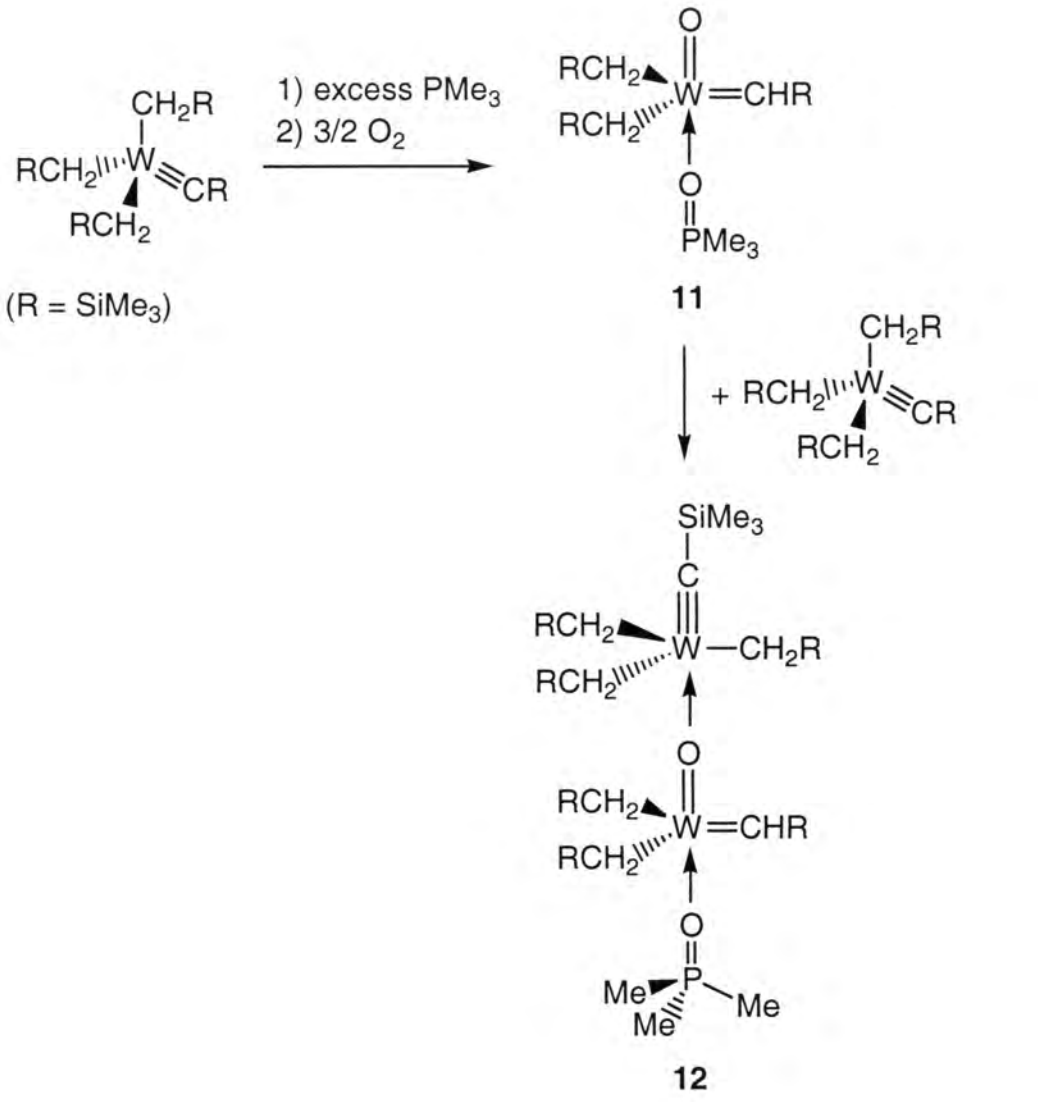

Scheme 3.12. Preparation of **11** and **12**.

Spectroscopic properties of **11** are consistent with the structural assignment. The alkylidene ligand in **11** was observed as a doublet ($^1J_{C\text{-}H}$ = 98.33 Hz) at 254.78 ppm in the ^{1}H-gated-decoupled ^{13}C spectrum, and at 7.98 ppm in ^{1}H NMR. Complex **11**, which is thermally stable at room temperature in the solid state, reacts further with excess O_2 to give unknown species.

The structure of the adduct **12** was determined by single-crystal X-ray crystallography. There are two independent adducts (**12a** and **12b**) in the solid state. The structures of **12a** and **12b** are similar, and the structural features of the two adducts are discussed below. The ORTEP views of **12a** and **12b** are shown in Figures 3.2 and 3.3, respectively. Two packing diagrams of **12** are shown in Figures 3.3 and 3.4. Crystallographic data are given in Tables 3.3 and 3.4. There is a crystallographically defined 3-fold axis through P=O→W=O→W≡C-Si in both adducts **12a** and **12b**. The P=O→W=O→W≡C-Si atoms are thus linearly arranged. The three-fold rotational disorder involving the two $-CH_2SiMe_3$ and one $=CHSiMe_3$ ligands on W(2A) and W(4) in $(Me_3SiCH_2)_2W(=O)(=CHSiMe_3)(O=PMe_3)$ (**11**) gave the average W-C bond distance of 2.088(4) Å for in **12a** and 2.100(4) Å in **12b**, respectively. It is the only known linear O=W←O=PMe$_3$ fragment in d^0 complexes.[48a] A rare linear O=W-O-W=O structure has been reported by Schrock, Lippard and coworkers.[48b] The methyl groups around the P atom and the ligands around the two W atom are almost eclipsed; The C(22)-P(2)-O(3)-W(4)-C(18) and C(18)-W(4)-O(4)-W(3)-C(12) torsion angles are 114.1° and 248.9°, respectively, in **12b**. The methyl groups around the Si(5) and the ligands around W(3) are twisted

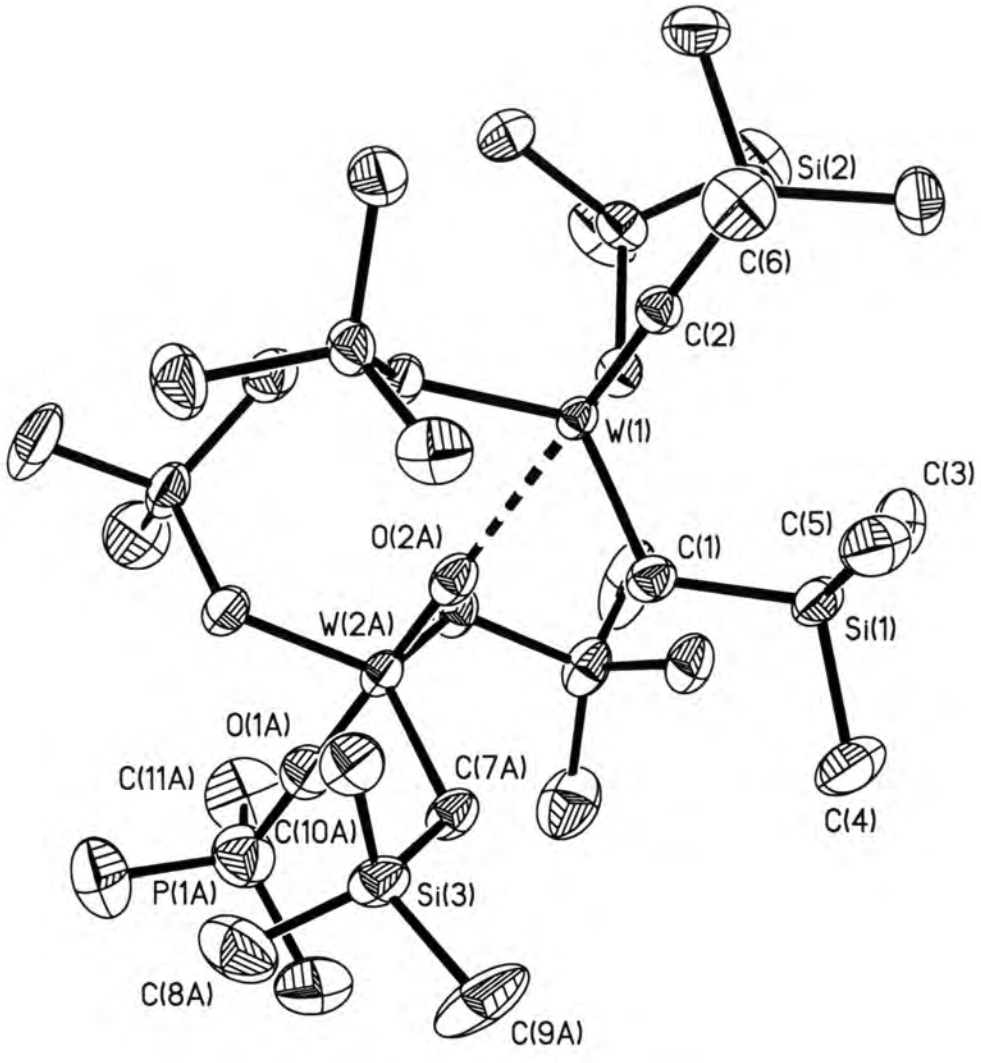

Figure 3.2. ORTEP of the first independent molecule of $(Me_3SiCH_2)_2W(=O)(=CHSiMe_3)(O=PMe_3)\bullet$ $(Me_3SiCH_2)W{\equiv}CSiMe_3$ (**12a**) showing 50% probability thermal ellipsoids. All hydrogen atoms are omitted and all methyl groups are unlabelled here for clarity.

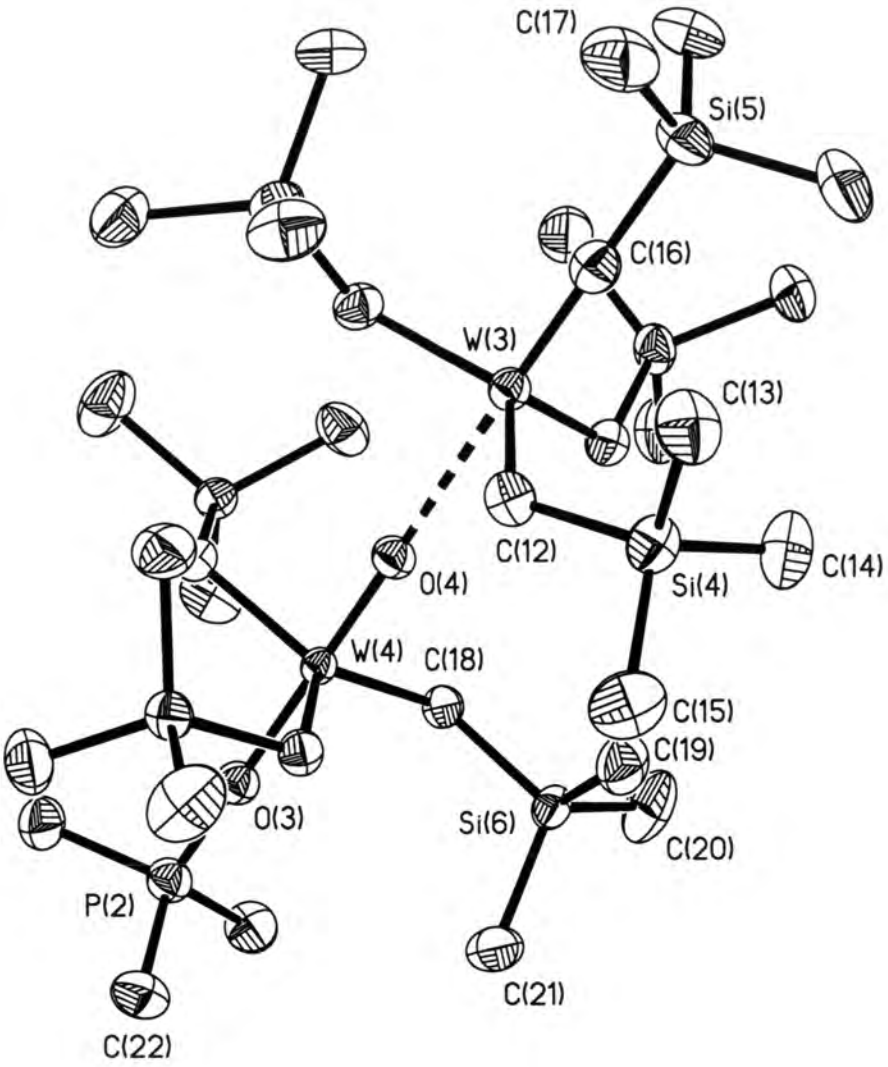

Figure 3.3. ORTEP view of the second molecule of $(Me_3SiCH_2)_2W(=O)(=CHSiMe_3)(O=PMe_3)\bullet (Me_3SiCH_2)W{\equiv}CSiMe_3$ (**12b**) showing 50% probability thermal ellipsoids. All hydrogen atoms are omitted and all methyl groups are unlabelled here for clarity.

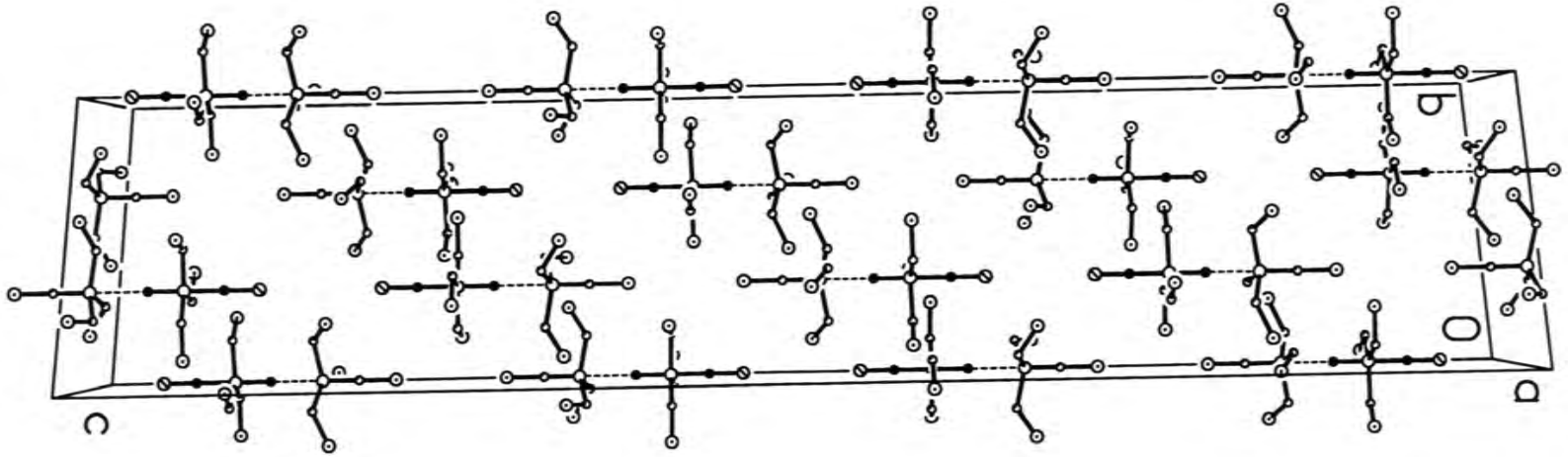

Figure 3.4. Packing diagram of **12**. View down the *a* axis. Methyl groups are omitted for clarity.

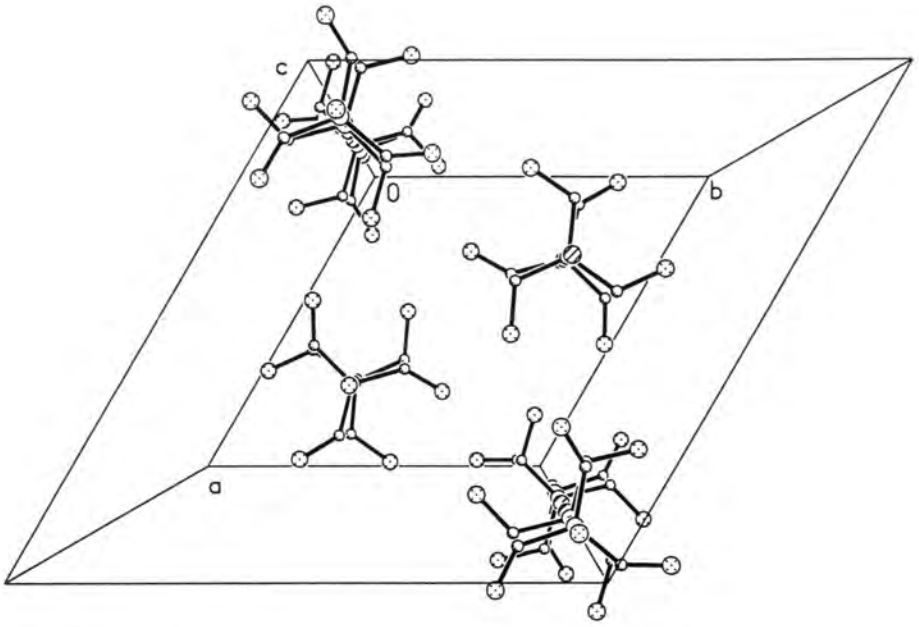

Figure 3.5. Packing diagram of **12**. View down the *c* axis. Methyl groups are omitted for clarity.

Table 3.3. Crystal data and structure refinement for **12**

Identification code	**12**	
Empirical formula	$C_{31}H_{84}O_2PSi_7W_2$	
Formula weight	1084.28	
Temperature	293(2) K	
Wavelength	0.71073 Å	
Crystal system	Hexagonal *R*-3	
Unit cell dimensions	a = 16.1077(7) Å	$\alpha = 90°$
	b = 16.1077(7) Å	$\beta = 90°$
	c = 68.397(4) Å	$\gamma = 120°$
Volume	15368.5(13) $Å^3$	
Z	12	
Density (calculated)	1.406 Mg/m^3	
Absorption coefficient	4.705 mm^{-1}	
F(000)	6564	
Crystal size	0.29 × 0.25 × 0.15 mm^3	
Theta range for data collection	1.49 to 28.28°	
Index ranges	$-21 \le h \le 21$, $-21 \le k \le 21$, $-91 \le l \le 91$	
Reflections collected	46502	
Independent reflections	8397 [R(int) = 0.0499]	

Table 3.3. Continued

Completeness to $\theta = 28.28°$	98.7%
Absorption correction	Semi-empirical from equivalents
Max. and min. transmission	0.5388 and 0.3424
Refinement method	Full-matrix least-squares on F^2
Data / restraints / parameters	8397 / 0 / 275
Goodness-of-fit on F^2	0.881
Final R indices $[I > 2\sigma(I)]$[a]	$R1$ = 0.0309, w$R2$ = 0.0673
R indices (all data)[a]	$R1$ = 0.0650, w$R2$ = 0.0859
Largest diff. peak and hole	3.430 and -0.859 e.Å^{-3}

[a] $wR2 = [\sum w(F_o^2 - F_c^2)^2 / \sum w(F_o^2)^2]^{1/2}$; $R = \sum \big| |F_o| - |F_c| \big| / \sum |F_o|$;

$w = 1 / [\sigma^2(F_o^2) + (aP)^2 + bP]$; $P = [2F_c^2 + \mathrm{Max}(F_o^2, 0)] / 3$

Table 3.4. Selected bond lengths (Å) and angles (°) for **12**[a]

C(1)-W(1)	2.095(4)	C(2)-W(1)	1.758(7)
C(1)-Si(1)	1.856(4)	C(2)-Si(2)	1.853(8)
C(7A)-W(2A)	2.088(4)	O(1A)-P(1A)	1.681(7)
O(1A)-W(2A)	1.908(6)	O(2A)-W(2A)	1.735(6)
C(7A)-Si(3)	1.879(5)	C(11A)-P(1A)	1.851(6)
O(2A)-W(1)	2.787		
C(12)-W(3)	2.101(4)	C(16)-W(3)	1.796(8)
C(12)-Si(4)	1.869(5)	C(16)-Si(5)	1.826(8)
C(18)-W(4)	2.100(4)	O(3)-P(2)	1.639(5)
O(3)-W(4)	1.915(5)	O(4)-W(4)	1.738(5)
C(18)-Si(6)	1.895(4)	C(22)-P(2)	1.857(5)
O(4)-W(3)	2.575(5)		
O(2)-W(2)-O(1)	180.0	P(1)-O(1)-W(2)	180.000(1)
C(2)-W(1)-C(1)	101.00(12)	C(1)-W(1)-C(1)#1	116.45(7)
Si(1)-C(1)-W(1)	123.1(2)	C(6)#1-Si(2)-C(6)	107.81(18)
C(2)-Si(2)-C(6)	111.08(18)	O(1)-W(2)-C(7)	88.15(14)
O(2)-W(2)-C(7)	91.85(14)	C(7)-W(2)-C(7)#1	119.897(16)
Si(3)-C(7)-W(2)	119.2(2)	C(11)#1-P(1)-C(11)	109.6(2)

Table 3.4. Continued

O(1)-P(1)-C(11)	109.4(2)		
W(3)-C(16)-Si(5)	180.0(1)	P(2)-O(3)-W(4)	180.0(1)
W(4)-O(4)-W(3)	180.0	C(16)-W(3)-O(4)	180.000(1)
O(4)-W(4)-O(3)	180.000(1)	C(16)-W(3)-C(12)	100.43(12)
C(12)#3-W(3)-C(12)	116.79(7)	Si(4)-C(12)-W(3)	123.9(2)
C(17)#3-Si(5)-C(17)	108.92(19)	C(16)-Si(5)-C(17)	110.02(18)
O(3)-W(4)-C(18)	87.65(11)	O(4)-W(4)-C(18)	92.35(11)
C(18)-W(4)-C(18)#3	119.834(16)	Si(6)-C(18)-W(4)	118.9(2)
C(22)#3-P(2)-C(22)	110.40(16)	O(3)-P(2)-C(22)	108.53(16)
C(12)-W(3)-O(4)	79.57(12)		

[a] Symmetry transformations are used to generate equivalent atoms:

#1 $-x+y,-x+1,z$ #3 $-x+y+1,-x+1,z$

with respect to one another; The C(12)-W(3)-C(16)-Si(5)-C(17) torsion angle is 302.7° in **12b**.

The W=O bond distances of 1.735(6) in **12a** and 1.738(5) Å in **12b** in the W=O→W moiety are slightly longer than those in other reported W oxo complexes.[42,48b,49-50] The O→W dative bond distances [1.908(6) in **12a** and 1.915(5) Å in **12b**] in the P=O→W moiety are much shorter than those in $W(=O)Cl_2[CH_2=CHCH_2P(=O)Ph_2]PMePh_2$ [2.177(3) Å][49a] and $WO_2Cl_2(O=PPh_3)$ [2.175(8) Å].[49b] The P=O bond distances of 1.681(7) Å in **12a** and 1.639(5) Å in **12b** are longer than those in d^2 $W(=O)Cl_2[CH_2=CHCH_2P(=O)Ph_2]PMePh_2$ [1.527(4) Å] and d^0 $W(=O)_2Cl_2(O=PPh_3)$ [1.500(7) Å].[49b] The long P=O and short O→W distances in the P=O→W moiety as well as long W=O bond distances in **12a** and **12b** may be a result of the conjugation in the P=O→W=O→W≡C-Si moiety in the adduct **12** (Scheme 3.13). Both d^0 **11** and $(Me_3SiCH_2)_3W{\equiv}CSiMe_3$ are highly electron deficient. Such conjugation may lead to electron transfer from $Me_3P=O$

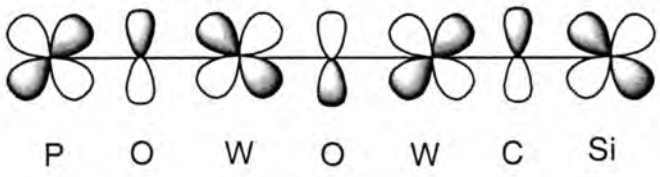

Scheme 3.13. Illustration of conjugation in the solid-state structure of **12**. (Only one set of π orbital overlapping is shown here.)

through **11** to $(Me_3SiCH_2)_3W{\equiv}CSiMe_3$. As a result, the charge separate resonance form Me_3P^+-O^- in $Me_3P{=}O \leftrightarrow Me_3P^+$-$O^-$ may become dominant.[49a]

The dative O→W bond distance in the O→W≡C-Si moiety is shorter in **12b** (2.575 Å) than in **12a** (2.787 Å). The W≡C bond distance is longer in **12b** [1.796(8) Å] than in **12a** [1.758(7) Å], and they are both longer than 1.739(8) Å in $(Me_3CCD_2)_3W{\equiv}CSiMe_3$.[20a] The shorter O→W bond and longer W≡C bond in **12b** suggest that the O and W atoms in the O→W≡C-Si moiety may have more π bond character through the conjugation in **12b** (Scheme 3.13). The O→W π bonding reduces the W≡C π bonding. The W≡C bond distances in **12a** and **12b** are however in the range of other reported W(VI)≡C distances (1.75–1.80 Å).[51] The structures of $(Me_3SiCH_2)_3W{\equiv}CSiMe_3$ in the adducts **12a** and **12b**, the second reported structure of d^0 W alkyl alkylidyne complex,[10c-d,20a,f] showed some additional features as a result of forming an adduct with **11**. The structures of both $(Me_3SiCH_2)_3W{\equiv}CSiMe_3$ here and $(Me_3CCD_2)_3W{\equiv}CSiMe_3$ [20a] are in distorted tetrahedral geometry. However, the interligand angles in $(Me_3SiCH_2)_3W{\equiv}CSiMe_3$ in **12a** [101.00(12)°] and **12b** [100.43(12)] are much smaller than 106.59(13)° in $(Me_3CCD_2)_3W{\equiv}CSiMe_3$,[20a] as a result of forming the adducts between **11** and $(Me_3SiCH_2)_3W{\equiv}CSiMe_3$.

The formation of the adduct **12** between **11** and $(Me_3SiCH_2)_3W{\equiv}CSiMe_3$ through the W=O→W bridge and the conjugation involving linear P=O→W=O→W≡C moiety are unusual.[48b] In addition, in this reaction of O_2 with

$(Me_3SiCH_2)_3W{\equiv}CSiMe_3$ in the presence of PMe_3, which is an alkyl analog of silyl alkylidyne $(Bu^tCH_2)_2W(\equiv CBu^t)(SiBu^tPh_2)$ (**2b**), we did not observe alkyl migration to the alkylidyne ligand. Instead we were surprised to find the formation of an oxo alkylidene complex **11**. The proposed byproduct "$Me_3SiCH{=}O$" in the reaction to form **11**, which is unstable above –25 °C,[52] was not observed (Scheme 3.14). It is not clear whether in the formation of **11** (in the presence of PMe_3), PMe_3 is oxidized by O_2 in a separate process. In similar reactions of d^n phosphine complexes with O_2, phosphine ligands either are oxidized to $O{=}PR_3$ [53a] or dissociate un-oxidized.[45] It is also known that oxo ligands in d^0 Cp^*ReO_3 transfer an O atom to PPh_3.[53b-c]

3.3. Conclusions

The reaction of O_2 with silyl alkylidyne **2b** $[(Bu^tCH_2)W(=CHBu^t)_2(SiBu^tPh_2)$ (**2a**) $\rightleftharpoons$ $(Bu^tCH_2)_2W(\equiv CBu^t)(SiBu^tPh_2)$ (**2b**)] is reported. A silyl migration product $(Bu^tCH_2)_2W(=O)[=C(Bu^t)(SiBu^tPh_2)]$ (**5**) was isolated and characterized. A siloxy analog of **2b**, $(Bu^tCH_2)_2W(\equiv CBu^t)(OSiBu^tPh_2)$ (**6**), was prepared and excluded as a possible intermediate in the formation of **5**. *Ab initio* calculations suggested a pathway involving silyl migration in **2b** to give a tungsten (IV) intermediate $(Bu^tCH_2)_2W{=}C(Bu^t)(SiBu^tPh_2)$ (**7**) *prior* to the reaction with O_2. The reaction of alkyl alkylidyne $(Me_3SiCH_2)_3W{\equiv}CSiMe_3$ with O_2 in the presence of PMe_3 was found to give an unusual alkylidene oxo complex $(Me_3SiCH_2)_2W(=O)(=CHSiMe_3)(O{=}PMe_3)$ (**11**). The crystal structure of **11** revealed that it formed an adduct with $(Me_3SiCH_2)_3W{\equiv}CSiMe_3$ to give

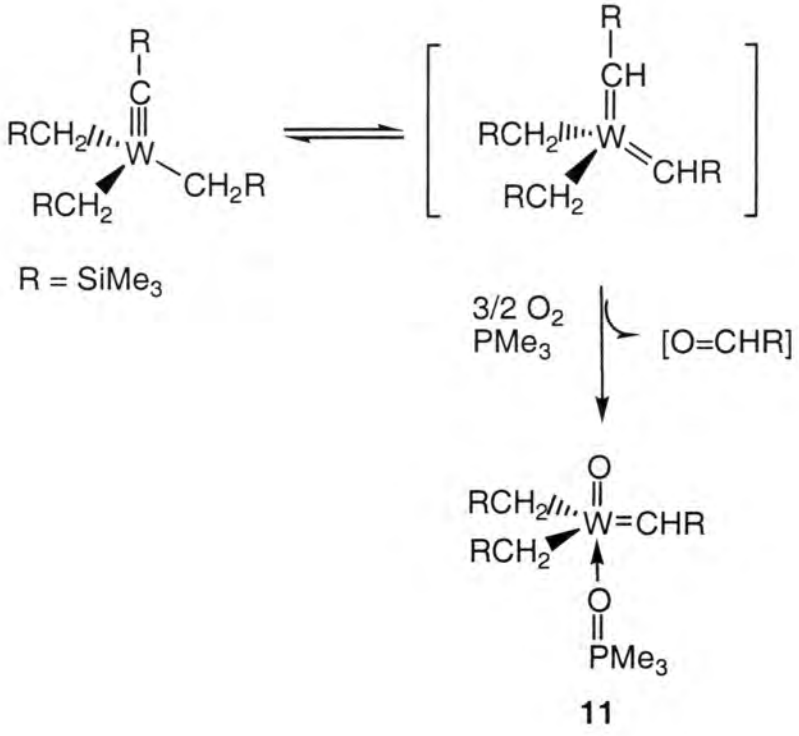

Scheme 3.14. Proposed reaction pathways to give **11**.

$(Me_3SiCH_2)_2W(=O)(=CHSiMe_3)(O=PMe_3)\bullet(Me_3SiCH_2)_3W{\equiv}CSiMe_3$ (**12**) in the solid.

3.4. Experiment Section

3.4.1. *General procedures*

All manipulations, unless noted, were performed under a dry nitrogen atmosphere with the use of either a drybox or standard Schlenk techniques. All solvents were purified by distillation from potassium/benzophenone ketyl. Benzene-d_6 and toluene-d_8 were dried over activated molecular sieves and stored under N_2. One-dimentional ^1H and ^{13}C NMR spectra, unless noted, were recorded at 23 °C on a Bruker AC-250 and referenced to solvents (residual protons in the ^1H spectra). ^1H-^{13}C heteronuclear correlation (HETCOR) and $^{29}Si\{^1H\}$ (DEPT) NMR experiments were conducted at 23 °C on a Bruker AMX-400 FT spectrometer. The $^{29}Si\{^1H\}$ (DEPT) NMR spectra were referenced to $SiMe_4$. $Li(THF)_3Si(SiMe_3)_3$,[24a] $Li(THF)_3SiBu^tPh_2$,[24b] $(Me_3SiCH_2)_3W{\equiv}CSiMe_3$,[32] and $(Bu^tCH_2)_3W{\equiv}CBu^t$ [23] were prepared by the literature procedures. HCl in Et_2O (1.0 M, Aldrich) was used as received. O_2 gas (99.6% purity) was dried by passing through a –78 °C trap, and was transferred quantitatively through a gas manifold. Elemental analyses were performed by Complete Analysis Laboratories Inc., E&R Microanalytical Division, Parsippany, New Jersey 07054-4909.

3.4.2. *Preparation of $(Bu^tCH_2)_2W(=O)[=C(Bu^t)(SiBu^tPh_2)]$ (5)*

Complex **2** (0.50 g, 0.79 mmol) was dissolved in 2.0 mL of benzene-d_6 in a J. Young NMR tube, and the solution was frozen at -60 °C. The tube was then evacuated, and O_2 (0.79 mmol) was introduced into the NMR tube. The solution was then warmed to room temperature. In 20 min, the color of the solution changed from brown to red orange. All the volatiles were then removed *in vacuo*. NMR spectra of the solid showed that ca. 32% (0.25 mmol) of **2** had reacted with O_2; 68% of **2** still remained in the reaction mixture. The solid was re-dissolved in pentane, and the solution was filtered. Slow cooling of the solution to -30 °C gave **3** as crystalline solid (isolated weight: 8.8 mg, 0.014 mmol, 5.6% yield based on the amount of **2** that had reacted with O_2). Data For **5**: ^{1}H NMR (benzene-d_6, 250.1 MHz) δ 7.79, 7.22-7.15 (m, 10H, SiBu^t*Ph*$_2$), 3.27 (d, 2H, C*H*$_a$H$_b$CMe$_3$, $^2J_{H\text{-}H}$ = 14.1 Hz), 1.31 (s, 9H, SiC*Me*$_3$Ph$_2$), 1.52 [s, 9H, =C(SiCMe$_3$Ph$_2$)C*Me*$_3$], 1.19 (s, 18H, CH$_a$H$_b$C*Me*$_3$), 0.34 (d, 2H, CH$_a$*H*$_b$CMe$_3$). ^{13}C{^{1}H} (benzene-d_6, 62.9 MHz) δ 269.65 (W=*C*), 138.56, 136.52, 130.68, 127.81 (SiBu^t*Ph*$_2$), 130.06 (*C*H$_2$CMe$_3$), 48.24 [=C(SiCMe$_3$Ph$_2$)*C*Me$_3$], 36.08 (*C*H$_2$CMe$_3$), 35.27 (CH$_2$*CMe*$_3$), 34.53 [=C(SiCMe$_3$Ph$_2$)C*Me*$_3$], 31.48 (SiC*Me*$_3$), 23.56 (Si*C*Me$_3$). Anal. Calcd. for $C_{31}H_{50}OSiW$: C, 57.22; H, 7.75. Found C, 56.93; H, 7.88.

3.4.3. *Preparation of $LiOSiBu^tPh_2$ (9)*

To a solution of hexamethylcyclotrisiloxane (0.31g, 0.52 mmol) in Et_2O at –78 °C was added dropwise Bu^{t}Li (0.19 mmol, 2.0 M in hexane, Aldrich). The

mixture was stirred at –78 °C and then allowed to slowly warm up to 0 °C in 1.5 h. All the volatiles were then removed *in vacuo* to give **9** as white solid powder (0.45 g, 0.0017 mmol, 89.5% yield). Data For **9**: ^{1}H NMR (benzene-d_6, 250.1 MHz) δ 7.71-7.55, 7.22-7.15 (m, 10H, C_6H_5), 0.97 (s, 9H, CMe_3). $^{13}C\{^{1}H\}$ (benzene-d_6, 62.9 MHz) δ 134.80, 129.08, 127.06, 126.67 (C_6H_5), 28.43 (CMe_3), 27.21 (CMe_3). Anal. Calcd. for $C_{16}H_{19}OSiLi$: C, 73.25; H, 7.30. Found C, 73.18; H, 7.29.

3.4.4. *Preparation of $(Bu^tCH_2)_2W(\equiv CBu^t)(OSiBu^tPh_2)$ (6)*

Anhydrous HCl (0.55 mmol, 1.0 M in Et_2O) was added dropwise with vigorous stirring over a 30 min period to $(Bu^tCH_2)_3W\equiv CBu^t$ (0.3465 g, 0.55 mmol) in Et_2O (20 mL) at –78 °C. The solution was warmed to 0 °C over a period of 2 h, and then stirred for 30 min. A solution of $LiOSiBu^tPh_2$ (0.1432 g, 0.55 mmol) in Et_2O (10 mL) was added at –30 °C. The mixture was warmed to room temperature and then stirred for 10 min. The volatiles were removed *in vacuo* and the residue was dissolved in a small amount of hexanes and cooled to –30 °C to give dark red powder (0.22 g, 0.34 mmol, 62.1% yield). Data For **6**: ^{1}H NMR (benzene-d_6, 250.1 MHz) δ 7.89, 7.25-7.15 (m, 10H, C_6H_5), 1.88 (d, 2H, $CH_aH_bCMe_3$, $^{2}J_{H\text{-}H}$ = 14.25 Hz), 1.21 (s, 9H, $SiCMe_3$), 1.19 (s, 9H, $\equiv CCMe_3$), 1.17 (s, 18H, $CH_aH_bCMe_3$), 0.27 (d, 2H, $CH_aH_bCMe_3$). $^{13}C\{^{1}H\}$ (benzene-d_6, 62.9 MHz) δ 314.13 ($W\equiv CCMe_3$), 135.44, 134.32, 129.94, 127.84 (C_6H_5), 131.21 (CH_2CMe_3), 52.01 ($\equiv CCMe_3$), 34.38 (CH_2CMe_3), 32.72 (CH_2CMe_3), 32.04 ($SiCMe_3$), 30.10 ($\equiv CCMe_3$), 20.19 ($SiCMe_3$). Anal. Calcd. for $C_{31}H_{50}OSiW$: C, 57.22; H, 7.75. Found C, 57.22; H, 8.06.

3.4.5. *Preparation of $(Me_3SiCH_2)_2W(=O)(=CHSiMe_3)(OPMe_3)$ (11) and $(Me_3SiCH_2)_2W(=O)(=CHSiMe_3)(O=PMe_3)$• $(Me_3SiCH_2)W{\equiv}CSiMe_3$ (12)*

Complex **2** (0.1182 g, 0.223 mmol) was dissolved in 1.0 mL of PMe_3 (9.67 mmol) in a J. Young NMR tube, and the solution was frozen at -60 °C. The tube was then evacuated, and O_2 (0.335 mmol) was introduced. The solution was then warmed to room temperature. In 20 min, the color of the solution changed from dark red to red orange. All volatiles were then removed *in vacuo*. NMR spectra of the solid showed that ca. 28% (0.062 mmol) of **2** had reacted with O_2 to yield **11**; 72% of the **2** still remained in the reaction mixture. The solid was re-dissolved in pentane, and the solution was filtered. Slow cooling of the solution to -30 °C gave **12** as a colorless crystalline solid (isolated weight: 2.9 mg, 0.0032 mmol, 4.8% yield based on the amount of **2** that had reacted with O_2). Data for **12**: ^{1}H NMR [benzene-d_6, 250.1 MHz; Only the spectra of $(Me_3SiCH_2)_2W(=O)(=CHSiMe_3)(O=PMe_3)$ (**11**) is reported here; The spectra of $(Me_3SiCH_2)W{\equiv}CSiMe_3$ are consistent with reported values[32]] δ 7.98 (s, 1H, C*H*SiMe$_3$), 1.03 (d, 9H, O=P*Me*$_3$, $^1J_{P\text{-}H}$ = 7.23 Hz), 0.37 (s, 4H, C*H*$_2$SiMe$_3$), 0.33 (s, 9H, =CHSi*Me*$_3$), 0.24 (s, 18H, CH$_2$Si*Me*$_3$). ^{13}C{^{1}H} (benzene-d_6, 62.9 MHz) δ 254.78 (W=*C*, $^1J_{C\text{-}H}$ = 98.33 Hz), 51.48 (*C*H$_2$SiMe$_3$), 19.37 (d, O=P*Me*$_3$, $^1J_{P\text{-}C}$ = 24.91 Hz), 2.99 (=CHSi*Me*$_3$), 1.80 (CH$_2$Si*Me*$_3$). Anal. Calcd. for $C_{31}H_{84}O_2Si_7PW$: C, 34.37; H, 7.72. Found C, 34.42; H, 7.86.

3.4.6. *General procedures for the studies of reactivities of 2 with PhN=O, PhN=NPh, pyridine oxide, $Me_3SiC{\equiv}CSiMe_3$, PhC≡CPh, PhC≡CH, and $Me_3SiC{\equiv}CH$*

The experiments were conducted in the drybox by mixing an equilibrium mixture **2a** ⇌ **2b** with excess PhN=O (PhN=NPh, pyridine oxide, $Me_3SiC{\equiv}CSiMe_3$, PhC≡CPh, PhC≡CH, or $Me_3SiC{\equiv}CH$) in benzene-d_6 in an aluminum weighing pan before the mixture was transferred to a J. Young NMR tube. After ca. 10 min at room temperature, the ^{1}H NMR spectra of the mixture were recorded every 20 min for a total of 2 h. The solution of the mixture was then kept in the J. Young NMR tube and stored in drybox. The ^{1}H NMR spectra of the mixture were then recorded daily for a week. Experiments at elevated temperatures were conducted similarly except that the solution in the J. Young NMR tube was heated in an oil bath at 40 °C before each NMR experiment at room temperature.

3.4.7. *X-ray crystal structure determination for 5 and 12*

The structures of **5** and **12** were determined at the University of Delaware (Professor Arnold L. Rheingold's group) and the University of Tennessee, respectively.

For the X-ray structure of **5,** a suitable crystal was selected and mounted in a thin-walled glass capillary under an inert atmosphere. The data were collected on a Siemens P4 diffractometer equipped with a SMART/CCD detector. The systematic absences in the diffraction data are consistent for space groups *Pna*2_1 and *Pnma*.

Even though the *E*-statistics suggested the centrosymmetric space group, the value of *Z* and the absence of a molecular mirror plane indicated the non-centrosymmetric space group. Both possibilities were explored, but the only solution in the non-centrosymmetric option yielded chemically reasonable and computationally stable results of refinement. The structures of **5** was solved using direct methods, completed by subsequent difference Fourier syntheses and refined by full-matrix least-squares procedures. Absorption corrections were not required because there was less than 10% variation in the integrated ψ-scan intensity data. All non-hydrogen atoms were refined with anisotropic displacement coefficients and hydrogen atoms were treated as idealized contributions. All software and sources of the scattering factors are contained in the SHELXTL (5.03) program library (G. Sheldrick, Siemens XRD, Madison, WI).

The X-ray crystal structure of **12** was determined on a Bruker AXS Smart 1000 X-ray diffractometer equipped with a CCD area detector and a graphite-monochromated Mo source (K_α radiation, 0.71073 Å) and fitted with an upgraded Nicolet LT-2 low temperature device. Suitable crystals were coated with paratone oil (Exxon) and mounted on a glass fiber under a stream of nitrogen at 173(2) K. The structure of **12** was solved by direct methods. All non-hydrogen atoms were anistropically refined. Empirical absorption correction for **12** was performed with SADABS.[35a] Global refinements for the unit cells and data reductions of structures **12** were performed under the Saint program (Version 6.02). All calculations were performed using SHELXTL (Version 5.1) proprietary software package.[35b]

CHAPTER 4

Synthesis and Characterization of

Bis(2,6-diisopropylphenylimido)molybdenum(VI) Complexes

4.1. Introduction

Transition metal imido chemistry has experienced significant growth in recent years.[54-57] The unique coordination mode of the metal-nitrogen double bonds in imido complexes has shown versatile reactivity.[54] Metal imido complexes have been used in metathesis of olefins[18g,42d,55a-d] and imines,[55e-o] and in C-H activation.[56] They have also been studied as mechanistic models for important industrial processes such as the Haber ammonia synthesis, reduction of nitriles, and ammoxidation of propylene, and for various enzymatic transformations.[57] Recently molecular approaches have been used to give Group 6 metal nitrides as diffusion barrier materials for Si-based microelectronic devices.[3b,58] In addition, M-Si-N ternary films have attracted much attention in recent years as excellent diffusion barriers in microelectronic devices.[3] We are interested in amido imido complexes $(R'N=)_xM(NR_2)_y$ and silyl imido complexes $(RN=)_xM(NR'_2)_y(SiR"_3)_z$ as potential precursors to metal nitride MN_n and M-Si-N ternary materials,[59] and we reported recently the first known Cp-free Group 5 silyl imido complexes.[60] Several molybdenum amido imido[61a-c] and silyl imido complexes[61d] are known. We report here the preparation and X-ray crystal structures of new molybdenum amido imido and silyl imido complexes $(ArN=)_2Mo(NMe_2)_2$ (**14**),

$(ArN=)_2Mo(NMe_2)[Si(SiMe_3)_3]$ (**15**), $(ArN=)_2MoCl[N(SiMe_3)_2]$ (**16**), and $(ArN=)_2Mo(NMe_2)[N(SiMe_3)_2]$ (**17**). In addition, a series of new, interesting secondary amine adducts $(ArN=)_2MoCl_2(HNMe_2)$ (**19**), $(ArN=)_2MoCl_2(HNEt_2)$ (**20**), $(ArN=)_2MoCl_2(HNMe_2)_2$ (**21**), and $(ArN=)_2MoCl_2(HNMe_2)\bullet(ArN=)_2MoCl_2(DME)$ (**22**) are described. The crystal structure of a previously reported amido imido complex $(ArN=)_2Mo(NHAr)_2$ (**18**)[61a-b] is also presented.

4.2. Results and Discussion

4.2.1. *Preparation and spectroscopic properties of $(ArN=)_2Mo(NMe_2)_2$ (14) $(ArN=)_2Mo(NMe_2)[Si(SiMe_3)_3]$ (15), $(ArN=)_2MoCl[N(SiMe_3)_2]$ (16), $(ArN=)_2Mo(NMe_2)[N(SiMe_3)_2]$ (17), $(ArN=)_2MoCl_2(HNMe_2)$ (19), $(ArN=)_2MoCl_2(HNEt_2)$ (20), $(ArN=)_2MoCl_2(HNMe_2)_2$ (21), and $(ArN=)_2MoCl_2(HNMe_2)\bullet(ArN=)_2MoCl_2(DME)$ (22)*

The diamido complex $(ArN=)_2Mo(NMe_2)_2$ (**14**) was prepared by the reaction of $(ArN=)_2MoCl_2(DME)$ (**13**) with 2 equiv of $LiNMe_2$ (Scheme 4.1). Reaction of $(ArN=)_2MoCl_2(DME)$ with one equiv of $LiNMe_2$ and one equiv of $Li(THF)_3Si(SiMe_3)_3$ was found to give silyl amido $(ArN=)_2Mo(NMe_2)[Si(SiMe_3)_3]$ (**15**) (Scheme 4.1). **15** is a silyl imido amido complex of molybdenum(VI), and its chloro and alkyl analogs have been reported by Tilley and coworkers.[61d] If $(ArN=)_2MoCl_2(DME)$ was treated with one equiv of $LiN(SiMe_3)_2$, $(ArN=)_2MoCl[N(SiMe_3)_2]$ (**16**) was obtained in 85% yield (Scheme 4.1). A further

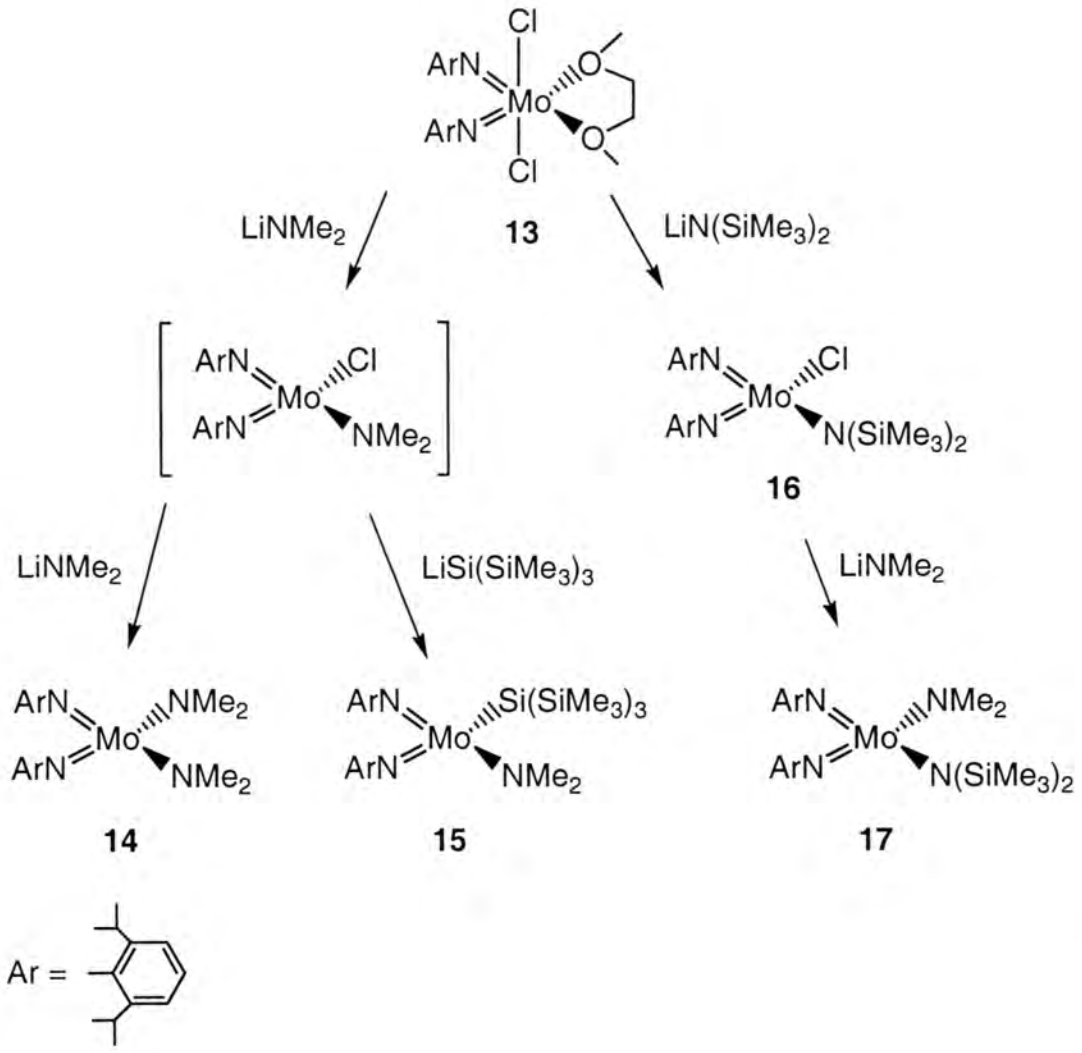

Scheme 4.1. Synthetic pathways to give complexes **14–17**.

reaction between **16** and one equiv of $LiNMe_2$ gave the diamido complex $(ArN=)_2Mo(NMe_2)[N(SiMe_3)_2]$ (**17**, Scheme 4.1). Similar procedures have been used to give other Mo silyl imido[61d] and amido imido complexes.[61a] The mixed amide **17** was also prepared by replacing the two chlorides in **13** with one equiv of $LiNMe_2$ followed by one equiv of $LiN(SiMe_3)_2$.

$(ArN=)_2Mo(NHAr)_2$ (**18**) was prepared by the reaction of $(ArN=)_2MoCl_2(DME)$ (**13**) with 2 equiv of LiNHAr in Et_2O in a procedure similar to that reported by Osborn, Wigley and their coworkers (Scheme 4.2).[61a-b] The reactions between $(ArN=)_2MoCl_2(DME)$ (**13**) and free amines ($HNMe_2$ and $HNEt_2$) led to formation of the amine adducts $(ArN=)_2MoCl_2(NHMe_2)$ (**19**), $(ArN=)_2MoCl_2(NHEt_2)$ (**20**), and $(ArN=)_2MoCl_2(NHMe_2)_2$ (**21**) (Scheme 4.3). In the reactions between $(ArN=)_2MoCl_2(DME)$ and $LiNMe_2$ or $LiNEt_2$ in Et_2O, **19**, **20** and **21** were sometimes obtained in low isolated yields presumably as a result of the presence of a small amount of moisture (Scheme 4.3). We have not been able to prepare "$(ArN=)_2MoCl(NMe_2)$" and "$(ArN=)_2MoCl(NEt_2)$" by these reactions. In an earlier report, a Schiff base adduct $[(ArN=)_2MoCl_2]\bullet[NH=C(C_6H_5)CH(SiMe_3)_2]$ was suspected as a result of di-hydrolysis of the 1-aza-allyl ligand $Li(THF)[N(SiMe_3)C(C_6H_5)=C(SiMe_3)_2]$ to $NH=C(C_6H_5)CH(SiMe_3)_2$, LiOH and Me_3SiOH, but was not confirmed.[62] Complex **23**, in which $(ArN=)_2MoCl_2(DME)$ (**13**) and $(ArN=)_2MoCl_2(NHMe_2)$ (**19**) coexisted in the solid state in a 1:1 molar ratio, was obtained in 3.06% isolated yield in the preparation of **19** with hydrolyzed

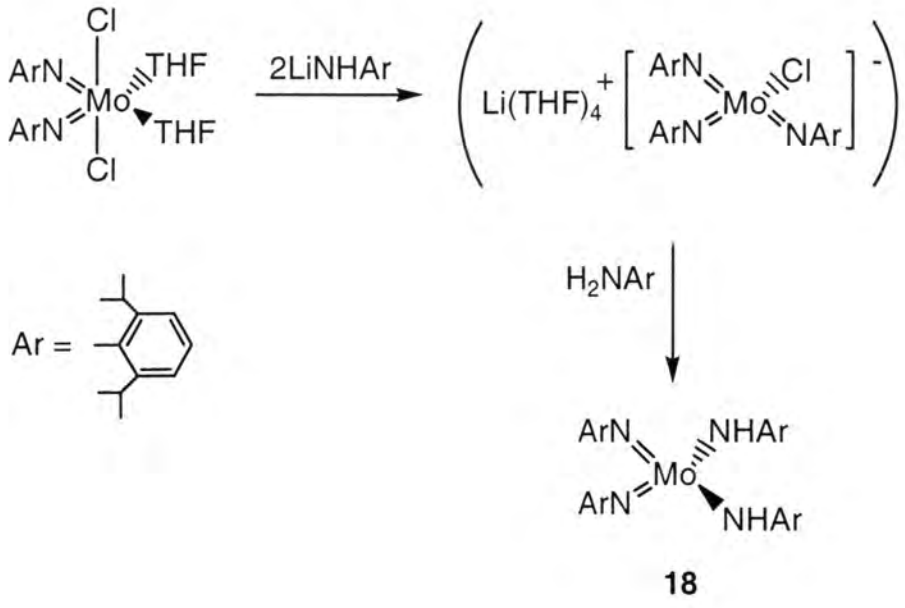

Scheme 4.2. Reported preparation of **18**.[61b] A trisimido complex was believed to be an intermediate in the formation of **18**.

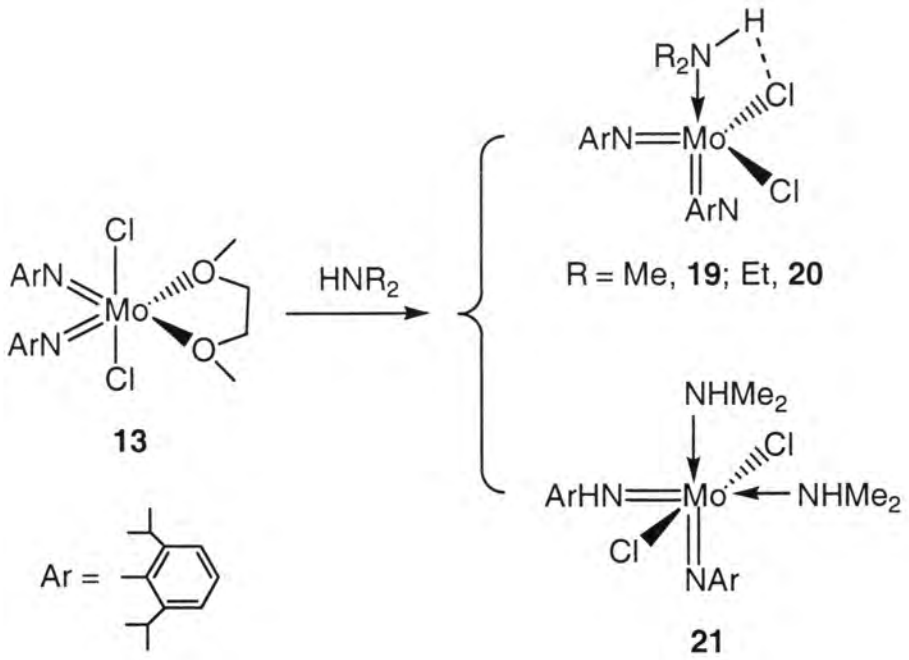

Scheme 4.3. Preparation of secondary amine adducts **19**-**21**.

$LiNMe_2$. Complexes **13-22** are air and moisture sensitive, but thermally stable both in solution and in the solid state at room temperature under an inert gas atmosphere.

Spectroscopic properties [^1H, $^{13}C\{^1H\}$ NMR] of the complexes are consistent with the structure assignments. The methyl resonances of the four *i*-Pr ortho substituents in the ArN= ligands in complexes **14-22** gave only one doublet in ^1H NMR spectra at room temperature, suggesting that both imido ligands in these complexes are equivalent in solution. ^1H NMR spectra confirmed that the ratios of the imido to amine are 2 : 1 in **19** and **20**, and 1 : 1 in **21**. Furthermore, the *H*-NR_2 protons in complexes **19**, **20**, and **21** showed broad single peaks in the ^1H NMR spectra. There was no sign of an α-H exchange process between the coordinate HNR_2 (R = Me, Et) and imido ligands. Such an exchange $[(RN=)_2(C_2X_4O_2)W(NH_2R) \rightleftharpoons (RHN)_2W(=NR)(C_2X_4O_2)$, R = Bu^t, X = CF_3, CH_3, Ph] was found in a homogeneous model for ammoxidation.[62]

4.2.2. *Reactivities of $(ArN=)_2Mo(NMe_2)_2$ (14), $(ArN=)_2Mo(NMe_2)[Si(SiMe_3)_3]$ (15), and $(ArN=)_2Mo(NMe_2)[N(SiMe_3)_2]$ (17)*

We studied the reactions of **14**, **15** and **17** with silanes to compare their reactivities with those of Group 4 and 5 amides toward silanes.[59] We did observe slow formation of aminosilanes [$H_2Si(NMe_2)Ph$ and $HSi(NMe_2)_2Ph$] in the reactions of **14**, **15** or **17** with H_3SiPh (Scheme 4.4). However, no metal-containing species was identified in these reactions, even at elevated temperatures (60 °C). In addition, no reaction of $H_2SiMePh$ or H_2SiPh_2 with **14**, **15** or **17** was observed.

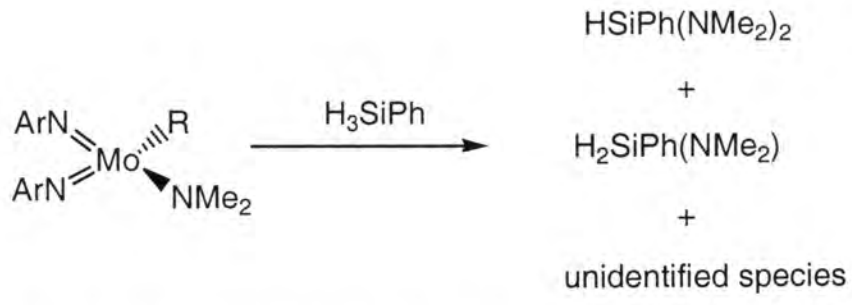

R = NMe_2, **14**; $Si(SiMe_3)_3$, **15**; $N(SiMe_3)_2$, **17**

Scheme 4.4. The reactions of **14, 15**, and **17** with H_3SiPh.

14, **15** and **17** might be relatively more inert towards the silanes than amides such as $Zr(NMe_2)_4$ [59a-c] and $Ta(NMe_2)_5$ [59d] for the following reasons. First, the bulky 2,6-diisopropylphenylimido groups in **14**, **15** and **17** make it difficult for the silane molecules to access the Mo metal center and the ligands. Second, all the Mo=N-C angles observed in **14**, **15** and **17** are linear, as discussed below, and it has been noted that bent imido ligands with formal M=N- double bonds were likely far more reactive than linear imido ligands with $M{\equiv}N-$ formal triple bonds.[54d]

4.2.3. *X-ray crystal structures of* $(ArN=)_2Mo(NMe_2)_2$ *(14)* $(ArN=)_2Mo(NMe_2)[Si(SiMe_3)_3]$ *(15)*, $(ArN=)_2MoCl[N(SiMe_3)_2]$ *(16),* $(ArN=)_2Mo(NMe_2)[N(SiMe_3)_2]$ *(17), and* $(ArN=)_2Mo(NHAr)_2$ *(18)*

The new complexes **14**-**17** in the current studies were characterized by X-ray crystallography. ORTEP views and packing diagrams of **14**-**17** are given in Figures 4.1-4.8. The crystallographic data are listed in Tables 4.1-4.8. The structures of **14**-

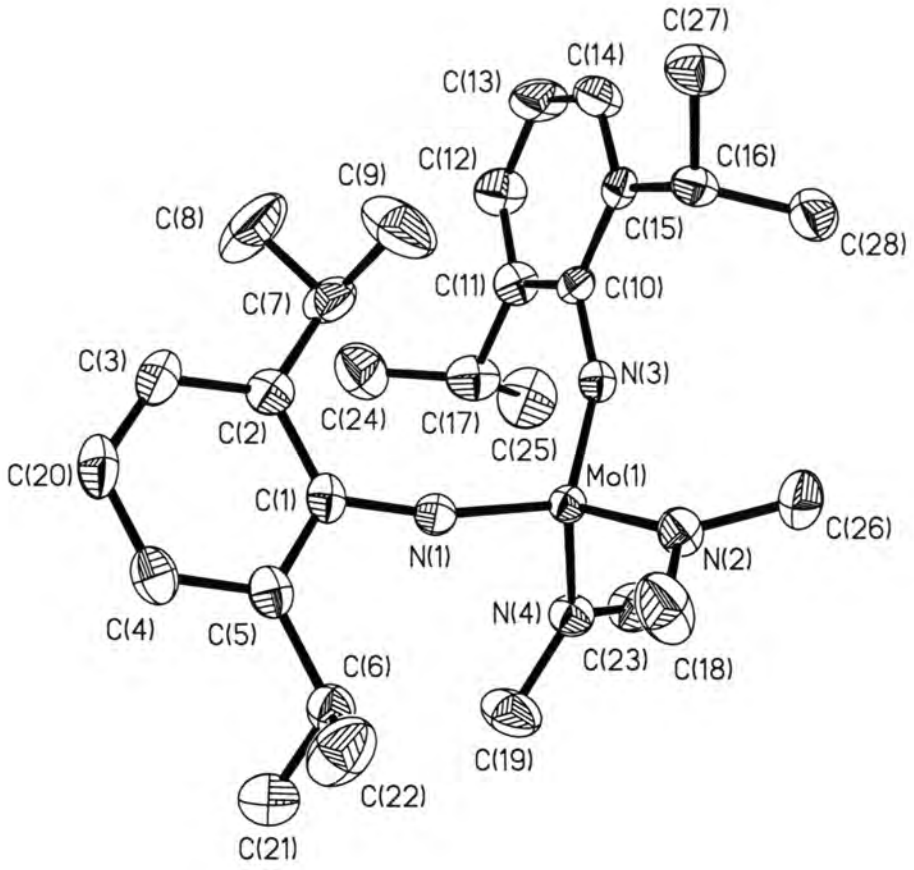

Figure 4.1. ORTEP view of **14** showing 50% probability thermal ellipsoids.

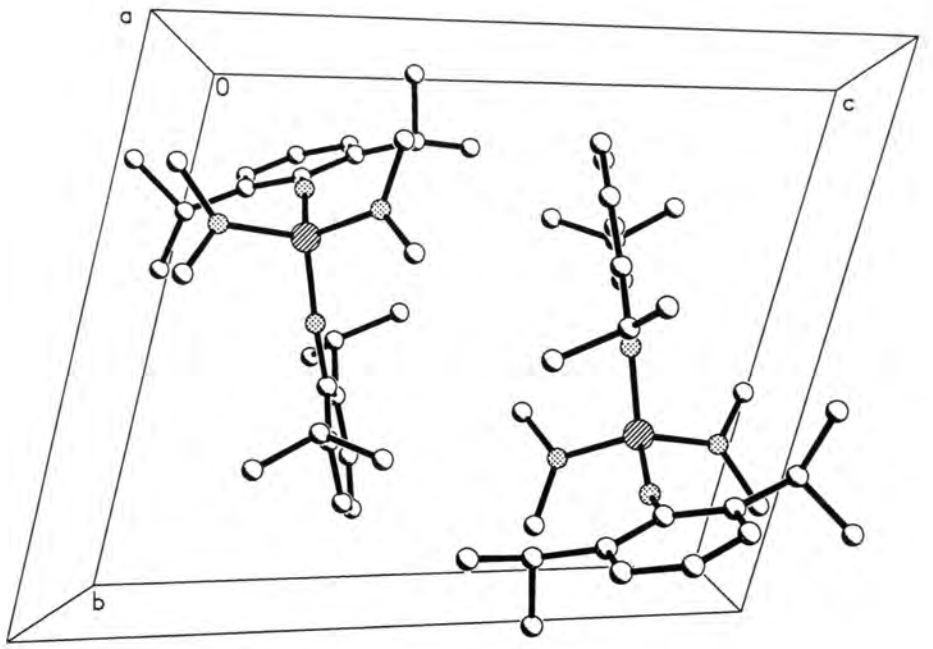

Figure 4.2. Packing diagram of **14**. View down the *a* axis.

Table 4.1. Crystal data and structure refinement for **14**

Identification code	**14**	
Empirical formula	$C_{28}H_{46}MoN_4$	
Formula weight	534.63	
Temperature	293(2) K	
Wavelength	0.71073 Å	
Crystal system	Triclinic	
Space group	$P\bar{1}$	
Unit cell dimensions	a = 9.956(2) Å	α = 99.62(3)°
	b = 11.456(2) Å	β =107.82(3)°
	c = 13.995(3) Å	γ = 104.03(3)°
Volume	1423.1(5) Å^3	
Z	2	
Density (calculated)	1.248 Mg/m^3	
Absorption coefficient	0.482 mm^{-1}	
F(000)	568	
Crystal size	0.31 × 0.29 × 0.12 mm^3	
θ range for data collection	1.90 to 22.55°	
Index ranges	$0 \le h \le 10$, $-12 \le k \le 11$, $-15 \le l \le 14$	
Reflections collected	4006	
Independent reflections	3748 [R(int) = 0.0308]	

Table 4.1. Continued

Completeness to $\theta = 22.55°$	100.0%
Absorption correction	Semi-empirical from equivalents
Max. and min. transmission	0.9444 and 0.8650
Refinement method	Full-matrix least-squares on F^2
Data / restraints / parameters	3748 / 0 / 310
Goodness-of-fit on F^2	1.055
Final R indices $[I > 2\sigma(I)]$[a]	$R1$ = 0.0372, $wR2$ = 0.0821
R indices (all data)	$R1$ = 0.0508, $wR2$ = 0.0883
Largest diff. peak and hole	0.299 and -0.304 e.Å^{-3}

[a] $wR2 = [\sum w(F_o^2 - F_c^2)^2 / \sum w(F_o^2)^2]^{1/2}$; $R = \sum \left| |F_o| - |F_c| \right| / \sum |F_o|$; $w = 1 / [\sigma^2(F_o^2) + (aP)^2 + bP]$; $P = [2F_c^2 + \mathrm{Max}(F_o^2, 0)] / 3$

Table 4.2. Selected bond lengths (Å) and angles (°) for **14**

Mo(1)-N(1)	1.765(3)	Mo(1)-N(3)	1.780(3)
Mo(1)-N(2)	1.947(3)	Mo(1)-N(4)	1.948(3)
N(1)-C(1)-C(5)	118.4(4)	N(1)-C(1)-C(2)	120.7(4)
N(1)-Mo(1)-N(3)	117.32(15)	N(1)-Mo(1)-N(2)	105.50(15)
N(3)-Mo(1)-N(2)	109.55(14)	N(1)-Mo(1)-N(4)	106.66(14)
N(3)-Mo(1)-N(4)	106.57(15)	N(2)-Mo(1)-N(4)	111.25(15)
C(1)-N(1)-Mo(1)	168.1(3)	C(26)-N(2)-C(18)	110.9(3)
C(26)-N(2)-Mo(1)	123.9(3)	C(18)-N(2)-Mo(1)	124.4(3)
C(10)-N(3)-Mo(1)	156.4(3)	C(19)-N(4)-C(23)	111.2(3)
C(19)-N(4)-Mo(1)	124.6(3)	C(23)-N(4)-Mo(1)	124.2(3)

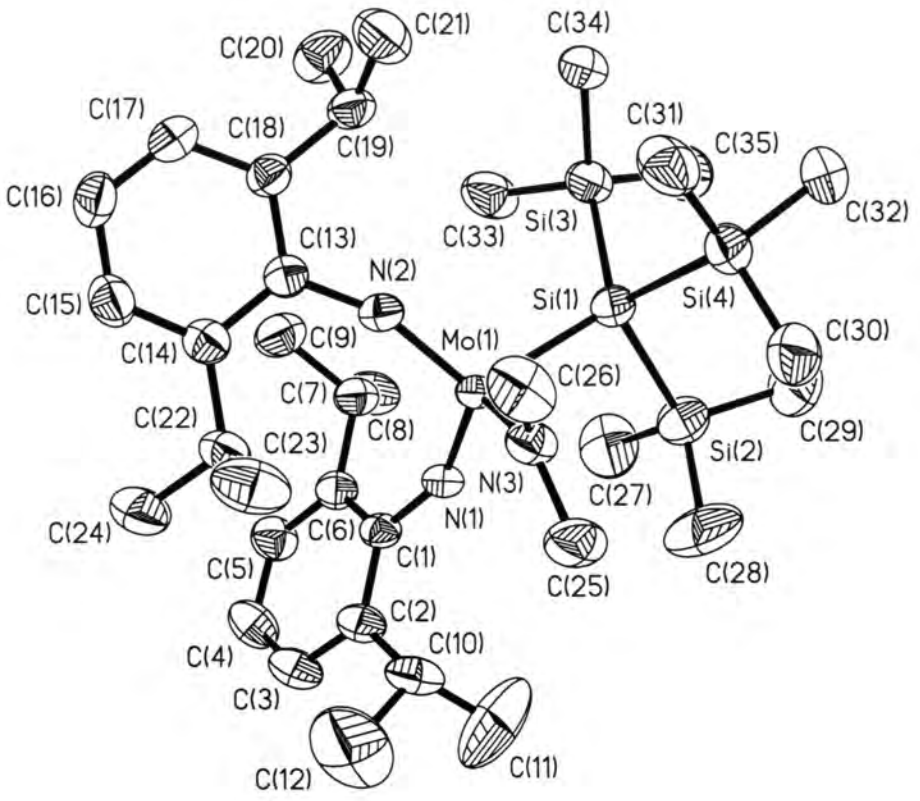

Figure 4.3. ORTEP view of **15** showing 50% probability thermal ellipsoids.

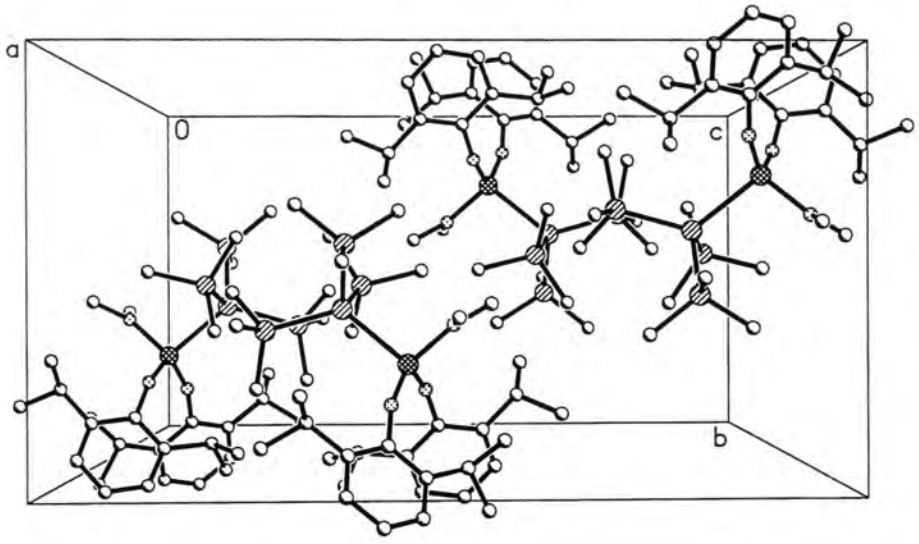

Figure 4.4. Packing diagram of **15**. View down the *a* axis.

Table 4.3. Crystal data and structure refinement for **15**

Identification code	**15**	
Empirical formula	$C_{35}H_{67}MoN_3Si_4$	
Formula weight	738.22	
Temperature	173(2) K	
Wavelength	0.71073 Å	
Crystal system	Monoclinic	
Space group	*C2/c*	
Unit cell dimensions	a = 35.776(5) Å	$\alpha = 90°$
	b = 11.5061(16) Å	$\beta = 93.240(4)°$
	c = 20.913(3) Å	$\gamma = 90°$
Volume	8595(2) $Å^3$	
Z	8	
Density (calculated)	1.141 Mg/m^3	
Absorption coefficient	0.441 mm^{-1}	
$F(000)$	3168	
Crystal size	0.42 × 0.31 × 0.15 mm^3	
θ range for data collection	1.14 to 26.38°	
Index ranges	$-44 \le h \le 44$, $-14 \le k \le 14$, $-26 \le l \le 26$	
Reflections collected	68384	

Table 4.3. Continued

Independent reflections	8795 [R(int) = 0.0402]
Completeness to $\theta = 26.38°$	99.9%
Absorption correction	Semi-empirical from equivalents
Max. and min. transmission	0.9367 and 0.8363
Refinement method	Full-matrix least-squares on F^2
Data / restraints / parameters	8795 / 0 / 407
Goodness-of-fit on F^2	1.089
Final R indices [$I > 2\sigma(I)$][a]	$R1$ = 0.0429, $wR2$ = 0.1120
R indices (all data)	$R1$ = 0.0585, $wR2$ = 0.1312
Largest diff. peak and hole	1.808 and -0.513 e.Å^{-3}

[a] $wR2 = [\sum w(F_o^2 - F_c^2)^2 / \sum w(F_o^2)^2]^{1/2}$; $R = \sum \big| |F_o| - |F_c| \big| / \sum |F_o|$;

$w = 1 / [\sigma^2(F_o^2) + (aP)^2 + bP]$; $P = [2F_c^2 + \mathrm{Max}(F_o^2, 0)] / 3$.

Table 4.4. Selected bond lengths (Å) and angles (°) for **15**

Mo(1)-N(1)	1.772(2)	Mo(1)-N(2)	1.760(2)
Mo(1)-Si(1)	2.6315(10)	Mo(1)-N(3)	1.948(3)
Si(1)-Si(4)	2.3605(14)	Si(1)-Si(3)	2.3589(15)
N(1)-C(1)-C(2)	118.6(3)	Si(1)-Si(2)	2.3616(14)
N(2)-Mo(1)-N(3)	108.00(12)	C(14)-C(22)-C(24)	113.4(3)
N(2)-Mo(1)-Si(1)	112.47(8)	N(2)-Mo(1)-N(1)	113.17(12)
N(3)-Mo(1)-Si(1)	104.18(9)	N(1)-Mo(1)-N(3)	113.19(11)
C(13)-N(2)-Mo(1)	161.3(2)	N(1)-Mo(1)-Si(1)	105.53(8)
C(26)-N(3)-Mo(1)	122.3(3)	C(1)-N(1)-Mo(1)	153.9(2)
Si(3)-Si(1)-Si(4)	104.04(5)	C(26)-N(3)-C(25)	111.4(3)
Si(4)-Si(1)-Si(2)	107.47(6)	C(25)-N(3)-Mo(1)	125.6(2)
Si(4)-Si(1)-Mo(1)	107.91(5)	Si(3)-Si(1)-Si(2)	108.52(6)
Si(2)-Si(1)-Mo(1)	105.32(5)	Si(3)-Si(1)-Mo(1)	122.83(5)

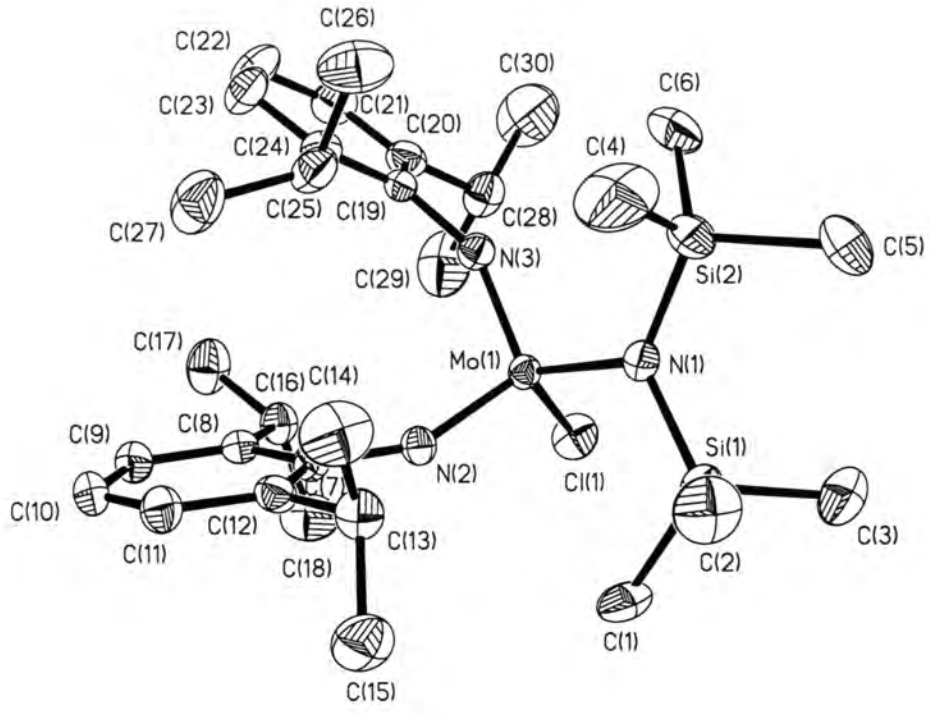

Figure 4.5. ORTEP view of **16** showing 50% probability thermal ellipsoids.

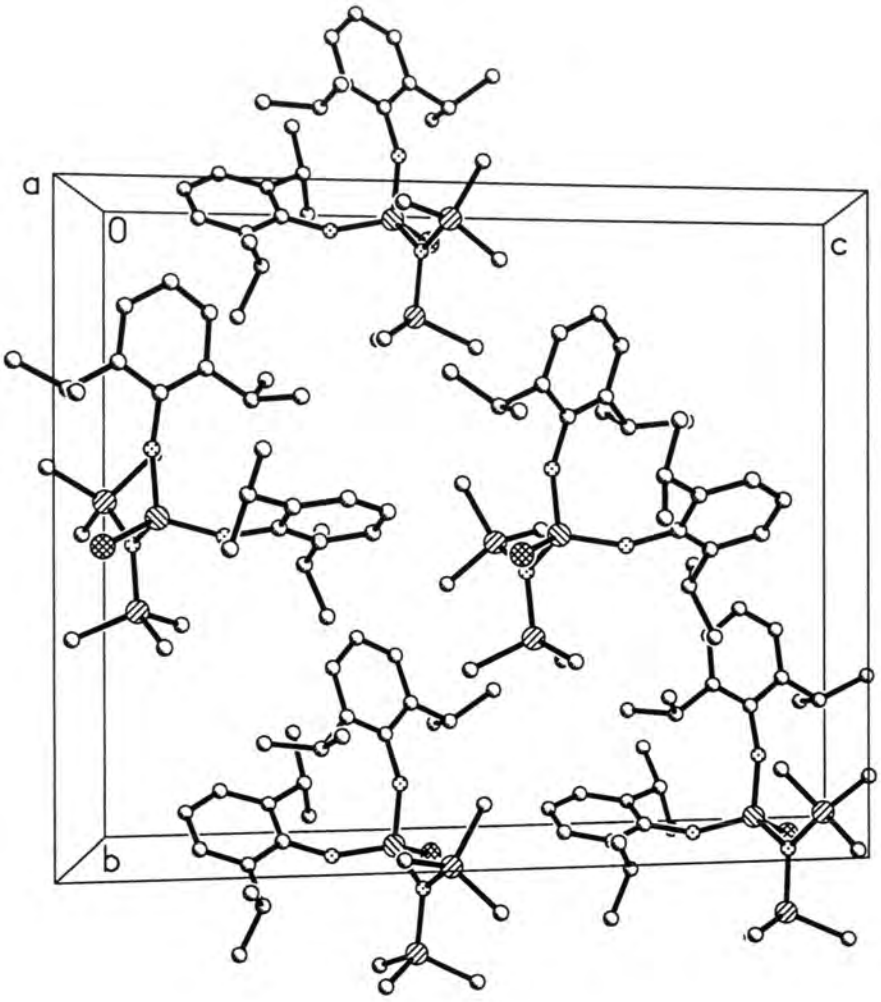

Figure 4.6. Packing diagram of **16**. View down the *a* axis.

Table 4.5. Crystal data and structure refinement for **16**

Identification code	**16**
Empirical formula	$C_{30}H_{52}ClMoN_3Si_2$
Formula weight	642.32
Temperature	173(2) K
Wavelength	0.71073 Å
Crystal system	Monoclinic
Space group	*P*2(1)
Unit cell dimensions	a = 10.1565(14) Å α = 90°
	b = 17.210(3) Å β = 104.015(3)°
	c = 20.936(3) Å γ = 90°
Volume	3550.6(9) Å^3
Z	4
Density (calculated)	1.202 Mg/m^3
Absorption coefficient	0.533 mm^{-1}
F(000)	1360
Crystal size	0.38 × 0.29 × 0.11 mm^3
θ range for data collection	1.00 to 26.39°
Index ranges	$-12 \le h \le 12$, $-21 \le k \le 21$, $-26 \le l \le 26$
Reflections collected	34891

Table 4.5. continued

Independent reflections	14392 [R(int) = 0.0618]
Completeness to $\theta = 26.39°$	99.7%
Absorption correction	Semi-empirical from equivalents
Max. and min. transmission	0.9437 and 0.8230
Refinement method	Full-matrix least-squares on F^2
Data / restraints / parameters	14392 / 1 / 695
Goodness-of-fit on F^2	1.037
Final R indices [$I > 2\sigma(I)$][a]	$R1$ = 0.0408, $wR2$ = 0.0894
R indices (all data)	$R1$ = 0.0607, $wR2$ = 0.1042
Absolute structure parameter	-0.04(3)
Largest diff. peak and hole	0.599 and -0.541 e.Å^{-3}

[a] $wR2 = [\sum w(F_o^2 - F_c^2)^2 / \sum w(F_o^2)^2]^{1/2}$; $R = \sum \left| |F_o| - |F_c| \right| / \sum |F_o|$;

$w = 1 / [\sigma^2(F_o^2) + (aP)^2 + bP]$; $P = [2F_c^2 + \mathrm{Max}(F_o^2, 0)] / 3$.

Table 4.6. Selected bond lengths (Å) and angles (°) for **16**

Cl(1)-Mo(1)	2.3353(11)	Cl(2)-Mo(2)	2.3283(12)
Mo(1)-N(3)	1.749(3)	Mo(1)-N(2)	1.757(4)
Mo(1)-N(1)	1.975(4)	Mo(2)-N(5)	1.740(4)
Mo(2)-N(4)	1.762(4)	Mo(2)-N(6)	1.972(4)
C(44)-C(52)-C(53)	113.0(4)	N(3)-Mo(1)-N(2)	105.58(17)
C(53)-C(52)-C(54)	109.5(5)	N(2)-Mo(1)-N(1)	112.82(16)
N(3)-Mo(1)-N(1)	109.15(16)	N(2)-Mo(1)-Cl(1)	108.65(11)
N(3)-Mo(1)-Cl(1)	107.52(12)	N(5)-Mo(2)-N(4)	109.99(17)
N(1)-Mo(1)-Cl(1)	112.75(11)	N(4)-Mo(2)-N(6)	112.68(16)
N(5)-Mo(2)-N(6)	107.65(16)	N(4)-Mo(2)-Cl(2)	107.09(11)
N(5)-Mo(2)-Cl(2)	106.11(12)	Si(2)-N(1)-Si(1)	120.0(2)
N(6)-Mo(2)-Cl(2)	113.12(12)	Si(1)-N(1)-Mo(1)	115.8(2)
Si(2)-N(1)-Mo(1)	124.2(2)	C(19)-N(3)-Mo(1)	153.3(3)
C(7)-N(2)-Mo(1)	154.3(3)	C(43)-N(5)-Mo(2)	165.5(3)
C(31)-N(4)-Mo(2)	155.6(3)	Si(3)-N(6)-Mo(2)	117.6(2)

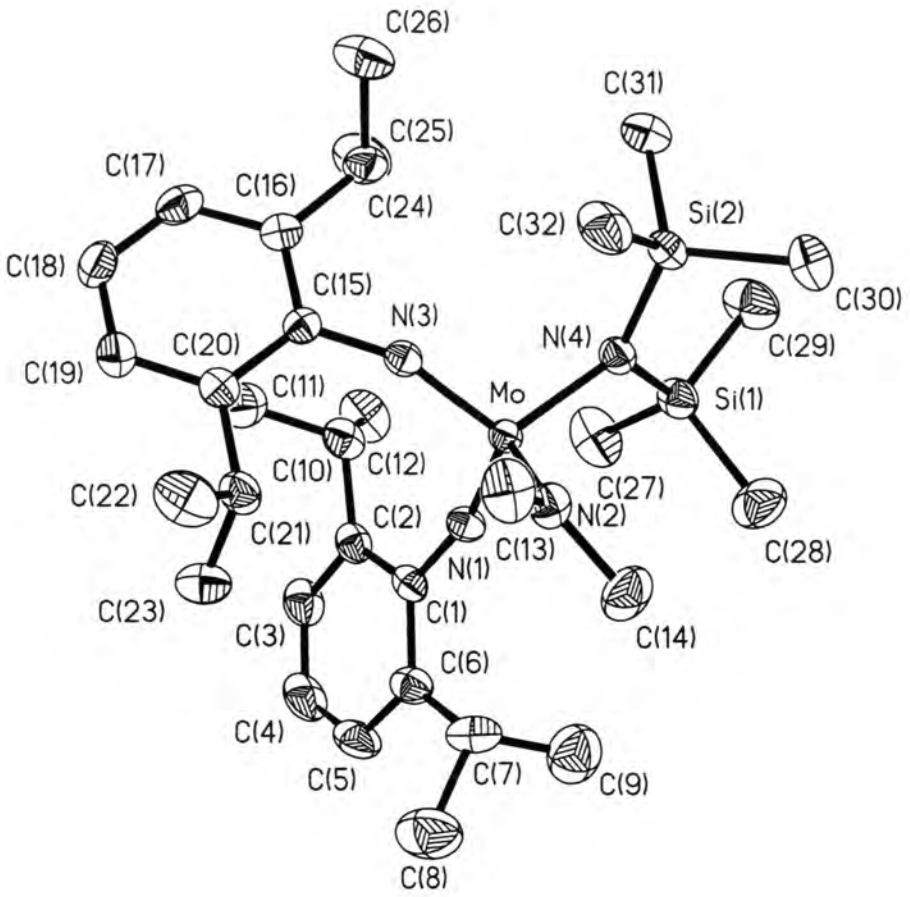

Figure 4.7. ORTEP view of **17** showing 50% probability thermal ellipsoids.

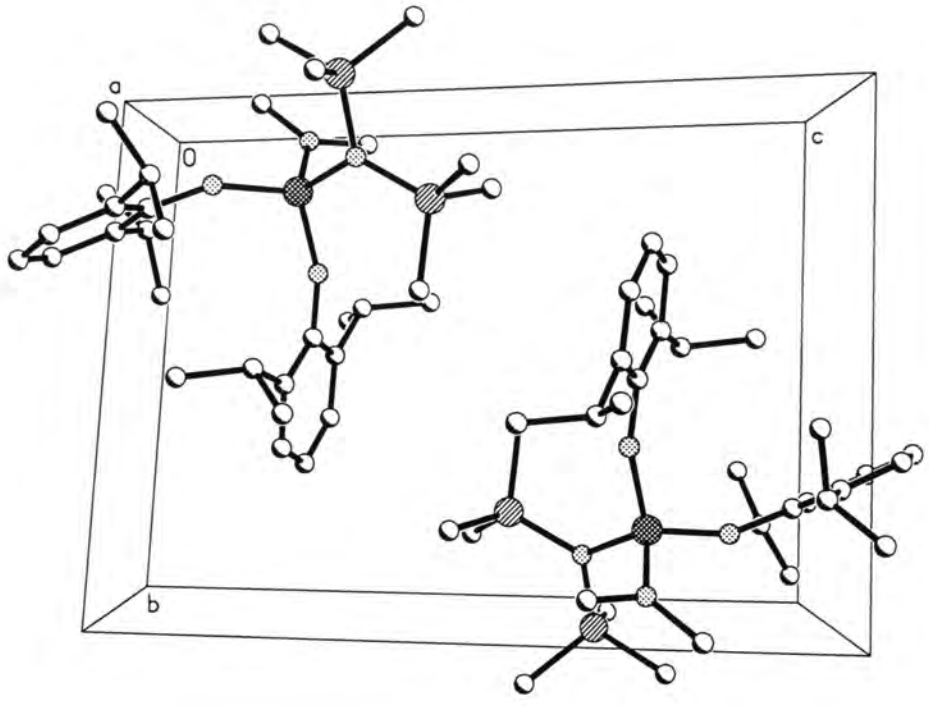

Figure 4.8. Packing diagram of **17**. View down the *a* axis.

Table 4.7. Crystal data and structure refinement for **17**

Identification code	**17**	
Empirical formula	$C_{32}H_{58}MoN_4Si_2$	
Formula weight	650.94	
Temperature	173(2) K	
Wavelength	0.71073 Å	
Crystal system	Triclinic	
Space group	$P\bar{1}$	
Unit cell dimensions	a = 10.3743(6) Å	α = 88.9340(10)°
	b = 11.5703(6) Å	β = 73.0650(10)°
	c = 16.1555(9) Å	γ = 76.8370(10)°
Volume	1804.00(17) Å^3	
Z	2	
Density (calculated)	1.198 Mg/m^3	
Absorption coefficient	0.455 mm^{-1}	
F(000)	696	
Crystal size	0.36 × 0.32 × 0.29 mm^3	
θ range for data collection	1.32 to 25.00°	
Index ranges	$-12 \le h \le 12$, $-13 \le k \le 13$, $-19 \le l \le 19$	
Reflections collected	26719	

Table 4.7. Continued

Independent reflections	6371 [R(int) = 0.0280]
Completeness to $\theta = 25.00°$	100.0%
Absorption correction	Semi-empirical from equivalents
Max. and min. transmission	0.8794 and 0.8534
Refinement method	Full-matrix least-squares on F^2
Data / restraints / parameters	6371 / 0 / 368
Goodness-of-fit on F^2	1.083
Final R indices [$I > 2\sigma(I)$][a]	$R1$ = 0.0227, $wR2$ = 0.0612
R indices (all data)	$R1$ = 0.0270, $wR2$ = 0.0630
Largest diff. peak and hole	0.651 and -0.206 e.Å^{-3}

[a] $wR2 = [\sum w(F_o^2 - F_c^2)^2 / \sum w(F_o^2)^2]^{1/2}$; $R = \sum \left| |F_o| - |F_c| \right| / \sum |F_o|$;

$w = 1 / [\sigma^2(F_o^2) + (aP)^2 + bP]$; $P = [2F_c^2 + \mathrm{Max}(F_o^2, 0)] / 3$.

Table 4.8. Selected bond lengths (Å) and angles (°) for **17**

Mo-N(3)	1.7562(14)	Mo-N(1)	1.7641(14)
Mo-N(2)	1.9529(15)	Mo-N(4)	2.0120(14)
N(3)-Mo-N(2)	104.17(7)	N(3)-Mo-N(1)	109.38(7)
N(3)-Mo-N(4)	112.02(6)	N(1)-Mo-N(2)	110.91(7)
N(2)-Mo-N(4)	111.00(6)	N(1)-Mo-N(4)	109.29(6)
C(14)-N(2)-Mo	120.62(13)	C(1)-N(1)-Mo	162.07(13)
Si(1)-N(4)-Mo	121.47(8)	C(13)-N(2)-Mo	127.95(13)
Si(2)-N(4)-Mo	117.73(8)	C(15)-N(3)-Mo	155.49(12)

17 show pseudo-tetrahedral geometry around Mo centers with interligand angles in the range of 104.18(7)–117.34(17)° (Tables 4.2, 4.4, 4.6, and 4.8, and Figures 4.1, 4.3, 4.5, and 4.7). The Mo=N bond lengths of 1.781(4)-1.749(3) Å and Mo-N bond lengths of 1.947(4)– 2.0115(15) Å in **14-17** are consistent with those in other Mo imido complexes.[61-64] The Mo-Si bond distance of 2.6314(10) Å in **14** is longer than Mo-Si bond lengths of 2.562(2) Å in $(ArN=)_2MoCl[Si(SiMe_3)_3]$,[61d] and 2.513(1) Å in $Cp_2Mo(SiMe_2Cl)H$,[28a] but is similar to those in $(ArN=)_2Mo(CH_2Bu^t)[Si(SiMe_3)_3]$ [2.608(9) Å][61d] and $Mo_2[Si(SiMe_3)_3]_2(NMe_2)_4$ [2.670(2) Å].[65]

It has been known that the imido moiety is a strong π-donor, and as such is generally found bound to metals in high oxidation states, which is usually with d^0–d^2 electronic configurations.[54d] There are two coordination geometries for M=N-R bonds - linear when the M=N-C angle is between 180 and 160°, and bent when this angle between 150 and 130° (Scheme 4.5).[54e] In the bent geometry, a lone electron

Scheme 4.5. Coordination modes for the imido moiety.[54d]

pair is localized on nitrogen (Mode **A**). In the linear geometry, this electron pair on N atom forms a dative bond between M and N atom (Mode **B**). If symmetry restrictions do not allow lone-pair donation, the imido ligand is then linear (Mode **C**) with a formal metal-nitrogen double bond. In the linear (**B**) and bent (**A**) modes, the imido ligand is formally a 4- and 2-electron donor ligand, respectively. When the M=N-C angles are between 160 and 150°, the term "semi-bent" has been used,[54d] although this range is now generally considered to be at the low end of thelinear coordination mode. The imido ligands in **14-17** are nearly linear with Mo=N-C angles from 153.4(3)° in **16** to 168.1(3)° in **14**, as in other Mo=NAr complexes.[64,66-67]

The crystal structure of $(ArN=)_2Mo(NHAr)_2$ (**18**) was reported earlier by Osborn and coworkers.[61a] Our structure of **18** gave similar bond angles and bond distances but a different unit cell in the same space group. An ORTEP view of the crystal structure of **18** in the current studies and a packing diagram are shown in Figures 4.9 and 4.10, respectively. Crystallographic data are given in Tables 4.9 and 4.10. To our knowledge, the structures of **18**, reported by Osborn and presented here, and **14** are the only known structural examples of d^0 bis(2,6-diisopropylphenylimido) bis(amido) Group 6 complexes.[54a,61a] The structure of **18** shows pseudo-tetrahedral geometry around the metal centers with interligand angles in the range of 104.19(15)–117.35(17)°. The Mo=N bond length in **18** [1.751(3) Å] is slightly shorter than those in **14** [1.767(4) Å, 1.781(4) Å]; **15** [1.760(2) Å, 1.772(2) Å] , **17** [1.7562(14) Å, 1.7641(14) Å] and longer than those in **16** [1.749(3)

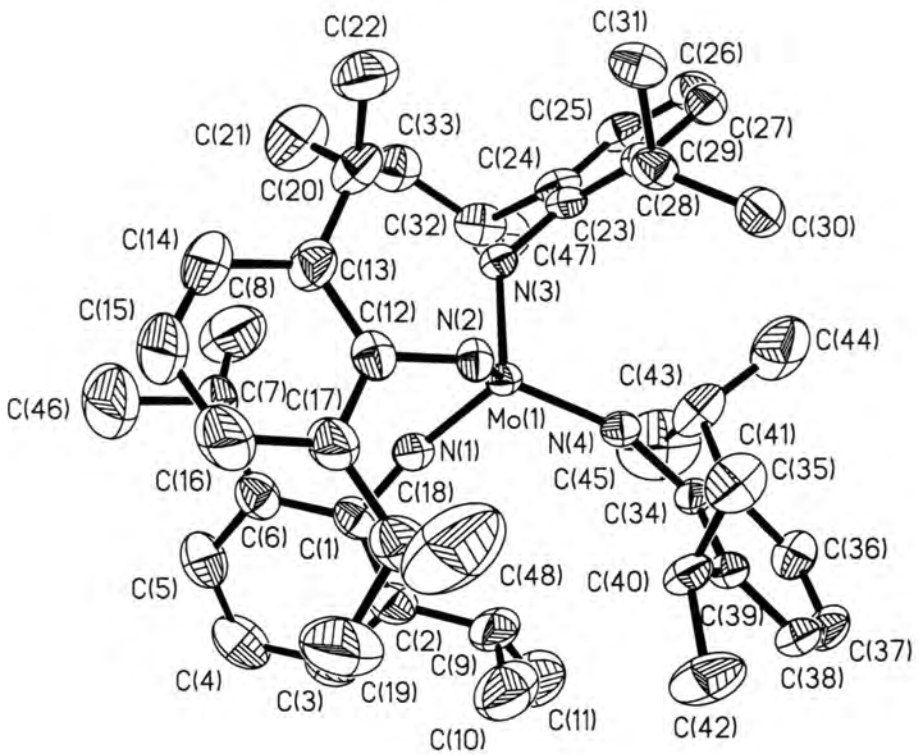

Figure 4.9. ORTEP view of **18** showing 50% probability thermal ellipsoid.

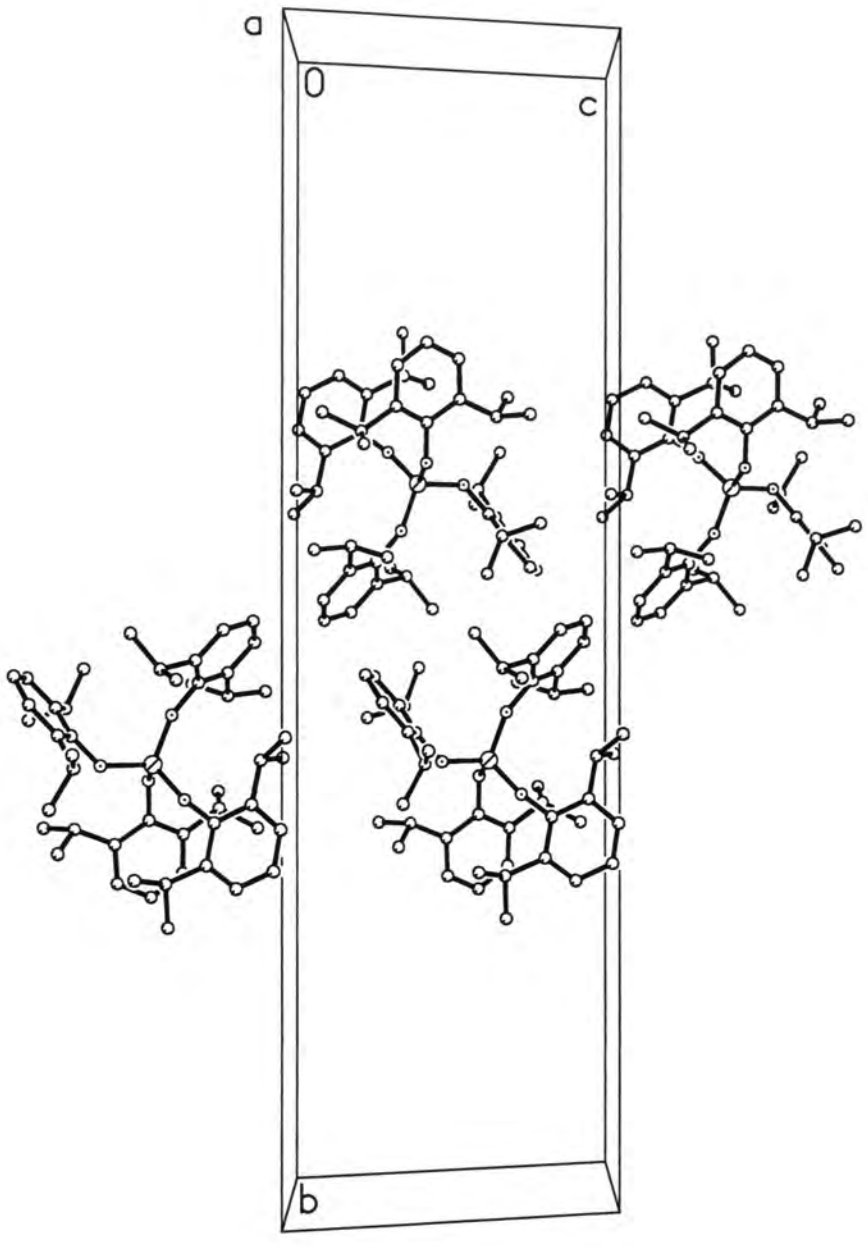

Figure 4.10. Packing diagram of **18**. View down the *a* axis.

Table 4.9. Crystal data and structure refinement for **18**

Identification code	**18**	
Empirical formula	$C_{48}H_{70}MoN_4$	
Formula weight	799.02	
Temperature	173(2) K	
Wavelength	0.71073 Å	
Crystal system	Monoclinic	
Space group	*P*2(1)/*c*	
Unit cell dimensions	a = 10.3327(16) Å	$\alpha = 90°$
	b = 39.554(6) Å	$\beta = 107.332(3)°$
	c = 11.7358(18) Å	$\gamma = 90°$
Volume	4578.7(12) $Å^3$	
Z	4	
Density (calculated)	1.159 Mg/m^3	
Absorption coefficient	0.321 mm^{-1}	
F(000)	1712	
Crystal size	0.30 × 0.21 × 0.05 mm^3	
θ range for data collection	1.03 to 26.41°	
Index ranges	$-12 \le h \le 12$, $-49 \le k \le 49$, $-14 \le l \le 14$	
Reflections collected	45223	
Independent reflections	9361 [*R*(int) = 0.1199]	

Table 4.9. Continued

Completeness to $\theta = 26.41°$	99.6%
Absorption correction	Semi-empirical from equivalents
Max. and min. transmission	0.9841 and 0.9099
Refinement method	Full-matrix least-squares on F^2
Data / restraints / parameters	9361 / 0 / 494
Goodness-of-fit on F^2	1.016
Final R indices $[I > 2\sigma(I)]^a$	$R1 = 0.0514$, $wR2 = 0.1205$
R indices (all data)	$R1 = 0.1057$, $wR2 = 0.1534$
Largest diff. peak and hole	0.536 and -0.639 e.Å^{-3}

[a] $wR2 = [\sum w(F_o^2 - F_c^2)^2 / \sum w(F_o^2)^2]^{1/2}$; $R = \sum \left| |F_o| - |F_c| \right| / \sum |F_o|$;

$w = 1 / [\sigma^2(F_o^2) + (aP)^2 + bP]$; $P = [2F_c^2 + \mathrm{Max}(F_o^2, 0)] / 3$.

Table 4.10. Selected bond lengths (Å) and angles (°) for **18**

Mo(1)-N(4)	1.751(3)	Mo(1)-N(1)	1.751(3)
Mo(1)-N(2)	1.980(3)	Mo(1)-N(3)	1.988(3)
N(4)-Mo(1)-N(2)	105.27(14)	N(4)-Mo(1)-N(1)	114.70(15)
N(4)-Mo(1)-N(3)	109.75(14)	N(1)-Mo(1)-N(2)	107.93(15)
N(2)-Mo(1)-N(3)	115.31(13)	N(1)-Mo(1)-N(3)	104.19(15)
C(12)-N(2)-Mo(1)	126.8(3)	C(1)-N(1)-Mo(1)	170.7(3)
C(34)-N(4)-Mo(1)	158.1(3)	C(23)-N(3)-Mo(1)	135.0(3)

Å, 1.757(4) Å]. Mo(VI)–amido length in **18** [1.980(3) Å, 1.989(3) Å] are longer than those in **14** [1.948(4) Å], **15** [1.948(4) Å], **16** [1.975(4)] Å, and **17** [1.9529 Å]. All imido groups in **18** are linear with Mo=N-C angles from 158.1(3) to 170.7(3)°.

4.2.4. *X-ray crystal structures of $(ArN=)_2MoCl_2(DME)$ (13), $(ArN=)_2MoCl_2(NHMe_2)$ (19), $(ArN=)_2MoCl_2(NHEt_2)$ (20), $(ArN=)_2MoCl_2(NHMe_2)_2$ (21), and $(ArN=)_2MoCl_2(NHMe_2)\bullet(ArN=)_2MoCl_2(DME)$ (22)*

The secondary amine adducts $(ArN=)_2MoCl_2(NHMe_2)$ (**19**), $(ArN=)_2MoCl_2(NHEt_2)$ (**20**), and $(ArN=)_2MoCl_2(NHMe_2)_2$ (**21**) are among the few reported structures of bis(imido) amine adducts of d^0 Group 6 metals, and, to our knowledge, no direct analogues have been reported.[64,68] ORTEP views of their crystal structures and packing diagrams are shown in Figures 4.11, 4.13, and 4.15, respectively. Packing diagrams are shown in Figures 4.12, 4.14, and 4.16, respectively. The crystallographic data are listed in Tables 4.11-4.16.

The Mo=N bond lengths in **19** [1.753(3) Å, 1.742(4) Å)], **21** [(1.756(2) Å], and **22** [1.759(4) Å, 1.753(4) Å] are within the range of the normal Mo=N bonds.[64] The structures of **19** and **20** are best described as distorted trigonal bipyramids. One imido and two chloride ligands occupy the equatorial positions, and the other apical linear imido ligand and the amine are in axial positions (Figures 4.11 and 4.13). There are large difference between the Mo=N-C angles of the two imido ligands in **19** and **20**. The axial imido ligands in both complexes [∠C(1)-N(1)-Mo(1) =

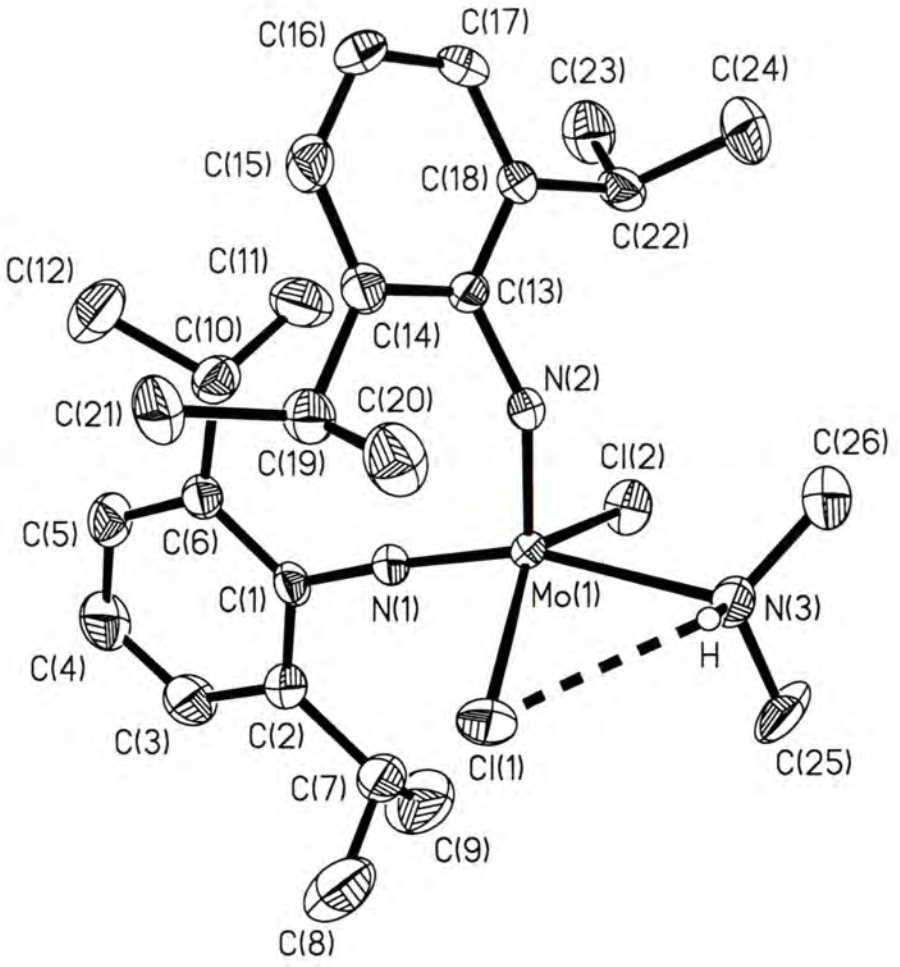

Figure 4.11. ORTEP view of **19** showing 50% probability thermal ellipsoids.

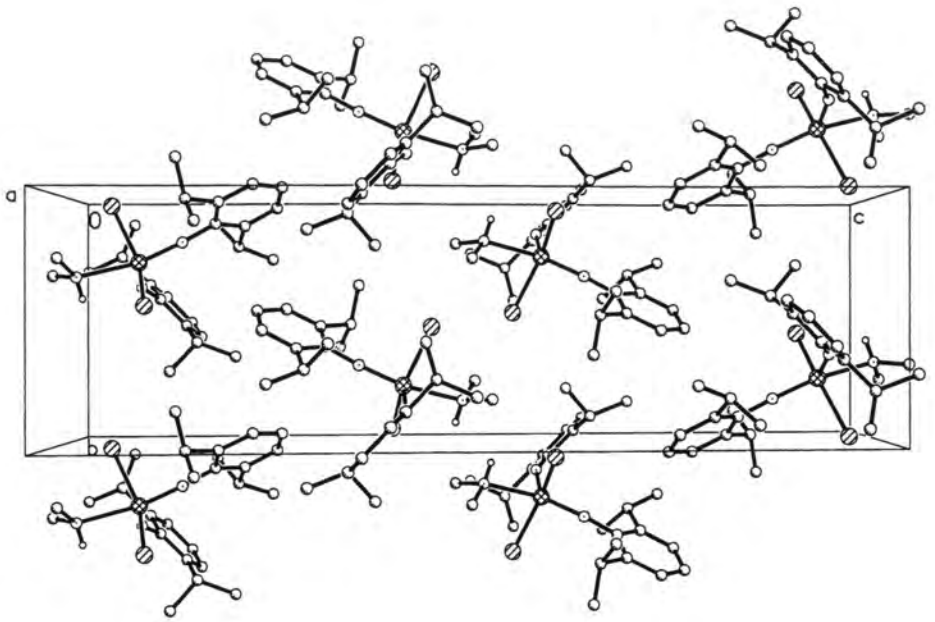

Figure 4.12. Packing diagram of **19**. View down the *a* axis.

Table 4.11. Crystal data and structure refinement for **19**

Identification code	**19**	
Empirical formula	$C_{26}H_{41}Cl_2MoN_3$	
Formula weight	562.46	
Temperature	173(2) K	
Wavelength	0.71073 Å	
Crystal system	Monoclinic	
Space group	*P*2(1)/*c*	
Unit cell dimensions	a = 10.6051(14) Å	$\alpha = 90°$
	b = 8.9182(12) Å	$\beta = 94.237(2)°$
	c = 29.677(4) Å	$\gamma = 90°$
Volume	2799.1(6) Å^3	
Z	4	
Density (calculated)	1.335 Mg/m^3	
Absorption coefficient	0.677 mm^{-1}	
F(000)	1176	
Crystal size	0.31 × 0.19 × 0.10 mm^3	
θ range for data collection	1.38 to 26.41°	
Index ranges	$-13 \le h \le 13$, $-11 \le k \le 10$, $-37 \le l \le 36$	
Reflections collected	26622	

Table 4.11. Continued

Independent reflections	5733 [R(int) = 0.0579]
Completeness to $\theta = 26.41°$	99.7%
Absorption correction	Semi-empirical from equivalents
Max. and min. transmission	0.9354 and 0.8175
Refinement method	Full-matrix least-squares on F^2
Data / restraints / parameters	5733 / 0 / 303
Goodness-of-fit on F^2	1.130
Final R indices [$I > 2\sigma(I)$][a]	$R1$ = 0.0354, $wR2$ = 0.0815
R indices (all data)	$R1$ = 0.0666, $wR2$ = 0.1093
Largest diff. peak and hole	0.450 and -0.448 e.Å^{-3}

[a] $wR^2 = [\sum w(F_o^2 - F_c^2)^2 / \sum w(F_o^2)^2]^{1/2}$; $R = \sum \big| |F_o| - |F_c| \big| / \sum |F_o|$;

$w = 1 / [\sigma^2(F_o^2) + (aP)^2 + bP]$; $P = [2F_c^2 + \mathrm{Max}(F_o^2, 0)] / 3$.

Table 4.12. Selected bond lengths (Å) and angles (°) for **19**

Cl(1)-Mo(1)	2.3837(10)	Cl(2)-Mo(1)	2.3564(10)
Mo(1)-N(2)	1.742(3)	Mo(1)-N(1)	1.753(3)
Mo(1)-N(3)	2.320(3)	N(2)-Mo(1)-N(3)	93.63(12)
N(2)-Mo(1)-N(1)	108.51(13)	N(2)-Mo(1)-Cl(2)	105.93(9)
N(1)-Mo(1)-N(3)	157.86(12)	N(3)-Mo(1)-Cl(2)	80.96(9)
N(1)-Mo(1)-Cl(2)	92.65(11)	N(1)-Mo(1)-Cl(1)	94.13(10)
N(2)-Mo(1)-Cl(1)	107.10(9)	Cl(2)-Mo(1)-Cl(1)	142.06(4)
N(3)-Mo(1)-Cl(1)	78.85(9)	C(13)-N(2)-Mo(1)	152.6(2)
C(1)-N(1)-Mo(1)	174.4(3)	C(26)-N(3)-Mo(1)	116.3(2)
C(25)-N(3)-Mo(1)	115.1(3)		

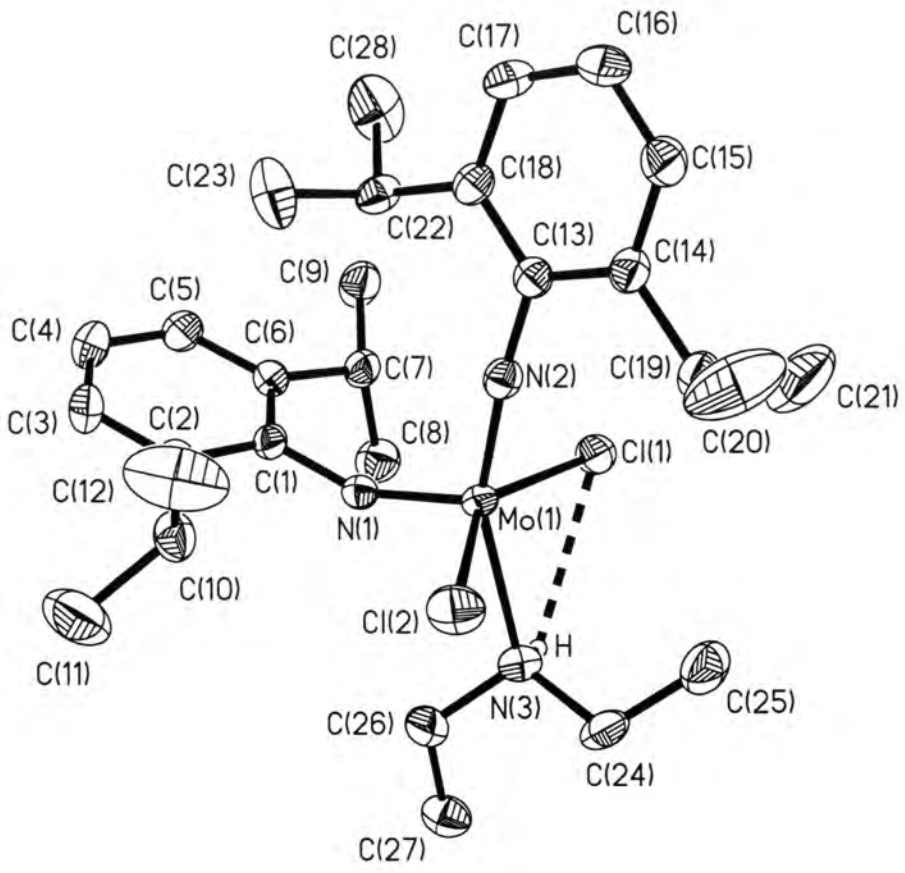

Figure 4.13. ORTEP of **20** showing 50% probability thermal ellipsoids.

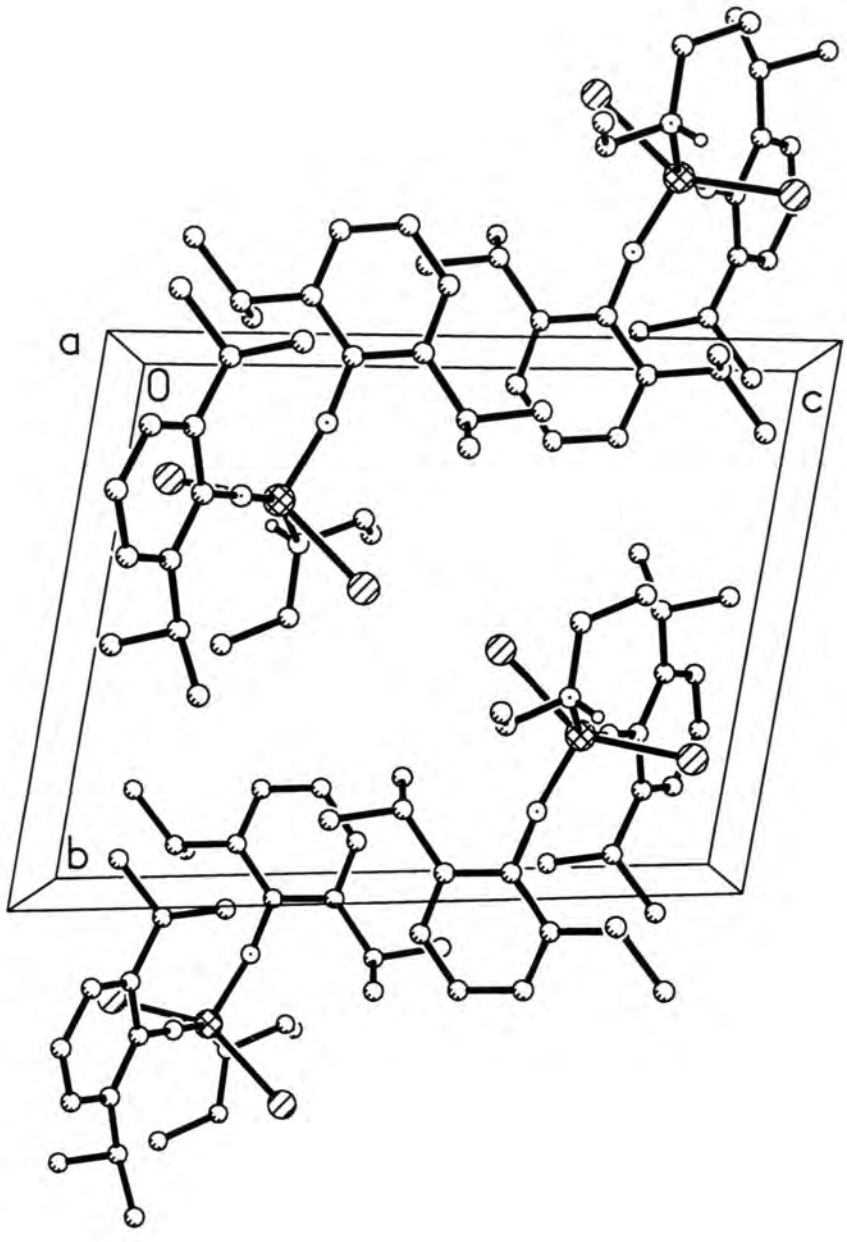

Figure 4.14. Packing diagram of **20**. View down the *a* axis.

Table 4.13. Crystal data and structure refinement for **20**

Identification code	**20**	
Empirical formula	$C_{28}H_{45}Cl_2MoN_3$	
Formula weight	590.51	
Temperature	173(2) K	
Wavelength	0.71073 Å	
Crystal system	Triclinic	
Space group	$P\bar{1}$	
Unit cell dimensions	a = 9.702(2) Å	α = 99.327(4)°
	b = 11.132(3) Å	β = 105.249(4)°
	c = 14.721(3) Å	γ = 92.024(4)°
Volume	1508.6(6) Å^3	
Z	2	
Density (calculated)	1.300 Mg/m^3	
Absorption coefficient	0.632 mm^{-1}	
F(000)	620	
Crystal size	0.29 × 0.18 × 0.09 mm^3	
θ range for data collection	1.46 to 26.43°	
Index ranges	$-12 \le h \le 12$, $-13 \le k \le 13$, $-18 \le l \le 18$	
Reflections collected	15030	

Table 4.13. Continued

Independent reflections	6142 [R(int) = 0.0528]
Completeness to $\theta = 26.43°$	99.0%
Absorption correction	Semi-empirical from equivalents
Max. and min. transmission	0.9453 and 0.8380
Refinement method	Full-matrix least-squares on F^2
Data / restraints / parameters	6142 / 0 / 321
Goodness-of-fit on F^2	1.037
Final R indices [$I>2\sigma(I)$][a]	$R1$ = 0.0391, $wR2$ = 0.0910
R indices (all data)	$R1$ = 0.0543, $wR2$ = 0.0994
Largest diff. peak and hole	0.975 and -0.578 e.Å^{-3}

[a] $wR2 = [\sum w(F_o^2 - F_c^2)^2 / \sum w(F_o^2)^2]^{1/2}$; $R = \sum \left| |F_o| - |F_c| \right| / \sum |F_o|$;

$w = 1 / [\sigma^2(F_o^2) + (aP)^2 + bP]$; $P = [2F_c^2 + \mathrm{Max}(F_o^2,0)] / 3$.

Table 4.14. Selected bond lengths (Å) and angles (°) for **20**

Cl(1)-Mo(1)	2.3696(9)	Cl(2)-Mo(1)	2.3622(9)
Mo(1)-N(1)	1.756(2)	Mo(1)-N(2)	1.756(2)
Mo(1)-N(3)	2.358(3)	N(1)-Mo(1)-N(3)	94.96(10)
N(1)-Mo(1)-N(2)	107.66(11)	N(1)-Mo(1)-Cl(2)	106.34(8)
N(2)-Mo(1)-N(3)	157.11(10)	N(3)-Mo(1)-Cl(2)	81.26(8)
N(2)-Mo(1)-Cl(2)	95.30(8)	N(2)-Mo(1)-Cl(1)	91.32(8)
N(1)-Mo(1)-Cl(1)	104.62(8)	Cl(2)-Mo(1)-Cl(1)	144.58(3)
N(3)-Mo(1)-Cl(1)	79.34(8)	C(13)-N(2)-Mo(1)	173.4(2)
C(1)-N(1)-Mo(1)	152.5(2)	C(24)-N(3)-Mo(1)	118.3(2)
C(26)-N(3)-Mo(1)	112.9(2)		

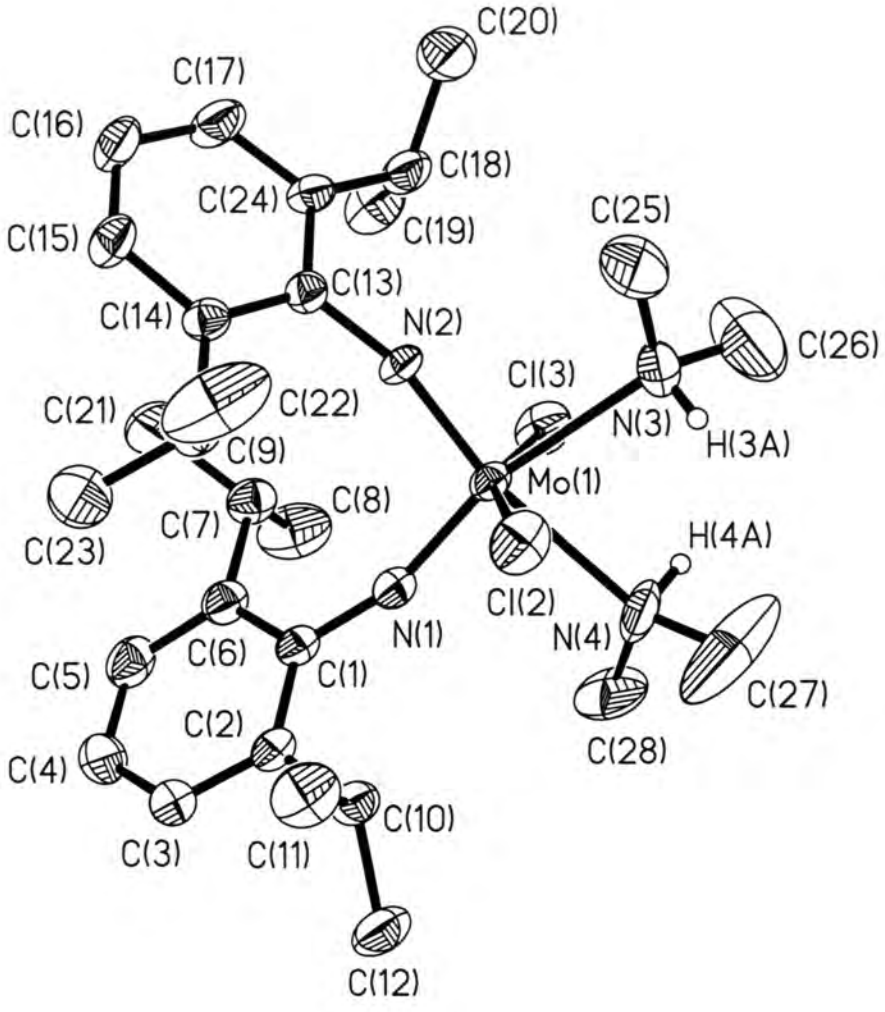

Figure 4.15. ORTEP view of **21** showing 50% probability thermal ellipsoids.

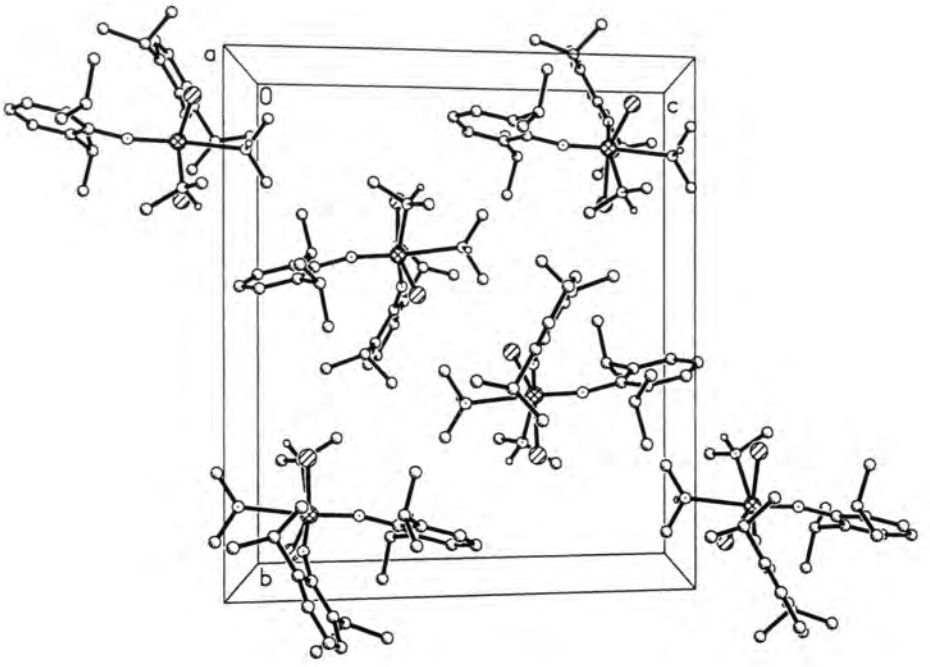

Figure 4.16. Packing diagram of **21**. View down the *a* axis.

Table 4.15. Crystal data and structure refinement for **21**

Identification code	**21**	
Empirical formula	$C_{28}H_{48}Cl_2MoN_4$	
Formula weight	607.54	
Temperature	173(2) K	
Wavelength	0.71073 Å	
Crystal system	Monoclinic	
Space group	*P*2(1)/*c*	
Unit cell dimensions	a = 11.185(3) Å	$\alpha = 90°$
	b = 17.932(5) Å	$\beta = 102.515(5)°$
	c = 15.961(4) Å	$\gamma = 90°$
Volume	3125.3(14) $Å^3$	
Z	4	
Density (calculated)	1.291 Mg/m^3	
Absorption coefficient	0.613 mm^{-1}	
F(000)	1280	
Crystal size	0.39 × 0.22 × 0.11 mm^3	
θ range for data collection	1.86 to 23.26°	
Index ranges	$-12 \le h \le 12$, $-19 \le k \le 19$, $-17 \le l \le 17$	
Reflections collected	22572	

Table 4.15. Continued

Independent reflections	4491 [R(int) = 0.0574]
Completeness to $\theta = 23.26°$	99.9%
Absorption correction	Semi-empirical from equivalents
Max. and min. transmission	0.9357 and 0.7961
Refinement method	Full-matrix least-squares on F^2
Data / restraints / parameters	4491 / 0 / 334
Goodness-of-fit on F^2	1.120
Final R indices $[I > 2\sigma(I)]$[a]	$R1$ = 0.0391, $wR2$ = 0.0960
R indices (all data)	$R1$ = 0.0664, $wR2$ = 0.1218
Largest diff. peak and hole	0.928 and -0.831 e.Å^{-3}

[a] $wR2 = [\sum w(F_o^2 - F_c^2)^2 / \sum w(F_o^2)^2]^{1/2}$; $R = \sum \big| |F_o| - |F_c| \big| / \sum |F_o|$;

$w = 1 / [\sigma^2(F_o^2) + (aP)^2 + bP]$; $P = [2F_c^2 + \mathrm{Max}(F_o^2, 0)] / 3$.

Table 4.16. Selected bond lengths (Å) and angles (°) for **21**

Cl(2)-Mo(1)	2.4088(14)	Cl(3)-Mo(1)	2.4034(15)
Mo(1)-N(2)	1.753(4)	Mo(1)-N(1)	1.759(4)
Mo(1)-N(4)	2.411(5)	Mo(1)-N(3)	2.444(5)
N(2)-Mo(1)-Cl(3)	95.74(13)	N(2)-Mo(1)-N(1)	102.11(18)
N(2)-Mo(1)-Cl(2)	98.27(13)	N(1)-Mo(1)-Cl(3)	99.56(13)
Cl(3)-Mo(1)-Cl(2)	156.40(5)	N(1)-Mo(1)-Cl(2)	95.96(13)
N(1)-Mo(1)-N(4)	88.99(18)	N(2)-Mo(1)-N(4)	168.26(19)
Cl(2)-Mo(1)-N(4)	84.16(16)	Cl(3)-Mo(1)-N(4)	78.47(17)
N(1)-Mo(1)-N(3)	166.01(18)	N(2)-Mo(1)-N(3)	91.05(17)
Cl(2)-Mo(1)-N(3)	77.25(16)	Cl(3)-Mo(1)-N(3)	83.61(16)
C(1)-N(1)-Mo(1)	162.4(3)	N(4)-Mo(1)-N(3)	78.23(17)
C(26)-N(3)-C(25)	108.4(6)	C(13)-N(2)-Mo(1)	163.9(3)
C(25)-N(3)-Mo(1)	113.3(4)	C(26)-N(3)-Mo(1)	127.6(5)
C(27)-N(4)-Mo(1)	127.9(5)	C(27)-N(4)-C(28)	111.2(6)
C(28)-N(4)-Mo(1)	114.8(4)		

174.4(3)° in **19** and ∠C(13)-N(2)-Mo(1) = 173.4(2)° in **20**] are more "linear" than the equatorial imido ligands [∠C(13)-N(2)-Mo(1) = 152.6(3)° in **19** and ∠C(1)-N(1)-Mo(1) = 152.5(2)° in **20**]. A similar significant bending of the equatorial imido ligands in the trigonal bipyramidal bis(imido) Mo complexes has been reported to be most likely the result of an electronic effect rather than crystal packing in such five coordinate trigonal bipyramidal systems.[64d,68a] In addition the C-N bond lengths in the axial imido ligands are shorter [N(1)-C(1) = 1.383(4) Å in **19** and N(2)-C(13) = 1.381(4) Å in **20**] than those of the equatorial imido ligands [N(2)-C(13) = 1.408(4) Å in **19** and N(1)-C(11) = 1.394(4) Å in **20**]. While the geometry around Mo in **21** is distorted octahedral (Figure 4.15) with two chloride ligands *trans* to each other, the two imido groups *cis* to each other and *trans* to the two *cis* amines, are approaching linear [∠C(1)-N(1)-Mo(1) = 162.4(3)° and ∠C(13)-N(2)-Mo(1) = 163.9(3)°] (Table 4.16). The Mo←NHR_2 dative bond lengths between Mo(VI) and N in amine [2.320(4) Å in **19**, 2.359(3) Å in **20**, and 2.411(5) Å, 2.444(5) Å in **21**] are longer than those reported in an α-aminoenolate Mo complex $Mo(=NAr)_2Cl\{\eta^2\text{-}CH(NMe_2)CO_2Et\}$ [2.198(4) Å][64a] and a dimeric structure of $[W(NBu^t)_2(NH_2But)Cl(\mu\text{-}Cl)]_2$ [2.202(15) Å],[68b] but are close to those in two pyridine adducts: $Mo(=NAr)_2Cl_2(Py)_2$ [Mo-N(Py) = 2.422(6) Å and 2.396(5) Å] and $WCl_2(=NPh)_2(Py)_2$ [W-N(Py) = 2.319(8) Å and 2.315(8) Å].[66b,68c] Furthermore, it has been reported that M-Cl moieties (M = transition metal) are good hydrogen-bond acceptors, especially when chlorine is an anion (Cl^-).[69] There are intramolecular hydrogen bonds N(3)-H···Cl(1) in **19** [$d_{N(3)\cdots Cl(1)}$ = 2.987(4) Å,

$d_{H\cdots Cl(1)}$ = 2.53(6) Å, $d_{N(3)\cdots H}$ = 0.84(6) Å, and ∠N(3)-H-Cl(1) = 116(5)°] and **20** [$d_{N(3)-Cl(1)}$ = 3.018(3) Å, $d_{H\cdots Cl(1)}$ = 2.69(3) Å, $d_{N(3-H}$ = 0.75(3) Å, and ∠N(3)-H-Cl(1) = 109(3)°]. The two amine N atoms in $(ArN=)_2MoCl_2(NHMe_2)_2$ (**21**) are also in close contact with the other chloride atom [$d_{N(3)-Cl(2)}$ = 3.029 Å and $d_{N(4)-Cl(3)}$ = 3.045 Å], and it is likely that hydrogen bonds N-H···Cl are present [$d_{H(4a)\cdots Cl(3)}$ = 2.634 Å].[68b] These interactions may contribute to the lack of α-hydrogen scrambling between amines and imido groups in **19**, **20** and **21**.[63] There is no evidence of interaction between the Mo centers and α-hydrogens of amines in the X-ray structures of **19**-**21** [d_{Mo-H} = 2.456 Å in **19**, 2.640 Å in **20**, $d_{Mo(1)-H(3a)}$ = 2.775 Å and $d_{Mo(1)-H(4a)}$ = 2.705 Å in **21**], although X-ray crystallography is, in general, not an accurate way to determine metal-hydrogen bond lengths.[64b,70]

The crystal structure of $(ArN=)_2MoCl_2(NHMe_2)\bullet(ArN=)_2MoCl_2(DME)$ (**22**) showed interesting coexistence of $(ArN=)_2MoCl_2(NHMe_2)$ (**19**) and $(ArN=)_2MoCl_2(DME)$ (**13**), the product and starting material in the preparation of **22**, respectively, in the same crystal lattice in a 1:1 molar ratio. An ORTEP view of **22** and its packing diagram are shown in Figures 4.17 and 4.18, respectively. Crystallographic data are given in Tables 4.17 and 4.18, respectively. The structure of $(ArN=)_2MoCl_2(DME)$ (**13**) was determined as well for comparison. ORTEP views of **13a** and **13b** are shown in Figures 4.19 and 4.21, respectively. Their packing diagrams are given in Figures 4.20 and 4.22, respectively. Crystallographic data for **13a** and **13b** are given in Tables 4.19-4.22. To our surprise, two different batches of crystals **13a** and **13b** which grew from different solvents (ether and

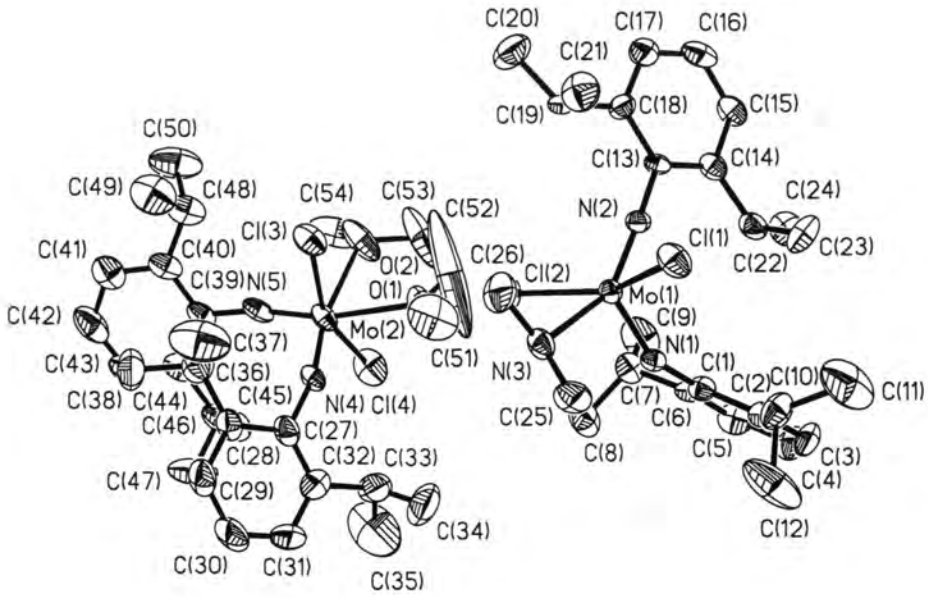

Figure 4.17. ORTEP view of **22** showing 50% probability thermal ellipsoids.

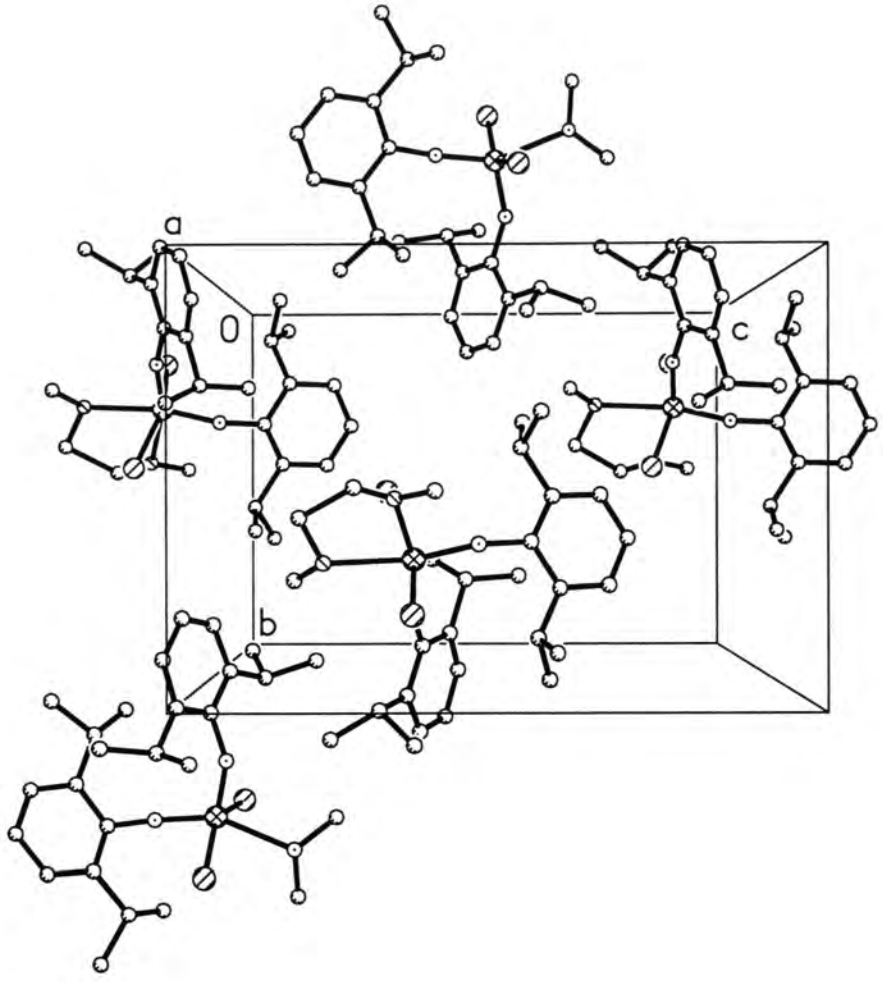

Figure 4.18. Packing diagram of **22**. View down the *a* axis.

Table 4.17. Crystal data and structure refinement for **22**

Identification code	**22**	
Empirical formula	$C_{27}H_{42.50}Cl_2MoN_{2.50}O$	
Formula weight	584.97	
Temperature	173(2) K	
Wavelength	0.71073 Å	
Crystal system	Orthorhombic	
Space group	$Pca2_1$	
Unit cell dimensions	a = 35.958(5) Å	$\alpha = 90°$
	b = 10.8417(15) Å	$\beta = 90°$
	c = 15.255(2) Å	$\gamma = 90°$
Volume	5947.3(14) Å^3	
Z	8	
Density (calculated)	1.307 Mg/m^3	
Absorption coefficient	0.642 mm^{-1}	
F(000)	2448	
Crystal size	0.29 × 0.16 × 0.03 mm^3	
θ range for data collection	1.13 to 26.41°	
Index ranges	$-44 \le h \le 44$, $-13 \le k \le 13$, $-19 \le l \le 19$	
Reflections collected	51499	

Table 4.17. Continued

Independent reflections	12150 [R(int) = 0.1374]
Completeness to $\theta = 26.41°$	99.8%
Absorption correction	Semi-empirical from equivalents
Max. and min. transmission	0.9810 and 0.8356
Refinement method	Full-matrix least-squares on F^2
Data / restraints / parameters	12150 / 1 / 627
Goodness-of-fit on F^2	0.960
Final R indices [$I > 2\sigma(I)$][a]	$R1$ = 0.0534, $wR2$ = 0.1173
R indices (all data)	$R1$ = 0.1085, $wR2$ = 0.1457
Absolute structure parameter	0.01(5)
Largest diff. peak and hole	0.738 and -0.778 e.Å^{-3}

[a] $wR2 = [\sum w(F_o^2 - F_c^2)^2 / \sum w(F_o^2)^2]^{1/2}$; $R = \sum \big| |F_o| - |F_c| \big| / \sum |F_o|$;

$w = 1 / [\sigma^2(F_o^2) + (aP)^2 + bP]$; $P = [2F_c^2 + \mathrm{Max}(F_o^2, 0)] / 3$.

Table 4.18. Bond lengths (Å) and angles (°) for **22**

Cl(2)-Mo(1)	2.3948(17)	Cl(1)-Mo(1)	2.373(2)
Cl(4)-Mo(2)	2.413(2)	Cl(3)-Mo(2)	2.4026(19)
Mo(1)-N(2)	1.750(6)	Mo(1)-N(1)	1.739(5)
Mo(2)-N(4)	1.733(6)	Mo(1)-N(3)	2.310(6)
Mo(2)-O(1)	2.356(7)	Mo(2)-N(5)	1.743(6)
N(1)-Mo(1)-N(3)	99.6(2)	Mo(2)-O(2)	2.373(7)
N(1)-Mo(1)-Cl(1)	103.04(18)	N(1)-Mo(1)-N(2)	109.2(3)
N(3)-Mo(1)-Cl(1)	81.15(17)	N(2)-Mo(1)-N(3)	151.1(2)
N(2)-Mo(1)-Cl(2)	93.8(2)	N(2)-Mo(1)-Cl(1)	91.8(2)
Cl(1)-Mo(1)-Cl(2)	147.40(7)	N(1)-Mo(1)-Cl(2)	105.28(18)
N(4)-Mo(2)-O(1)	92.5(3)	N(3)-Mo(1)-Cl(2)	78.52(17)
N(4)-Mo(2)-O(2)	166.4(3)	N(4)-Mo(2)-N(5)	102.7(3)
O(1)-Mo(2)-O(2)	74.1(2)	N(5)-Mo(2)-O(1)	164.6(3)
N(5)-Mo(2)-Cl(3)	96.47(19)	N(5)-Mo(2)-O(2)	90.8(3)
O(2)-Mo(2)-Cl(3)	81.70(18)	N(4)-Mo(2)-Cl(3)	98.2(2)
N(5)-Mo(2)-Cl(4)	97.4(2)	O(1)-Mo(2)-Cl(3)	79.1(2)
O(2)-Mo(2)-Cl(4)	79.55(19)	N(4)-Mo(2)-Cl(4)	96.9(2)
C(1)-N(1)-Mo(1)	152.1(5)	O(1)-Mo(2)-Cl(4)	82.7(2)
C(25)-N(3)-C(26)	110.2(7)	Cl(3)-Mo(2)-Cl(4)	156.75(9)
C(26)-N(3)-Mo(1)	111.5(5)	C(13)-N(2)-Mo(1)	174.6(5)

Table 4.18. Continued

C(39)-N(5)-Mo(2)	164.7(6)	C(25)-N(3)-Mo(1)	117.5(5)
C(52)-O(1)-Mo(2)	123.0(13)	C(27)-N(4)-Mo(2)	161.1(6)
C(54)-O(2)-C(53)	110.2(9)	C(52)-O(1)-C(51)	116.8(12)
C(53)-O(2)-Mo(2)	115.7(9)	C(51)-O(1)-Mo(2)	116.1(7)
C(54)-O(2)-Mo(2)	116.8(6)		

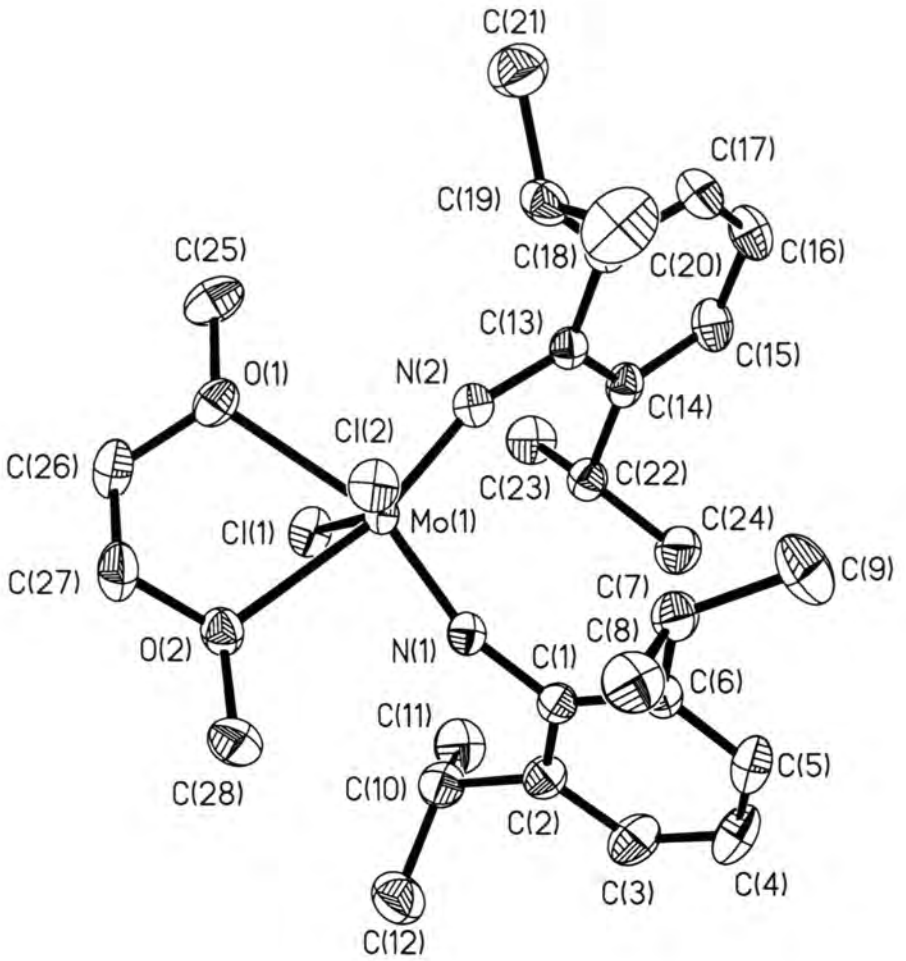

Figure 4.19. ORTEP view of **13a** showing 50% thermal ellipsoids.

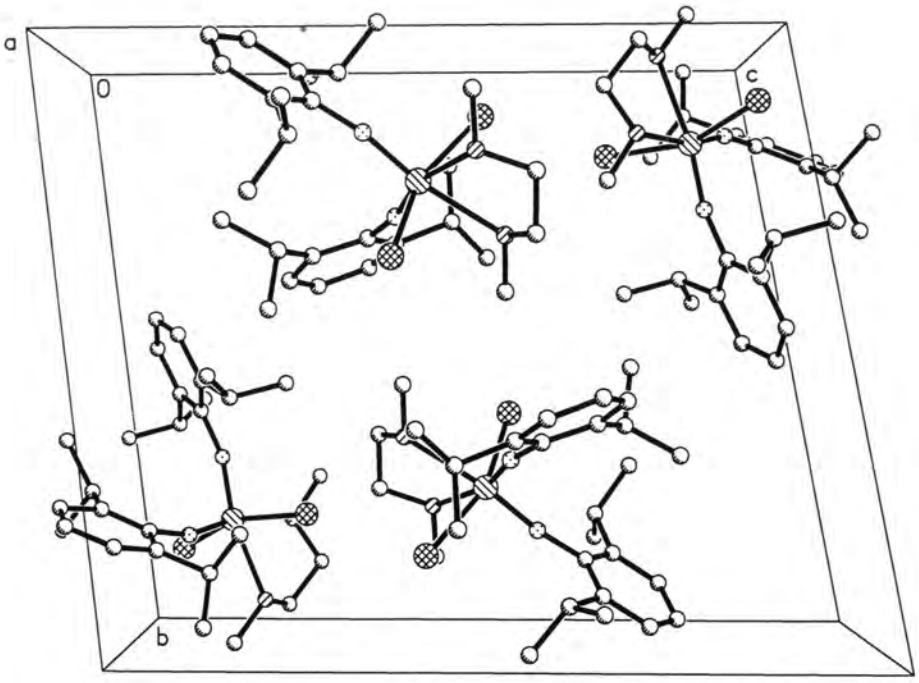

Figure 4.20. Packing diagram of **13a**. View down the *a* axis.

Table 4.19. Crystal data and structure refinement for **13a**

Identification code	**13a**	
Empirical formula	$C_{28}H_{44}Cl_2MoN_2O_2$	
Formula weight	607.49	
Temperature	173(2) K	
Wavelength	0.71073 Å	
Crystal system	Triclinic	
Space group	$P\bar{1}$	
Unit cell dimensions	a = 10.6216(6) Å	α = 80.8140(10)°
	b = 16.0603(9) Å	β = 87.5300(10)°
	c = 18.7632(10) Å	γ = 76.9920(10)°
Volume	3078.5(3) Å^3	
Z	4	
Density (calculated)	1.311 Mg/m^3	
Absorption coefficient	0.625 mm^{-1}	
F(000)	1272	
Crystal size	0.48 × 0.22 × 0.19 mm^3	
θ range for data collection	1.10 to 26.40°	
Index ranges	$-13 \le h \le 13$, $-20 \le k \le 20$, $-23 \le l \le 23$	
Reflections collected	30929	

Table 4.19. Continued

Independent reflections	12555 [R(int) = 0.0387]
Completeness to $\theta = 26.40°$	99.3%
Absorption correction	Semi-empirical from equivalents
Max. and min. transmission	0.8905 and 0.7535
Refinement method	Full-matrix least-squares on F^2
Data / restraints / parameters	12555 / 0 / 651
Goodness-of-fit on F^2	1.034
Final R indices [$I > 2\sigma(I)$][a]	$R1$ = 0.0317, $wR2$ = 0.0752
R indices (all data)	$R1$ = 0.0477, $wR2$ = 0.0901
Largest diff. peak and hole	0.463 and -0.390 e.Å^{-3}

[a] $wR^2 = [\sum w(F_o^2 - F_c^2)^2 / \sum w(F_o^2)^2]^{1/2}$; $R = \sum \left| |F_o| - |F_c| \right| / \sum |F_o|$;

$w = 1 / [\sigma^2(F_o^2) + (aP)^2 + bP]$; $P = [2F_c^2 + \mathrm{Max}(F_o^2,0)] / 3$.

Table 4.20. Selected bond lengths (Å) and angles (°) for **13a**

Cl(1)-Mo(1)	2.4038(7)	Cl(2)-Mo(1)	2.3980(7)
Cl(5)-Mo(2)	2.3981(8)	Cl(6)-Mo(2)	2.3957(8)
Mo(1)-N(1)	1.747(2)	Mo(1)-N(2)	1.749(2)
Mo(1)-O(2)	2.3599(19)	Mo(1)-O(1)	2.3639(17)
Mo(2)-N(3)	1.749(2)	Mo(2)-N(4)	1.749(2)
Mo(2)-O(3)	2.346(2)	Mo(2)-O(4)	2.3728(19)
N(1)-Mo(1)-O(2)	89.91(8)	N(1)-Mo(1)-N(2)	103.31(10)
N(1)-Mo(1)-O(1)	159.70(9)	N(2)-Mo(1)-O(2)	166.77(8)
O(2)-Mo(1)-O(1)	69.88(7)	N(2)-Mo(1)-O(1)	96.89(8)
N(2)-Mo(1)-Cl(2)	97.10(7)	N(1)-Mo(1)-Cl(2)	99.69(7)
O(1)-Mo(1)-Cl(2)	79.50(5)	O(2)-Mo(1)-Cl(2)	80.85(5)
N(2)-Mo(1)-Cl(1)	96.90(7)	N(1)-Mo(1)-Cl(1)	96.48(7)
O(1)-Mo(1)-Cl(1)	78.97(5)	O(2)-Mo(1)-Cl(1)	80.94(5)
N(3)-Mo(2)-N(4)	104.55(10)	Cl(2)-Mo(1)-Cl(1)	155.54(2)
N(4)-Mo(2)-O(3)	162.62(9)	N(3)-Mo(2)-O(3)	92.82(9)
N(4)-Mo(2)-O(4)	92.65(8)	N(3)-Mo(2)-O(4)	162.76(9)
N(3)-Mo(2)-Cl(6)	98.31(8)	O(3)-Mo(2)-O(4)	69.97(7)
O(3)-Mo(2)-Cl(6)	80.21(6)	N(4)-Mo(2)-Cl(6)	97.12(7)
N(3)-Mo(2)-Cl(5)	96.95(8)	O(4)-Mo(2)-Cl(6)	80.25(6)
O(3)-Mo(2)-Cl(5)	80.87(6)	N(4)-Mo(2)-Cl(5)	96.62(7)

Table 4.20. Continued

Cl(6)-Mo(2)-Cl(5)	156.17(3)	O(4)-Mo(2)-Cl(5)	79.75(6)
C(13)-N(2)-Mo(1)	161.59(18)	C(1)-N(1)-Mo(1)	161.80(19)
C(29)-N(4)-Mo(2)	167.97(19)	C(41)-N(3)-Mo(2)	164.3(2)
C(25)-O(1)-Mo(1)	118.92(17)	C(26)-O(1)-Mo(1)	112.78(15)
C(28)-O(2)-Mo(1)	119.85(16)	C(27)-O(2)-Mo(1)	114.63(17)
C(52)-O(3)-Mo(2)	119.2(2)	C(52)-O(3)-C(55)	112.0(3)
C(51)-O(4)-C(54)	111.5(3)	C(55)-O(3)-Mo(2)	113.84(19)
C(54)-O(4)-Mo(2)	113.48(19)	C(51)-O(4)-Mo(2)	119.51(19)

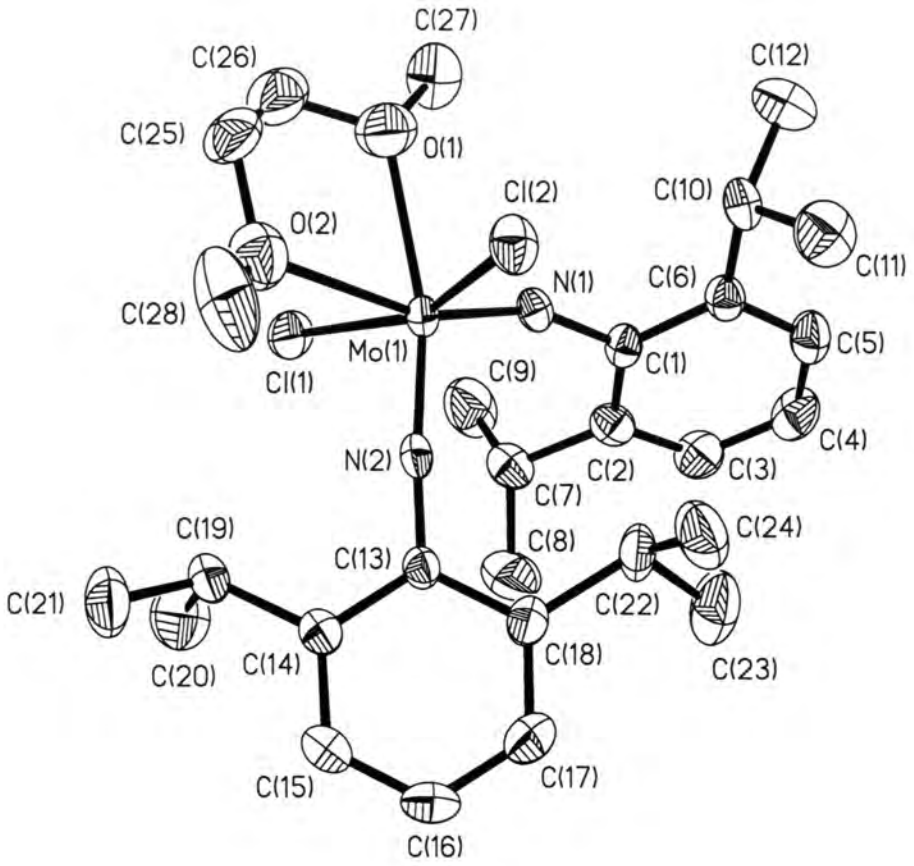

Figure 4.21. ORTEP view of **13b** showing 50% probability thermal ellipsoids.

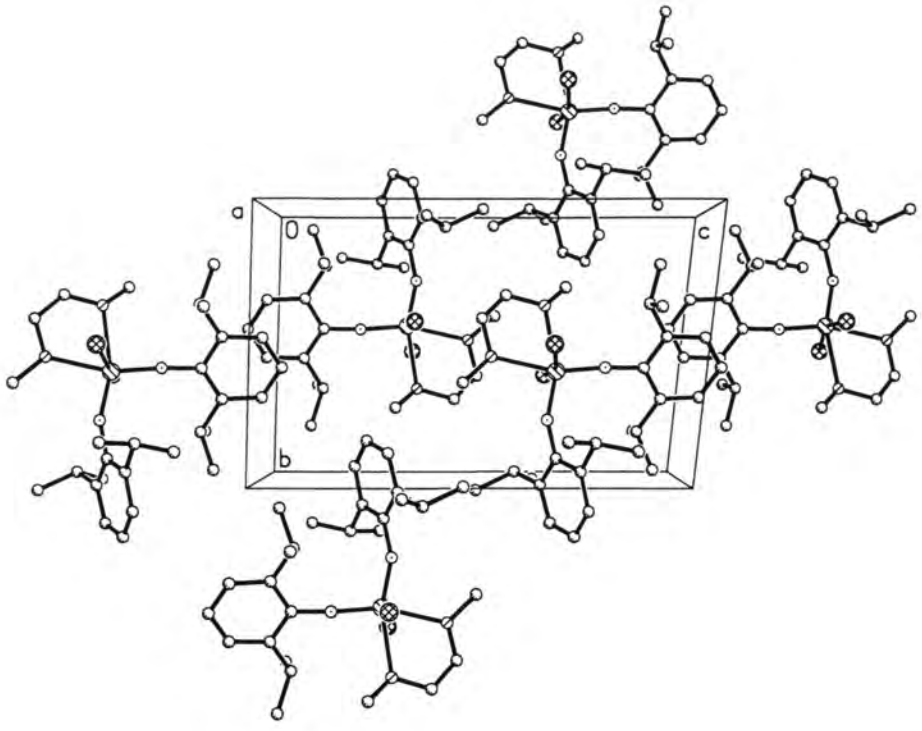

Figure 4.22. Packing diagram of **13b**. View down the *a* axis.

Table 4.21. Crystal data and structure refinement for **13b**

Identification code	**13b**	
Empirical formula	$C_{28}H_{44}Cl_2MoN_2O_2$	
Formula weight	607.49	
Temperature	173(2) K	
Wavelength	0.71073 Å	
Crystal system	Triclinic	
Space group	$P\bar{1}$	
Unit cell dimensions	a = 10.1333(18) Å	α = 93.281(3)°
	b = 10.6453(19) Å	β = 90.861(3)°
	c = 15.532(3) Å	γ = 113.424(3)°
Volume	1533.5(5) Å^3	
Z	2	
Density (calculated)	1.316 Mg/m^3	
Absorption coefficient	0.627 mm^{-1}	
F(000)	636	
Crystal size	0.50 × 0.21 × 0.11 mm^3	
θ range for data collection	1.31 to 26.41°	
Index ranges	$-12 \le h \le 12$, $-13 \le k \le 13$, $-19 \le l \le 19$	
Reflections collected	14652	

Table 4.21. Continued

Independent reflections	6224 [R(int) = 0.0423]
Completeness to $\theta = 26.41°$	98.7%
Absorption correction	Semi-empirical from equivalents
Max. and min. transmission	0.9342 and 0.7444
Refinement method	Full-matrix least-squares on F^2
Data / restraints / parameters	6224 / 0 / 326
Goodness-of-fit on F^2	1.059
Final R indices $[I>2\sigma(I)]$[a]	$R1 = 0.0469$, $wR2 = 0.1105$
R indices (all data)	$R1 = 0.0748$, $wR2 = 0.1276$
Largest diff. peak and hole	1.841 and -0.882 e.Å^{-3}

[a] $wR^2 = [\sum w(F_o^2 - F_c^2)^2 / \sum w(F_o^2)^2]^{1/2}$; $R = \sum \left| |F_o| - |F_c| \right| / \sum |F_o|$;

$w = 1 / [\sigma^2(F_o^2) + (aP)^2 + bP]$; $P = [2F_c^2 + \mathrm{Max}(F_o^2,0)] / 3$

Table 4.22. Selected bond lengths (Å) and angles (°) for **13b**

Cl(2)-Mo(1)	2.4059(12)	Cl(1)-Mo(1)	2.3985(11)
Mo(1)-N(1)	1.757(3)	Mo(1)-N(2)	1.750(3)
Mo(1)-O(2)	2.398(4)	Mo(1)-O(1)	2.323(4)
N(2)-Mo(1)-N(1)	105.50(15)	N(2)-Mo(1)-O(1)	162.70(15)
N(1)-Mo(1)-O(1)	91.80(15)	N(2)-Mo(1)-O(2)	94.04(14)
N(1)-Mo(1)-O(2)	160.39(14)	O(1)-Mo(1)-O(2)	68.66(14)
N(2)-Mo(1)-Cl(1)	95.69(10)	N(1)-Mo(1)-Cl(1)	99.59(11)
O(1)-Mo(1)-Cl(1)	81.65(10)	O(2)-Mo(1)-Cl(1)	79.79(10)
N(2)-Mo(1)-Cl(2)	93.87(11)	N(1)-Mo(1)-Cl(2)	97.45(11)
O(1)-Mo(1)-Cl(2)	83.16(10)	O(2)-Mo(1)-Cl(2)	79.20(10)
Cl(1)-Mo(1)-Cl(2)	157.45(4)	C(1)-N(1)-Mo(1)	157.1(3)
C(13)-N(2)-Mo(1)	175.0(3)	C(27)-O(1)-Mo(1)	121.8(3)
C(26)-O(1)-Mo(1)	116.3(4)	C(28)-O(2)-Mo(1)	121.7(4)
C(25)-O(2)-Mo(1)	114.8(3)		

pentane) gave two different unit cells and packings (Figures 4.20 and 4.22) in the same space group. Both structures showed distorted octahedral geometry. The Mo, two O, and two N atoms are coplanar, and the two imido ligands are *cis* to each other (Figures 4.19 and 4.21). The bond lengths and angles for **13a-b** (Tables 4.20 and 4.22) are almost identical to those in **22** (Table 4.12) and **19** (Table 4.18). In addition, the shorter Mo=N bond lengths in **13a-b** were preserved in **22**. A disparity between the bond angles of the two imido ligands, which is similar to those in **19** and **20**, was observed in **13b** [$\angle$C(13)-N(2)-Mo(1) = 175.0(3)° and $\angle$C(1)-N(1)-Mo(1) = 157.1(3)°], but surprisingly not observed in **13a** [$\angle$C(13)-N(2)-Mo(1) = 161.6(2)°; $\angle$C(1)-N(1)-Mo(1) = 161.7(2)°, $\angle$C(29)-N(4)-Mo(2) = 167.8(2)°, and $\angle$C(41)-N(3)-Mo(2) = 164.3(2)°]. It is apparently the crystal packing (not the electronic effect) that led to the observed difference between **13b** and **13a**.[68b,68d-e]

4.3. Conclusions

Preparation and characterization of bis(2,6-diisopropylphenylimido)molybdenum(VI) amide and silyl complexes $(ArN=)_2Mo(NMe_2)_2$ (**14**), $(ArN=)_2Mo(NMe_2)[Si(SiMe_3)_3]$ (**15**), $(ArN=)_2MoCl[N(SiMe_3)_2]$ (**16**), $(ArN=)_2Mo(NMe_2)[N(SiMe_3)_2]$ (**17**), and $(ArN=)_2Mo(NHAr)_2$ (**18**) are reported. The precursor to these complexes $(ArN=)_2MoCl_2(DME)$ was found to form amine adducts $(ArN=)_2MoCl_2(NHMe_2)$ (**19**), $(ArN=)_2MoCl_2(NHEt_2)$ (**20**), $(ArN=)_2MoCl_2(NHMe_2)_2$ (**21**), and

$(ArN=)_2MoCl_2(NHMe_2)\bullet(ArN=)_2MoCl_2(DME)$ (**22**). The preparation and characterization of these adducts are reported as well.

4.4. Experimental Section

4.4.1. *General procedures*

All manipulations, unless noted, were performed under a dry nitrogen atmosphere with the use of either a drybox or standard Schlenk techniques. All solvents were purified by distillation from potassium/benzophenone ketyl. H_2NAr and $HNEt_2$ were purchased from Aldrich and distilled from CaH_2 before use. Benzene-d_6 was dried over activated molecular sieves and stored under N_2. ^1H and $^{13}C\{^1H\}$ NMR spectra, unless noted, were recorded at 23 °C on a Bruker AC-250 NMR spectrometer and referenced to the solvent (residual protons in the ^1H NMR spectra). $(ArN=)_2MoCl_2(DME)$ (**13**)[71] and $LiSi(SiMe_3)_3(THF)_3$ [24a] were prepared by the literature procedures. $LiNMe_2$ (Aldrich) in hexanes was removed from the suspension before use. $LiN(SiMe_3)_2$ (Aldrich) and n-BuLi (Aldrich) were used as received. O_2-free water was prepared by freezing distilled water at -78 °C and evacuating the system. Elemental analyses were performed by Complete Analysis Laboratories Inc., E&R Microanalytical Division, Parsippany, New Jersey 07054-4909.

4.4.2. *Preparation of* $(ArN=)_2Mo(NMe_2)_2$ *(Ar = 2,6-diisopropylphenyl, 14)*

A chilled suspension (-60 °C) of $LiNMe_2$ (0.118 g, 2.31 mmol) in ether (20 mL) was added over 10 min to a chilled (-60 °C) solution of $(ArN=)_2MoCl_2(DME)$ (0.702 g, 1.16 mmol) in ether (30 mL). The mixture was stirred and allowed to warm gradually to room temperature overnight. The color turned from brick red to orange-red. Removal of volatiles *in vacuo*, followed by extraction with pentane, filtration, and crystallization at -30 °C gave 0.545 g of **14** (1.02 mmol, 88.2% yield). ^1H NMR (benzene-d_6, 250.1 MHz) δ 7.12–6.93 (m, 6H, C_6H_3), 3.85 (sep, 4H, $CHMe_2$, $^3J_{H\text{-}H}$ = 6.08 Hz), 3.48 (s, 12H, NMe_2), 1.16 (d, 24H, $CHMe_2$). $^{13}C\{^1H\}$ NMR (benzene-d_6, 62.9 MHz) δ 154.02, 142.10, 125.27, 120.78 (C_6H_3), 53.42 (NMe_2), 28.55 ($CHMe_2$), 23.69 ($CHMe_2$). Anal. Calcd for $C_{28}H_{46}N_4Mo$: C, 62.90; H, 8.67. Found: C, 62.54; H, 8.87.

4.4.3. *Preparation of* $(ArN=)_2Mo(NMe_2)[Si(SiMe_3)_3]$ *(15)*

A chilled suspension (-60 °C) of $LiNMe_2$ (0.091 g, 1.78 mmol) in ether (10 mL) was added over 10 min to a chilled (-60 °C) solution of $(ArN=)_2MoCl_2(DME)$ (1.081 g, 1.78 mmol) in ether (20 mL). The mixture was stirred and allowed to warm gradually to room temperature overnight. Then a chilled solution of $LiSi(SiMe_3)_3(THF)_3$ (0.838 g, 1.78 mmol) in ether (20 mL) was added to the mixture at -60 °C. The color turned from brick red to dark brown. Removal of volatiles *in vacuo*, followed by extraction with pentane, filtration, and crystallization at -30 °C gave 0.785 g of **15** (1.06 mmol, 59.8% yield). ^1H NMR (benzene-d_6,

250.1 MHz) δ 7.03–6.98 (m, 6H, C_6H_3), 3.79 (sep, 4H, CHMe$_2$, $^3J_{H\text{-}H}$ = 7.01 Hz), 3.45 (s, 6H, NMe_2), 1.13 (d, 24H, CHMe_2), 0.43 (s, 27H, SiMe_3). $^{13}C\{^1H\}$ NMR (benzene-d_6, 62.9 MHz) δ 142.10, 127.27, 125.67, 123.01 (C_6H_3), 53.97 (NMe_2), 26.49 (CHMe$_2$), 24.16 (CHMe_2), 4.22 (SiMe_3). Anal. Calcd for $C_{35}H_{67}N_3Si_4Mo$: C, 56.95; H, 9.15. Found: C, 56.79; H, 9.21.

4.4.4. *Preparation of (ArN=)$_2$MoCl[N(SiMe$_3$)$_2$] (16)*

A suspension of LiN(SiMe$_3$)$_2$ (0.115 g, 0.687 mmol) in ether (20 mL) was added over 10 min to a chilled solution (-60 °C) of (ArN=)$_2$MoCl$_2$(DME) (0.418 g, 0.687 mmol) in ether (20 mL). The resulting mixture was refluxed at 40 °C overnight. The color turned from brick red to orange-yellow. Removal of volatiles *in vacuo*, followed by extraction with pentane, filtration, and crystallization at -30 °C gave 0.375 g of **16** (0.584 mmol, 85.0% yield). ^{1}H NMR (benzene-d_6, 250.1 MHz) δ 7.05–6.90 (m, 6H, C_6H_3), 3.81 (sep, 4H, CHMe$_2$, $^3J_{H\text{-}H}$ = 6.75 Hz), 1.09 (d, 24H, CHMe_2), 0.422 (s, 18H, SiMe_3). $^{13}C\{^1H\}$ NMR (benzene-d_6, 62.9 MHz) δ 147.23, 143.21, 129.24, 122.44 (C_6H_3), 28.50 (CHMe$_2$), 23.45 (CHMe_2), 6.26 (SiMe_3). Anal. Calcd for $C_{30}H_{52}N_3Si_2MoCl$: C, 56.10; H, 8.16. Found: C, 55.98; H, 8.43.

4.4.5. *Preparation of (ArN=)$_2$Mo(NMe$_2$)[N(SiMe$_3$)$_2$] (17)*

A suspension of LiNMe$_2$ (0.025 g, 0.490 mmol) in ether (15 mL) was added over 10 min to a chilled solution (-60 °C) of **16** (0.315 g, 0.490 mmol) in ether (20

mL). The resulting mixture was stirred and allowed to warm gradually to room temperature overnight. The color turned from brick red to dark yellow. Removal of volatiles *in vacuo*, followed by extraction with pentane, filtration, and crystallization at -30 °C gave 0.165 g of **17** (0.253 mmol, 51.7% yield). **17** was also prepared by replacing the two chlorides in **13** with one equiv of $LiNMe_2$ followed by one equiv of $LiN(SiMe_3)_2$. ^1H NMR (benzene-d_6, 250.1 MHz) δ 7.03–6.93 (m, 6H, C_6H_3), 3.81 (sep, 4H, $CHMe_2$, $^3J_{H\text{-}H} = 6.75$ Hz), 3.35 (s, 6H, NMe_2), 1.11 (d, 24H, $CHMe_2$), 0.48 (s, 18H, $SiMe_3$). $^{13}C\{^1H\}$ NMR (benzene-d_6, 62.9 MHz) δ 142.61, 127.03, 126.25, 123.07 (C_6H_3), 52.67 (NMe_2), 27.99 ($CHMe_2$), 24.31 ($CHMe_2$), 5.79 ($SiMe_3$). Anal. Calcd for $C_{32}H_{58}N_4Si_2Mo$: C, 59.05; H, 8.98. Found: C, 59.11; H, 9.04.

4.4.6. *Preparation of LiNHAr*

This preparation is a modification of a literature procedure.[61a-b] A solution of n-BuLi (70.51 mL, 1.6 M in hexane, 0.113 mol) was added dropwise to a solution of H_2NAr (21.27 mL, 0.113 mol) in hexane (20 mL) at 0 °C. The solution gradually turned orange with white precipitation. The mixture was allowed to warm to room temperature over 2 h. Removal of volatile *in vacuo*, followed by washing with hexanes, filtration, and drying in *vacuo* gave 18.32 g (0.100 mol, 88.9% yield) of pale yellow solid. ^1H and ^{13}C NMR of the solid were consistent with those reported.[61a-b]

4.4.7. *Preparation of* $(ArN=)_2Mo(NHAr)_2$ *(18)*

This preparation is a modification of the literature procedure.[61a-b] A suspension of LiNHAr (0.335 g, 1.83 mmol) in ether (30 mL) was added over 30 min to a red-brick solution of **13** (0.554 g, 0.913 mmol) in ether (40 mL). The mixture was stirred at room temperature overnight. No obvious color change was observed. Removal of volatiles *in vacuo*, followed by extraction with pentane, filtration, and crystallization at -30 °C gave 0.722 g of **18** (0.903 mmol, 98.9% yield). ^{1}H NMR and $^{13}C\{^1H\}$ NMR of the sample were consistent with those reported.[61a-b]

4.4.8. *Preparation of* $(ArN=)_2MoCl_2(NHMe_2)$ *(19)*

A solution of **13** (2.53 g, 4.16 mmol) in ether (25 mL) was added to a suspension of hydrolyzed $LiNMe_2$ [0.212 g, 4.16 mmol in a mixture of ether (20 mL) and O_2-free H_2O (0.08 mL, 4.44 mmol)]. The mixture was stirred in a closed system at room temperature overnight. Removal of volatiles *in vacuo*, followed by extraction with pentane, filtration, and crystallization at -30 °C gave 1.52 g of **19** (2.70 mmol, 65.0% yield). ^{1}H NMR (benzene-d_6, 250.1 MHz, 23 °C) δ 7.03–6.91 (m, 6H, C_6H_3), 3.95 (sep, 4H, $CHMe_2$, $^3J_{H\text{-}H}$ = 6.73 Hz), 3.31 (br s, 1H, $NHMe_2$), 2.39 (s, 6H, $NHMe_2$), 1.19 (d, 24H, $CHMe_2$). $^{13}C\{^1H\}$ NMR (benzene-d_6, 62.9 MHz) δ 154.02, 145.58, 128.96, 122.92 (C_6H_3), 40.37 ($NHMe_2$), 28.77 ($CHMe_2$), 24.06 ($CHMe_2$). Anal. Calcd for $C_{26}H_{41}N_3MoCl_2$: C, 55.52; H, 7.35; N, 7.47. Found: C, 55.63; H, 7.93, N, 7.37.

4.4.9. *Preparation of (ArN=)$_2$MoCl$_2$(NHEt$_2$) (20)*

$HNEt_2$ (0.366 mL, 3.43 mmol) was added to a solution of **13** (2.085 g, 3.43 mmol) in ether (35 mL). The mixture was stirred at room temperature overnight. Removal of volatiles *in vacuo*, followed by extraction with pentane, filtration, and crystallization at -30 °C gave 1.72 g of **20** (2.92 mmol, 85.0% yield). ^{1}H NMR (benzene-d_6, 250.1 MHz) δ 7.06–6.90 (m, 6H, C_6H_3), 4.09 (sep, 4H, C*H*Me$_2$, $^3J_{H\text{-}H}$ = 6.52 Hz), 3.35 (br s, 1H, N*H*Et$_2$), 2.69 (m, 4H, NHCH_2CH$_3$), 1.22 (d, 24H, CH*Me*$_2$), 1.14 (t, 6H, CH$_2$CH_3). ^{13}C{^{1}H} NMR (benzene-d_6, 62.9 MHz) δ 154.14, 145.71, 128.77, 123.03 (C_6H_3), 32.61 (NH*C*H$_2$CH$_3$), 28.17 (*C*HMe$_2$), 24.35 (HNCH$_2$*C*H$_3$), 22.61 (CH*Me*$_2$). Anal. Calcd for $C_{28}H_{45}N_3MoCl_2$: C, 56.95; H, 7.68. Found: C, 57.24; H, 7.97.

4.4.10. *Preparation of (ArN=)$_2$MoCl$_2$(NHMe$_2$)$_2$ (21)*

A solution of **13** (3.37 g, 2.77 mmol) in ether (20 mL) was added to a suspension of hydrolyzed $LiNMe_2$ [0.283 g, 5.54 mmol in a mixture of ether (25 mL) and O_2-free H_2O (0.10 mL, 5.56 mmol)]. The resulting mixture was stirred in a closed system at room temperature overnight. Removal of volatiles in *vacuo*, followed by extraction with pentane, filtration, and crystallization at -30 °C gave 0.76 g of **21** (1.25 mmol, 45.0% yield). ^{1}HNMR (benzene-d_6, 250.1 MHz) δ 7.11–6.89 (m, 6H, C_6H_3), 3.97 (sep, 4H, C*H*Me$_2$, $^3J_{H\text{-}H}$ = 6.85 Hz), 3.19 (br s, 2H, N*H*Me$_2$), 2.24 (s, 12H, NH*Me*$_2$), 1.20 (d, 24H, CH*Me*$_2$). ^{13}C{^{1}H} NMR (benzene-d_6, 62.9 MHz) δ 153.97, 145.31, 128.69, 122.96 (C_6H_3), 40.01 (NH*Me*$_2$), 28.67

($CHMe_2$), 24.16 ($CHMe_2$). Anal. Calcd for $C_{26}H_{41}N_3MoCl_2$: C, 55.36; H, 7.96. Found: C, 55.64; H, 7.93.

4.4.11. *Preparation of $(ArN=)_2MoCl_2(NHMe_2)$•$(ArN=)_2MoCl_2(DME)$ (22)*

A solution of **13** (1.27 g, 2.08 mmol) in ether (15 mL) was added to a suspension of hydrolyzed $LiNMe_2$ [0.106 g, 2.08 mmol in a mixture of ether (20 mL) and O_2-free H_2O (0.04 mL, 2.22 mmol)]. The mixture was stirred in a closed system at room temperature overnight. Removal of volatiles *in vacuo*, followed by extraction with pentane, filtration, and crystallization at -30 °C gave 0.042 g of **22** (0.032 mmol, 3.06% isolated yield). ^1H NMR (benzene-d_6, 250.1 MHz, 23 °C) and $^{13}C\{^1H\}$ NMR (benzene-d_6, 62.9 MHz, 23 °C) of **7** showed it to be a 1:1 mixture of **19** and **13**.

4.4.12. *Crystallization of $(ArN=)_2MoCl_2(DME)$ (13)*

13a, prepared by the literature procedure,[71] was recrystallized from ether and pentane at -30 °C to give the crystals **13a** and **13b**, respectively.

4.4.13. *X-ray crystal structure determinations of 13-22*

The crystal structure of **14** was determined on a Siemens R3m/V diffractometer equipped with a graphite-monochromated Mo source (K_α radiation, 0.71073 Å) and fitted with a Nicolet LT-2 low temperature device. The unit cell parameters and orientation matrix were determined from a least-square fit of 30

reflections obtained from a rotation photograph and an automatic peak search routine. The crystal structures of **13** and **15-22** were determined on a Bruker AXS Smart 1000 X-ray diffractometer equipped with a CCD area detector and a graphite-monochromated Mo source (K_α radiation, 0.71073 Å) and fitted with an upgraded Nicolet LT-2 low temperature device. Suitable crystals were coated with paratone oil (Exxon) and mounted on a glass fiber under a stream of nitrogen at 173(2) K. The structures of **13**, **15-18** and **21-22** were solved by direct methods while automatic Patterson interpretation was applied to the structures of **14** and **19**. Non-hydrogen atoms were anistropically refined. All hydrogen atoms for structures **13-22** were treated as idealized contributions except for hydrogen atoms attached directly to the amine groups (*H*NMe_2 in **19** and *H*NEt_2 in **20**), which were located from the electron density maps and were refined isotropically. Empirical absorption correction was performed with SADABS.[35a] In addition the global refinements for the unit cells and data reductions of structures **13** and **15-22** were performed using the Saint program (Version 6.02). All calculations were performed using SHELXTL (Version 5.1) proprietary software package.[35b]

CHAPTER 5

Synthesis, Characterization and Dynamic Studies of Tantalum(V) Amide Silyl and Disilyl Complexes

5.1. Introduction

Early-transition-metal amide complexes have attracted much attention in recent years in part because of their important applications as precursors in the formation of microelectronic diffusion barriers as metal nitride (MN_x) and M-Si-N ternary films.[3a-b,58,72] Although numerous well-characterized Ta(IV)[54c,73] and Ta(V)[54c,60a,73-76] amide complexes and a few Ta silyl complexes[1,16a-b,16e,16g,77] have been reported, few Ta(V) amide silyl complexes are known.[1,22,39r] We are interested in the synthesis of Cp-free early-transition-metal amide silyl complexes as they are potential precursors to Ta-Si-N ternary materials. Ta-Si-N thin films have attracted much attention lately as a new diffusion barrier material in Si-based microelectronic devices.[3b,3f] Unlike, e.g., TiN films that are often polycrystaline and thus have grain boundaries for diffusion, M-Si-N ternary films are often amorphous and have shown better diffusion barrier properties. We report herein the synthesis and structural characterization of a series of Ta(V) amide silyl and amide bis(silyl) complexes $(Me_2N)_3Ta(SiR_3)Cl$ [SiR_3 = $Si(SiMe_3)_3$ (**23**),[78] $SiBu^tPh_2$ (**24**)], $(Me_2N)_3Ta(SiR_3)_2$ [SiR_3 = $Si(SiMe_3)_3$ (**25**),[78] $SiBu^tPh_2$ (**26**)], and $(Me_2N)_3Ta(SiBu^tPh_2)[Si(SiMe_3)_3]$ (**27**) and NMR studies of the exchanges among **25** ⇌ **27** ⇌ **26**.

5.2. Results and Discussion

5.2.1. *Synthesis and spectroscopic properties of 23-27*

Monosilyl complexes **23** and **24** were prepared by the reactions of $(Me_2N)_3TaCl_2$ [75] with $Li(THF)_3Si(SiMe_3)_3$ [24a] and $Li(THF)_3SiPh_2Bu^t$,[24b] respectively (Scheme 5.1). **23** and **24** are intermediates to bis(silyl) complexes **25-27**. **25** and **26** can be readily prepared by either the reactions of **23** and **24** with one equiv of the corresponding silyl lithium reagent or by the reactions of $(Me_2N)_3TaCl_2$ with two equiv of silyl lithium (Scheme 5.1). The mixed bis(silyl) complex $(Me_2N)_3Ta(SiBu^tPh_2)[Si(SiMe_3)_3]$ (**27**) was prepared by the reaction of **24** with one equiv of $Li(THF)_3Si(SiMe_3)_3$ (Scheme 5.1). However, attempts to prepare **26** by the reaction of $(Me_2N)_3Ta(Cl)Si(SiMe_3)_3$ (**23**) with one equiv of $Li(THF)_3SiPh_2Bu^t$ only led the formation of a mixture of $(Me_2N)_3Ta[Si(SiMe_3)_3]_2$ (**25**), $(Me_2N)_3Ta(SiBu^tPh_2)_2$ (**26**), and $(Me_2N)_3Ta(SiBu^tPh_2)[Si(SiMe_3)_3]$ (**27**).

The NMR spectra of **23-27** are consistent with the structural assignment of the complexes. It is interesting to note that the ^1H NMR spectrum of $(Me_2N)_3Ta[Si(SiMe_3)_3]Cl$ (**23**) at 296 K displays two resonances of the NMe_2 ligands at 3.14 ppm and 3.10 ppm in a 2:1 ratio. This observation is consistent with the X-ray structure of **23**,[39r] showing a trigonal bipyramid geometry with two NMe_2 ligands in the equatorial and one NMe_2 ligand in the axial position. At 253 K, the ^1H NMR spectrum of **24** consists of two amide signals at 3.06 and 3.02 ppm in a ratio of 2:1. These two amide resonances coalesce at 316 K as the result of an exchange between the axial and equatorial amide ligands in **23** (Scheme 5.2A). Variable-temperature ^1H NMR experiments of **23** was performed.[39r] The free

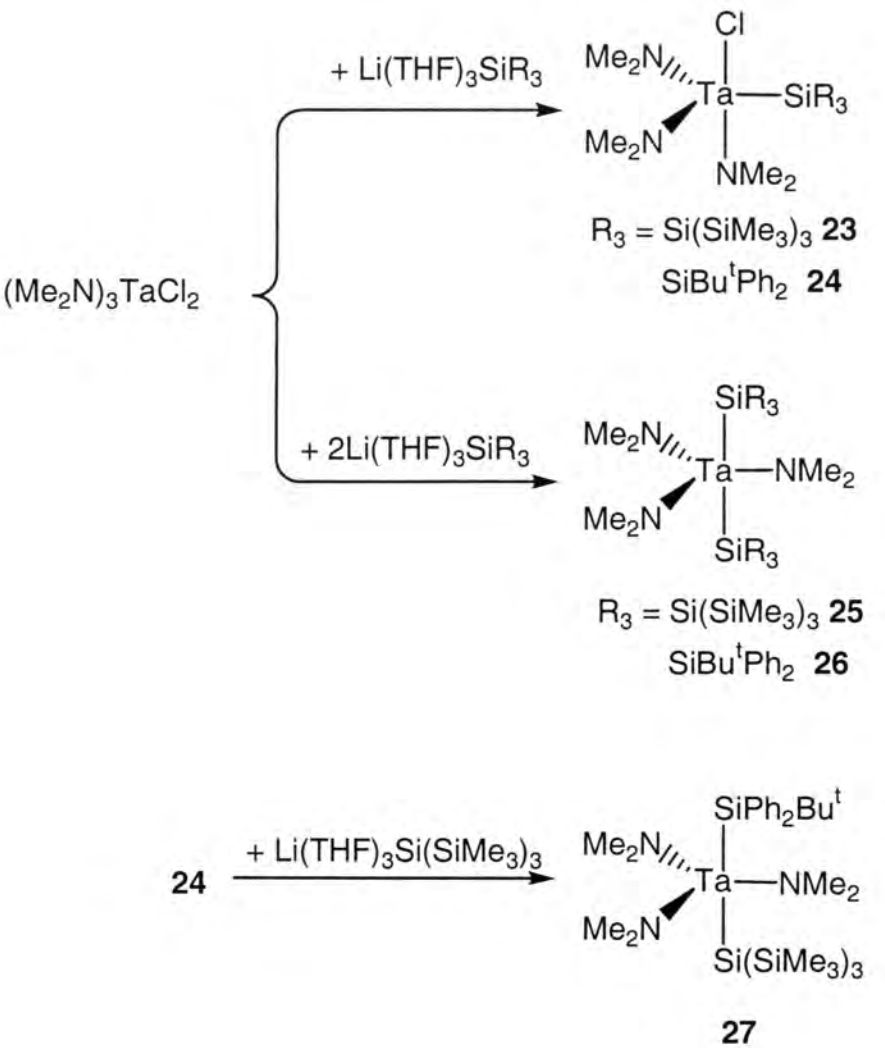

Scheme 5.1. Synthetic pathways to complexes **23–27**.

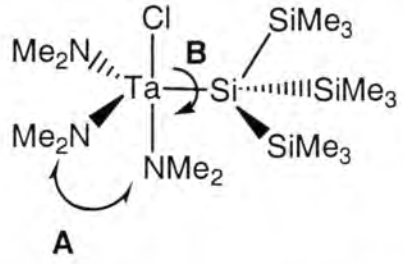

Scheme 5.2. Illustration of the amide ligands (**A**) and $SiMe_3$ ligands (**B**) in complex **23**.

energy of activation $\Delta G^{\ddagger}$ for this exchange was estimated to be 16.3 ± 0.5 kcal/mol.[39r] In the less sterically crowded $(Me_2N)_3Ta(SiBu^tPh_2)Cl$ (**24**), one ^1H NMR peak for the amide ligands was observed at 296 K, indicating a faster exchange at room temperature. Another dynamic process in **23** is the slow rotation of the $Si(SiMe_3)_3$ ligand in **23**. There are two peaks for the $SiMe_3$ groups at 5.8 and 5.9 ppm in the ^{13}C NMR spectrum of **23** at 296 K, although its ^1H NMR spectrum (400 MHz) at 296 K showed only one resonance for the $Si(SiMe_3)_3$ ligand. This difference between the two spectra indicates a slow rotation of the $Si(SiMe_3)_3$ ligand on the ^{13}C NMR time scale at room temperature (Scheme 5.2B). Two resonances of the $SiMe_3$ ligands were observed at 253 K, and they coalesced at 296 K.

The ^1H NMR spectra of bis(silyl) complexes **23-27** show only one resonance for NMe_2 ligands at both low and room temperature, suggesting that complexes **23-27** may adopt a trigonal bipyramidal structure with two silyl ligands in the axial and three amide ligands in the equatorial positions (Scheme 5.1).

The ^{29}Si NMR of the α-Si atom (-51.3 ppm) in the $Si(SiMe_3)_3$ ligand in $(Me_2N)_3Ta[Si(SiMe_3)_3]Cl$ (**23**) is similar to that (-53.47 ppm) in $(Bu^tCH_2)_2(Bu^tCH=)TaSi(SiMe_3)_3$.[16a] In the ^{29}Si NMR, the resonance of triamide silyl complex **24** (64.6 ppm) is downfield shifted from that of $SiMe_4$ (0.00 ppm). This trend is consistent with some other known complexes containing $-SiPh_2Bu^t$ ligands such as $(Me_2N)_3ZrSiBu^tPh_2(THF)_{0.5}$ (19.6 ppm),[60b] $(Me_2N)_3HfSiBu^tPh_2(THF)$ (46.8 ppm),[60b] $(Me_2N)_3TiSiBu^tPh_2$ (17.8 ppm),[60b] $(Me_2N)_2[(Me_3Si)_2N]ZrSiBu^tPh_2$ (18.1 ppm),[60b] and $(Me_3SiO)_2ZrCl(SiBu^tPh_2)(THF)_2$ (49.6 ppm).[16d]

5.2.2. *Thermodynamic studies of the exchanges 25 ⇌ 27 ⇌ 26*

Silyl exchanges were observed among **25**, **26** and **27** (Scheme 5.3). Silyl anion $SiBu^tPh_2$ in $Li(THF)_3SiBu^tPh_2$ replaces a silyl ligand $-Si(SiMe_3)_3$ in **25** to give **26** and $Li(THF)_3Si(SiMe_3)_3$. This reaction is reversible, and reaches an equilibrium (Eq. 5.1). There is a similar equilibrium among **27**, $Li(THF)_3SiBu^tPh_2$, **26**, and $Li(THF)_3Si(SiMe_3)_3$ (Eq. 5.2).

$$\mathbf{25} + Li(THF)_3SiBu^tPh_2 \rightleftharpoons \mathbf{27} + Li(THF)_3Si(SiMe_3)_3 \qquad \text{(Eq. 5.1)}$$

$$\mathbf{27} + Li(THF)_3SiBu^tPh_2 \rightleftharpoons \mathbf{26} + Li(THF)_3Si(SiMe_3)_3 \qquad \text{(Eq. 5.2)}$$

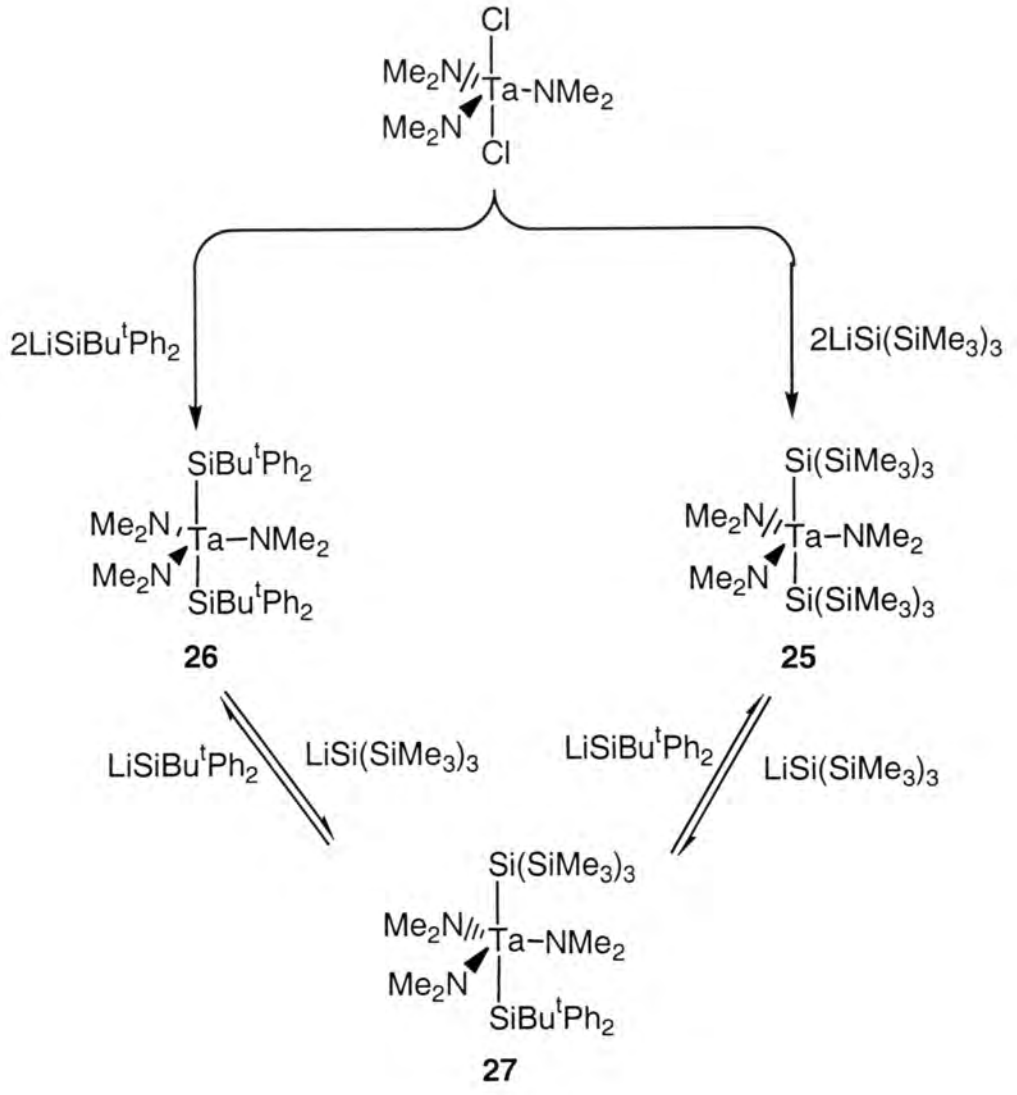

Scheme 5.3. The equilibria among complexes **25** ⇌ **27** ⇌ **26**.

The triamide disilyl complexes **25**-**27** may adopt a trigonal bipyramidal structure with the two silyl ligands in the axial positions (Scheme 5.1), as observed in a triamide disilyl anion $[(Me_2N)_3Zr(SiBu^tPh_2)_2]^-$.[78] However, we were not able to obtain a crystal structure of these three disilyl Ta compounds. These three complexes were found photosensitive, and decomposed on the X-ray diffractometer. Variable-temperature NMR spectra of the exchanges **25** ⇌ **27** ⇌ **26** were studied. The equilibrium constants for the exchange between **25** and **27** in Eq. 5.1, K_{eq} = {[**27**][$Li(THF)_3Si(SiMe_3)_3$]}/{[**25**][$Li(THF)_3SiBu^tPh_2$]}, were calculated from ^1H NMR spectra between 238 and 298 K, and are listed in Table 5.1. A plot of $\ln K_{eq}$ vs $1/T$ (Figure 5.1) gave a linear fit and yielded $\Delta H°$ = -0.54(0.17) kcal/mol and $\Delta S°$ = -0.79(0.65) eu (Eq. 2.1).[25]

$$-RT \ln K_{eq} = \Delta H° - T\Delta S° \qquad \text{(Eq. 2.1)}$$

The equilibrium constants K_{eq} range from 2.119(0.004) at 238 K to 1.687(0.004) at 298 K, indicating that the mixed disilyl complex **27** is favored, and increasing the temperature shifts the equilibrium towards **25**. The process **25** ⇌ **27** is slightly exothermic with $\Delta H°$ = -0.54(0.17) kcal/mol.

For the second equilibrium between **27** and **26**, the equilibrium constants, K_{eq} = {[**26**][$Li(THF)_3Si(SiMe_3)_3$]}/{[**27**][$Li(THF)_3SiBu^tPh_2$]}, were calculated from ^1H NMR spectra between 238 and 298 K, and are listed in Table 5.2. A plot of $\ln K_{eq}$ vs $1/T$ (Figure 5.2) gave a linear fit and yielded $\Delta H°$ = -0.56(0.17) kcal/mol

Table 5.1. Equilibrium constants (K_{eq}) for **25** + $LiSiBu^tPh_2$ ⇌ **27** + $LiSi(SiMe_3)_3$

T (K)	$K_{eq} \pm \delta K_{eq(ran)}$ [a]
298 ± 1	1.687 ± 0.004
293 ± 1	1.706 ± 0.006
288 ± 1	1.742 ± 0.003
283 ± 1	1.775 ± 0.015
278 ± 1	1.809 ± 0.004
273 ± 1	1.842 ± 0.002
268 ± 1	1.876 ± 0.006
263 ± 1	1.919 ± 0.011
258 ± 1	1.954 ± 0.004
253 ± 1	1.998 ± 0.002
248 ± 1	2.034 ± 0.006
243 ± 1	2.073 ± 0.007
238 ± 1	2.119 ± 0.004

[a] The largest random uncertainty is $\sigma K_{eq(ran)}/K_{eq} = 0.015/1.775 = 0.85\%$. The total uncertainty $\sigma K_{eq}/K_{eq}$ of 5.1% was calculated from $\sigma K_{eq(ran)}/K_{eq} = 0.85\%$ and the estimated systematic uncertainty $\sigma K_{eq(sys)}/K_{eq} = 5\%$ by $\sigma K_{eq}/K_{eq} = [(\sigma K_{eq(ran)}/K_{eq})^2 + (\sigma K_{eq(sys)}/K_{eq})^2]^{1/2}$.

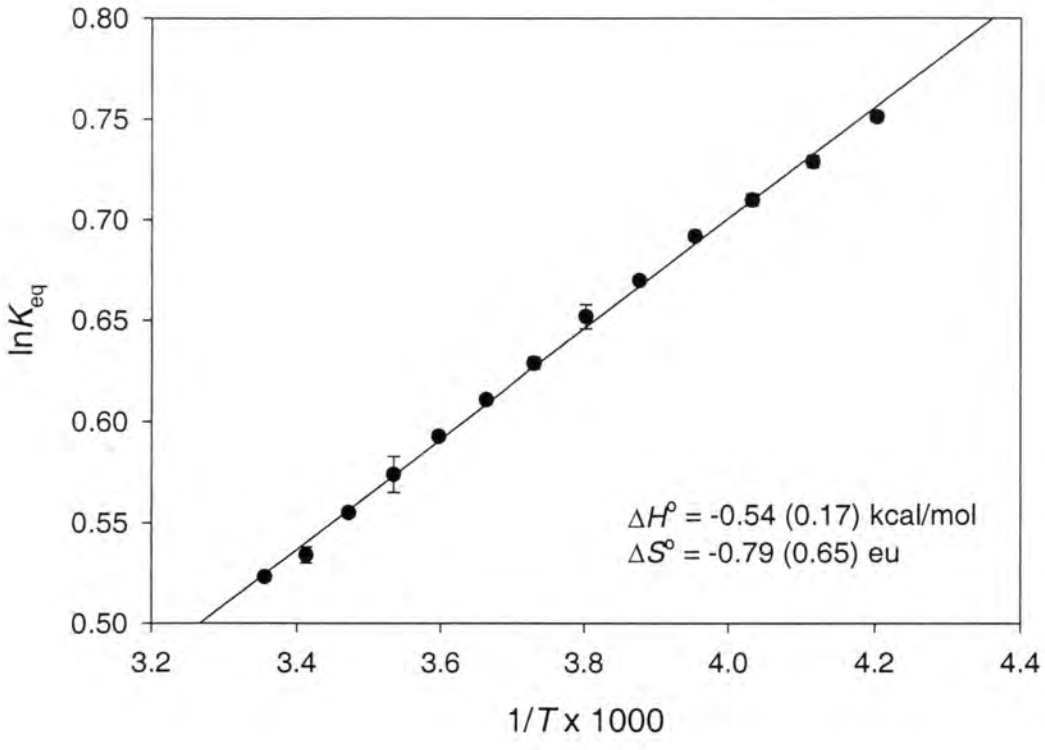

Figure 5.1. Plot of $\ln K_{eq}$ vs $1/T$ of the equilibrium **25** + $LiSiBu^tPh_2$ ⇌ **27** + $LiSi(SiMe_3)_3$.

Table 5.2. Equilibrium constants (K_{eq}) for **27** + $LiSiBu^tPh_2$ ⇌ **26** + $LiSi(SiMe_3)_3$

T (K)	$K_{eq} \pm \delta K_{eq(ran)}$ [a]
298 ± 1	1.119 ± 0.005
293 ± 1	1.224 ± 0.005
288 ± 1	1.249 ± 0.006
283 ± 1	1.273 ± 0.008
278 ± 1	1.300 ± 0.006
273 ± 1	1.326 ± 0.007
268 ± 1	1.353 ± 0.005
263 ± 1	1.381 ± 0.011
258 ± 1	1.408 ± 0.014
253 ± 1	1.436 ± 0.003
248 1	1.466 ± 0.008
243 ± 1	1.496 ± 0.009
238 ± 1	1.526 ± 0.003

[a] The largest random uncertainty is $\sigma K_{eq(ran)}/K_{eq} = 0.011/1.381 = 0.80\%$. The total uncertainty $\sigma K_{eq}/K_{eq}$ of 5.1% was calculated from $\sigma K_{eq(ran)}/K_{eq} = 0.80\%$ and the estimated systematic uncertainty $\sigma K_{eq(sys)}/K_{eq} = 5\%$ by $\sigma K_{eq}/K_{eq} = [(\sigma K_{eq(ran)}/K_{eq})^2 + (\sigma K_{eq(sys)}/K_{eq})^2]^{1/2}$.

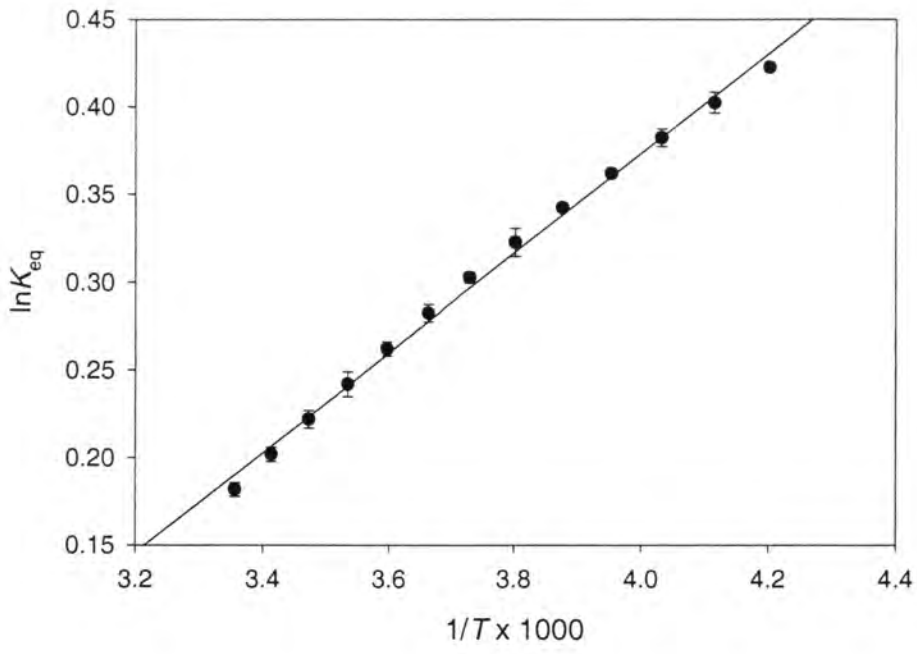

Figure 5.2. Plot of $\ln K_{eq}$ vs $1/T$ of the equilibrium **27** + $LiSiBu^tPh_2$ ⇌ **26** + $LiSi(SiMe_3)_3$.

and $\Delta S°$ = -1.52(0.65) eu.[25] The equilibrium constants K_{eq} range from 1.526(0.003) at 238 K to 1.119(0.005) at 298 K, indicating that the disilyl complex **26** is favored, and increasing the temperature shifts the equilibrium towards **27**. The process **27** ⇌ **26** is slightly exothermic with $\Delta H°$ = -0.56(0.17) kcal/mol.

It is interesting to note that the preference for **27** and eventually **26** in our tantalum silyl ligand exchange systems follows the trend that we observed in an equilibrium involving zirconium silyl amides: $(Me_2N)_3Zr\text{-}Si(SiMe_3)_3 + LiSiBu^tPh_2$ ⇌ $(Me_2N)_3Zr\text{-}SiBu^tPh_2 + LiSi(SiMe_3)_3$ [K_{eq} = 82.83(0.02) at 293(1) K; $\Delta H°$ = -4.6(5) kcal/mol and $\Delta S°$ = -7(2) eu measured between 263(1) and 293(1) K].[78] The relative stabilities of Ta amide silyl complexes are in contrast to those of $(RCH_2)_3Zr\text{-}Si(SiMe_3)_3$ (R = Bu^t, Me_3Si) and "$(RCH_2)_3Zr\text{-}SiBu^tPh_2$;" the former is stable to sublimation at 50 °C, and attempts to prepare the latter have to date been unsuccessful.

5.3. Conclusions

Preparation and characterization of Cp-free tantalum(V) amide silyl complexes have been investigated and reported. Thermodynamics of the interesting equilibria $(Me_2N)_3Ta[Si(SiMe_3)_3]_2$ (**25**) ⇌ $(Me_2N)_3Ta(SiBu^tPh_2)[Si(SiMe_3)_3]$ (**27**) ⇌ $(Me_2N)_3Ta(SiBu^tPh_2)_2$ (**26**) was studied. In the equilibrium **25** + $Li(THF)_3SiBu^tPh_2$ ⇌ **27** + $Li(THF)_3Si(SiMe_3)_3$, $\Delta H°$ = -0.54(0.17) kcal/mol and $\Delta S°$ = -0.79(0.65) eu. In the equilibrium **27** + $Li(THF)_3SiBu^tPh_2$ ⇌ **26** + $Li(THF)_3Si(SiMe_3)_3$, $\Delta H°$ = -0.56(0.17) kcal/mol and $\Delta S°$ = -1.52(0.65) eu.

5.4. Experimental Section

5.4.1. *General procedures*

All manipulations were performed under a dry nitrogen atmosphere with the use of either standard Schlenk techniques or a glovebox. Solvents were purified by distillation over potassium/benzophenone ketyl. Benzene-d_6 and toluene-d_8 were dried over activated molecular sieves and stored under nitrogen. $TaCl_5$ (Strem) was sublimed prior to use. $LiNMe_2$ (Aldrich) was separated from the hexanes suspension. $(Me_2N)_3TaCl_2$,[75] and silyl lithium reagents $Li(THF)_3Si(SiMe_3)_3$ [24a] and $Li(THF)_3SiBu^tPh_2$ [24b] were prepared according to the literature procedures. NMR spectra, unless noted, were recorded at 23 °C on a Bruker AC-250 or AMX 400 Fourier transform spectrometer and referenced to the solvents (residue protons in the ^1H NMR spectra). $^{29}Si\{^1H\}$ NMR (DEPT) data were obtained on an AMX 400 Fourier transform spectrometer and referenced to TMS. Elemental analyses were performed by Complete Analysis Laboratories Inc., E&R Microanalytical Division, Parsippany, New Jersey 07054-4909.

For the thermodynamic studies, the equilibrium constants K_{eq} were obtained from ^1H NMR spectra. At least two separate experiments at a given temperature, and their averages are listed (Tables 5.1 and 5.2). The *maximum* random uncertainty in the equilibrium constants was combined with the estimated systematic uncertainty, ca. 5%. The total uncertainties in the equilibrium constants were used in the $\ln K_{eq}$ vs. $1/T$ plots in Figures 5.1 and 5.2 and in error propagation calculations. The estimated uncertainty in the temperature measurements for an

NMR probe was 1 K. The enthalpy ($\Delta H°$) and entropy ($\Delta S°$) changes were calculated from an unweighted nonlinear least-squares procedure contained in the SigmaPlot Scientific Graph System, which is available from Jandel Corporation. The uncertainties in $\Delta H°$ and $\Delta S°$ were computed from the following error propagation formulas (Eqs. 2.9 and 2.10), which were derived from

$$-RT \ln K_{eq} = \Delta H° - T\Delta S° \qquad \text{(Eq. 2.1)}$$

$$(\sigma\Delta S°)^2 = 2R^2T_{min}{}^2T_{max}{}^2[\ln(K_{eq(max)}/K_{eq(min)})]^2(\sigma T/T)^2/\Delta T^4 + R^2(T_{max}{}^2 + T_{min}{}^2)(\sigma K_{eq}/K_{eq})^2/\Delta T^2 \qquad \text{(Eq. 2.8)}$$

$$(\sigma\Delta H°)^2 = (\Delta T/T)^2R^2(T_{max}{}^2T_{min}{}^4 + T_{min}{}^2T_{max}{}^4)[\ln(K_{eq(max)}/K_{eq(min)})]^2/\Delta T^4 + 2R^2T_{max}{}^2T_{min}{}^2(\sigma K_{eq}/K_{eq})^2/\Delta T^2 \qquad \text{(Eq. 2.9)}$$

where $\Delta T = (T_{max} - T_{min})$.[34]

5.4.2. *Preparation of $(Me_2N)_3Ta[Si(SiMe_3)_3]Cl$ (23)*

To a yellow slurry of $(Me_2N)_3TaCl_2$ (0.50 g, 1.30 mmol) in pentane (20 mL) was added one equiv of $Li(THF)_3Si(SiMe_3)_3$ (0.65 g, 1.40 mmol) in pentane (20 mL) with stirring at -20 °C. The reaction mixture was then slowly warmed to room temperature. Stirring at room temperature for 24 h and removal of volatiles afforded a yellow solid. Extraction of the solid with pentane, followed by filtration and crystallization at -20 °C yielded bright yellow crystals of **23** (0.38 g, 0.64 mmol,

49% yield). ^{1}H NMR (benzene-d_6, 250.1 MHz) δ 3.12 (s, 12H, NMe_2), 3.09 (s, 6H, NMe_2), 0.50 (s, 27H, SiMe_3). ^{13}C NMR (benzene-d_6, 62.9 MHz) δ 43.4 (NMe_2), 5.9 (SiMe_3), 5.8 (SiMe_3). ^{29}Si{^{1}H} NMR (DEPT, benzene-d_6, 79.5 MHz) δ 4.2 (SiSiMe$_3$), -51.3 (SiSiMe$_3$). Anal. Calcd for $C_{15}H_{45}N_3ClSi_4Ta$: C, 30.21; H, 7.61. Found: C, 30.05; H, 7.39.

5.4.3. *Preparation of $(Me_2N)_3Ta(SiBu^tPh_2)Cl$ (24)*

A slurry of $(Me_2N)_3TaCl_2$ (1.00 g, 2.60 mmol) in toluene (20 mL) was treated with one equiv of Li(THF)$_3$SiPh$_2$Bu^t (1.21 g, 2.62 mmol) in toluene (20 mL) at -20 °C. After stirring for 4 h at room temperature, the volatiles were removed *in vacuo*. The yellow solid was extracted with pentane, and the solution was filtered, concentrated, and cooled to -20 °C to give 0.46 g (0.78 mmol, 30% yield) of yellow crystals of **24**. ^{1}H NMR (benzene-d_6, 250.1 MHz) δ 7.97-7.14 (m, 10H, C$_6H_5$), 2.87 (s, 18H, NMe_2), 1.50 (s, 9H, CMe_3). ^{13}C NMR (benzene-d_6, 62.9 MHz) δ 144.9, 137.6, 127.8, 127.7 (C_6H$_5$), 42.8 (NMe_2), 30.5 (CMe_3), 25.2 (CMe$_3$). ^{29}Si{^{1}H} NMR (DEPT, benzene-d_6, 79.5 MHz) δ 64.6 (SiPh$_2$Bu^t). Anal. Calcd for $C_{22}H_{37}N_3ClSiTa$: C, 44.94; H, 6.34. Found: C, 44.85; H, 6.35.

5.4.4. *Preparation of $(Me_2N)_3Ta[Si(SiMe_3)_3]_2$ (25)*

To a yellow slurry of $(Me_2N)_3TaCl_2$ (0.51 g, 1.33 mmol) in pentane (25 mL) was added 2 equiv of Li(THF)$_3$Si(SiMe$_3$)$_3$ (1.25 g, 2.66 mmol) at room temperature. The reaction solution immediately turned deep purple. After stirring for 3 h at room

temperature, the volatiles were removed *in vacuo* yielding a purple solid. Extraction of the solid with pentane, followed by filtration and crystallization at -20 °C afforded deep red crystals of **25** (0.31 g, 0.38 mmol, 29% yield). ^{1}H NMR (toluene-d_8, 400.1 MHz, -30 °C) δ 3.22 (s, 18H, NMe_2), 0.37 (s, 54H, SiMe_3). ^{13}C NMR (toluene-d_8, 100.6 MHz, -30 °C) δ 44.9 (NMe_2), 6.5 (SiMe_3). ^{29}Si{^{1}H} NMR (DEPT, toluene-d_8, 79.5 MHz, -30 °C) δ 0.95 (SiSiMe$_3$), -6.25 (SiSiMe$_3$). Anal. Calcd for $C_{24}H_{72}N_3Si_8Ta$: C, 35.65; H, 8.98. Found: C, 35.42; H, 8.75.

5.4.5. *Preparation of $(Me_2N)_3Ta(SiBu^tPh_2)_2$ (26)*

Complex **26** was prepared by a procedure similar to that for the preparation of **5** and isolated as purple solid (yield 35%). It was found to be unstable and to decompose at room temperature. The structural assignment for **26** was thus based on its spectroscopic data. ^{1}H NMR (benzene-d_6, 250.1 MHz) δ 7.58-7.14 (m, 20H, C_6H_5), 2.99 (s, 18H, NMe_2), 1.07 (s, 18H, CMe_3). ^{13}C NMR (benzene-d_6, 62.9 MHz) δ 148.7, 137.3, 127.1, 126.8 (C_6H_5), 44.5 (NMe_2), 31.1 (CMe_3), 24.2 (CMe$_3$).

5.4.6. *Preparation of $(Me_2N)_3Ta(SiBu^tPh_2)[Si(SiMe_3)_3]$ (27)*

A yellow solution of $(Me_2N)_3Ta[Si(SiMe_3)_3]Cl$ (**23**) (0.10 g, 0.17 mmol) in hexanes (20 mL) was treated with one equiv of $Li(THF)_3SiPh_2Bu^t$ (0.08 g, 0.17 mmol) at room temperature. The reaction solution immediately turned purple. After the solution was stirred for 30 min at room temperature, the volatiles were removed *in vacuo* to give a purple solid. Extraction of the solid with toluene,

followed by filtration and crystallization at -20 °C afforded a purple solid product of **27** (0.20 g, 25% yield). The complex was found unstable at room temperature. The structural assignment for **27** was thus based on its spectroscopic data. ^{1}H NMR (benzene-d_6, 250.1 MHz) δ 7.61-7.15 (m, 10H, C_6H_5), 3.14 (s, 18H, NMe_2), 1.08 (s, 9H, CMe_3), 0.32 (s, 27H, $SiMe_3$). ^{13}C NMR (benzene-d_6, 62.9 MHz) δ 147.3, 137.2, 127.2, 127.1 (C_6H_5), 44.8 (NMe_2), 30.9 (CMe_3), 24.7 (CMe_3), 6.8 ($SiMe_3$).

CHAPTER 6

Future Studies

The synthesis and characterization of the novel Groups 5 and 6 complexes that are free of anionic π-ligands such as cyclopentadienyl (Cp) are presented in this dissertation. Their reactions with oxygen and silanes have been investigated.

CVD reactions of d^0 early transition metal complexes with O_2 have been studied to yield high-κ metal oxides or M-Si-O ternary oxides as gate and DRAM materials.[5h-l] The mechanistic pathways in these reactions with O_2 are largely unknown. Our current studies of reactions of O_2 with d^0 alkylidyne complexes $(Bu^tCH_2)_2W(\equiv CBu^t)(SiBu^tPh_2)$ (**2b**) and $(Me_3SiCH_2)_3W\equiv CSiMe_3$ revealed some unusual and interesting chemistry in these reactions. Further studies of the reactions of d^0 metal complexes with O_2 may provide a better understanding of the factors controlling the reactivities of these largely oxophilic metals and their complexes with O_2. The reactions of early transition metal silyl complexes with O_2 may be of particular significance, as both Si and metals are oxophilic. These studies may also lead to new CVD processes to microelectronic high-κ metal oxides or M-Si-O ternary oxides.

The roles that silicon in the silyl ligand in **2b** and in $CH_2SiMe_3/\equiv CSiMe_3$ ligands in $(Me_3SiCH_2)_3W\equiv CSiMe_3$ play in their reactions with O_2 may be further explored. In addition, studies with $^{16}O_2$-$^{18}O_2$ may reveal whether the two O atoms in $(Me_3SiCH_2)_2W(=O)(=CHSiMe_3)(O=PMe_3)$ (**11**) are from the same O_2 molecule.

It may also show in our current preparation of **11** whether the oxidation of PMe_3 by O_2 is separate from the reaction of $(Me_3SiCH_2)_3W{\equiv}CSiMe_3$. In other words, whether PMe_3 is directly oxidized by O_2 to $O{=}PMe_3$ which then assisted the reaction of $(Me_3SiCH_2)_3W{\equiv}CSiMe_3$ with O_2.[45,80] The fate of the Me_3SiCH_2- ligands in $(Me_3SiCH_2)_3W{\equiv}CSiMe_3$ in this reaction with O_2 is not clear, although we currently propose that an unstable $Me_3SiCH{=}O$[52] is one product. Theoretical studies may help us elucidate the mechanisms of this reaction.

Studies of the reactions of O_2 with the novel Mo(VI) amides and imdes [$(ArN{=})_2Mo(NMe_2)_2$ (**14**), $(ArN{=})_2Mo(NMe_2)[Si(SiMe_3)_3]$ (**15**), $(ArN{=})_2MoCl[N(SiMe_3)_2]$ (**16**), $(ArN{=})_2Mo(NMe_2)[N(SiMe_3)_2]$ (**17**), and $(ArN{=})_2Mo(NHAr)_2$ (**18**)] in the current dissertation can provide a comparison with the reactivities of Mo-N single bonds and Mo=N double bonds toward O_2 and shed light on the mechanistic pathways in the CVD of metal oxide thin films from metal amide complexes.[5h-l]

REFERENCES

1. Corey, J. Y.; Braddock-Wilking, J. *Chem. Rev.* 1999, *99*, 175. (b) Tilley, T. D. In *The Silicon-Heteroatom Bond*; Patai, S.; Rappoport, Z.; Eds.; Wiley: New York, 1991, Chs. 9 and 10. (c) Eisen, M. S.; In *The Chemistry of Organic Silicon Compounds*; Rappoport, Z.; Apeloig, Y., Eds.; Wiley: New York, 1998, Part 3, Vol. 2, Ch. 35. (d) Sharma, H. K.; Pannell, K. H. *Chem. Rev.* 1995, *95*, 1351. (e) Schubert, U. *Transition Met. Chem.* 1991, *16*, 136. (f) Schubert, U. *Adv. Organomet. Chem.* 1990, *30*, 151. (g) Schubert, U. *Angew. Chem., Int. Ed. Engl.* 1994, *33*, 419. (h) Gauvin, F.; Harrod, J. F.; Woo, H. G. *Adv. Organomet. Chem.* 1998, *42*, 363.

2. (a) Allinson, J. S.; Aylett, B. J.; Colquhoun, H. M. *J. Organomet. Chem.* **1976**, *112*, C7. (b) Isaacs, E. E.; Graham, W. A. G. *Can. J. Chem.* **1975**, *53*, 467. (c) Darensbourg, D. J.; Bauch, C. G.; Riebenspies, J. H.; Rheingold, A. L. *Inorg. Chem.* **1988**, *27*, 4203. (d) Graham, W. A. G.; Jetz, W. *Inorg. Chem.* **1971**, *10*, 4. (e) Schubert, U.; Müller, J.; Alt, H. G. *Organometallics* **1987**, *6*, 469. (f) Bennett, M. J.; Simpson, K. A. *J. Am. Chem. Soc.* **1971**, *93*, 7156. (g) Schubert, U.; Kirchgässner, U.; Grönen, J.; Piana, H. *Polyhedron* **1989**, *8*, 1589. (h) Handwerker, H.; Paul, M.; Blümel, J.; Zybill, C. *Angew. Chem. Int. Ed. Engl.* **1993**, *32*, 1313. (i) Heyn, R. H.; Tilley, T. D. *Inorg. Chem.* **1990**, *29*, 4051. (j) Luo, X.–L.; Kubas, G. J.; Bryan, J. C.; Burns, C. J.; Unkefer, C. J. *J. Am. Chem. Soc.* **1994**, *116*, 10312.

3. (a) *The Chemistry of Metal CVD*, Kodas, T. T.; Hampden-Smith, M. J.; Eds.; VCH: Weinheim, Germany, 1994. (b) Winter, C. H. *Aldrichimica Acta* **2000**, *33*, 3. (c) Raaijmakers, I. J. *Thin Solid Films* **1994**, *247*, 85. (d) Reid, J. S.;

Kolawa, E.; Garland, C. M.; Nicolet, M.–A.; Cardone, F.; Gupta, D.; Ruiz, R. P. *J. Appl. Phys.* **1996**, *79*, 1109. (e) Smith, P. M.; Custer, J. S.; *Appl. Phys. Lett.* **1997**, *70*, 3116. (f) Custer, J. S.; Smith, P. M.; Fleming, J. G.; Roherty-Osmun, E. *ACS Symp. Ser.* **1999**, *727*, 86.

4. Scott, J. F. *Annu. Rev. Mater. Sci.* **1998**, *28*, 79.
5. (a) Wilk, G. D.; Wallace, R. M.; Anthony, J. M. *J. Appl. Phys.* **2001**, *89*, 5243. (b) Senzaki, Y.; Hochberg, A. K.; Norman, J. A. *Adv. Mater. Opt. Electron.* **2000**, *10*, 93. (c) Smith, R. C.; Ma, T.–Z.; Hoilien, N.; Tsung, L. Y.; Bevan, M. J.; Colombo, L.; Roberts, J.; Campbell, S. A.; Gladfelter, W. L. *Adv. Mater. Opt. Electron.* **2000**, *10*, 105. (d) Huff, H. R.; Richter, C. A.; Green, M. L.; Lucovsky, G.; Hattori, T. Eds. *Mater. Res. Soc. Symp. Proc.* **1999**, 567. (e) Buchanan, D. A.; Edwards, A. H.; Von Bardeleben, H. J.; Hattori, T. Eds. *Mater. Res. Soc. Symp. Proc.* **2000**, 592. (f) Wolfe, D. M.; Flock, K.; Therrien, R.; Johnson, R.; Rayner, G. Jr.; Günther, L.; Brown, N.; Claflin, B.; Lucovsky, G. *Mater. Res. Soc. Symp. Proc.* **1999**, *567*, 343. (g) Rayner, G. Jr.; Therrien, R.; Lucovsky, G. *Mater. Res. Soc. Symp. Proc.* **2001**, *611*, C1.3.1. (h) Senzaki, Y.; Hamilton, R. F.; Reid, K. G.; Hobbs, C. C.; Hedge, R. I.; Tiner, M. J. *Mater. Res. Soc. Symp. Proc.* **2000**, *606*, 13. (i) Son, K.–A.; Mao, A. Y.; Kim, B. Y.; Liu, F.; Pylant, E. D.; Hess, D. A.; White, J. M.; Kwong, D. L.; Roberts, D. A.; Vrtis, R. N. *J. Vac. Sci. Technol.* A. **1998**, *16*, 1670. (j) Son, K.–A.; Mao, A. Y.; Kim, B. Y.; Liu, F.; Pylant, E. D.; Hess, D. A.; White, J. M.; Kwong, D. L.; Roberts, D. A.; Vrtis, R. N. *Appl. Phys. Lett.* **1998**, *72*, 1187. (k) Niimi, H.; Johnson, R. S.; Lucovsky, G.; Massoud, H. Z. *Proc. Electrochem Soc.* **2000**,

2000, 487. (l) Chiu, H.–T.; Wang, C.–N.; Chuang, S.–H. *Chem. Vap. Deposition* **2000**, *6*, 223. (m) Smith, R. C.; Taylor, C. J.; Roberts, J.; Campbell, S. A.; Tiner, M.; Hegde, R.; Hobbs, C.; Gladfelter, W. L. *Chem. Mater.* **2000**, *12*, 2822. (n) Taylor, C. J.; Gilmer, D. C.; Colombo, D. G.; Wilk, G. D.; Campbell. S. A.; Roberts, J.; Gladfelter, W. L. *J. Am. Chem. Soc.* **1999**, *121*, 5220. (o) Wilk, G. D.; Wallace, R. M.; Anthony, J. M. *J. Appl. Phys.* **2000**, *87*, 484. (p) Chambers, J. J.; Parsons, G. N. *Mater. Res. Soc. Symp. Proc.* **2001**, *611*, C1.6.1.

6. (a) Sheldon, R. A.; Kochi, J. K. *Metal Catalyzed Oxidations of Organic Compounds*; Academic Press: New York, 1981. (b) *The Activation of Dioxygen and Homogeneous Catalytic Oxidation*, Barton, D. H.; Martell, A. E.; Sawyer, D. T. Eds.; Plenum, Press: New York, 1993. (c) *Oxygen Complexes and Activation by Transition Metals*, Martell, A. E.; Sawyer, D. T. Eds.; Plenum, Press: New York, 1988. (d) Feig, A. L.; Lippard, S. J. *Chem. Rev.* **1994**, *94*, 759. (e) Holm, R. H. *Chem. Rev.* **1987**, *87*, 1401.
7. Chen, T.; Wu, Z.; Li, L.; Sorasaenee, K. R.; Diminnie, J. B.; Pan, H.; Guzei, I. A.; Rheingold, A. L.; Xue Z. *J. Am. Chem. Soc.* **1998**, *120*, 13519.
8. (a) Davidson, P. J.; Lappert, M. F.; Pearce, R. *J. Organomet. Chem.* **1973**, *57*, 269. (b) McAlexander, L. H., Ph.D dissertation, University of Tennessee, 1997. (c) Li, L.-T., Ph.D dissertation, University of Tennessee, 1996.
9. (a) Schrock, R. R. *J. Am. Chem. Soc.* **1974**, *96*, 6796. (b) Schrock, R. R.; Fellman, J. D. *J. Am. Chem. Soc.* **1978**, *100*, 3359.

10. (a) Schrock, R. R.; Clark, D. N.; Sancho, J.; Wengrovius, J. H.; Rocklage, S. M.; Pedersen, S. F. *Organometallics* **1982**, *1*, 1645. (b) *Carbyne Complexes*, Fischer, H.; Hoffman, P.; Kreissl, F. R.; Schrock, R. R.; Schubert, U.; Weiss, K. Eds.; VCH: New York, 1988. (c) Schrock, R. R. *Acc. Chem. Res.* **1986**, *19*, 342. (d) Mayr, A.; Hoffmeister, H. *Adv. Organomet. Chem.* **1991**, *32*, 227.

11. Murarka, S. P. *Silicides for VLSI Applications*; Academic Press: New York, 1983.

12. *High Temperature Silicides and Refractory Alloys*. Papers presented at Symposium F, Materials Research Society Fall Meeting 1993, *Mat. Res. Soc. Symp. Proc.* 1994, Vol. *322*.

13. Silverman, J.; Mooney, J. M.; Shepherd, F. D. *Scien. Amer.* **March 1992**, 78.

14. (a) Heyn, R. H.; Tilley, T. D. *Inorg. Chem.* **1989**, *28*, 1768. (b) Barron, A. R.; Wilkinson, G.; Montevalli, M.; Hursthouse, M. B. *J. Chem. Soc., Dalton Trans.* **1987**, 837.

15. (a) Kingston, B. M.; Lappart, M. F. *J. Chem. Soc., Dalton Trans.* **1972**, 69. (b) Berry, D. H.; Koloski, T. S.; Carroll, P. J. *Organometallics* **1990**, *9*, 2952. (c) Berry, D. H.; Chey, J. H.; Zipin, H. S.; Carroll, P. J. *J. Am. Chem. Soc.* **1990**, *112*, 452. (d) Aitken, C. T.; Harrod, J. F.; Samuel, E. *J. Am. Chem. Soc.* **1986**, *108*, 4059. (e) Woo, H-G.; Heyn, R. H.; Tilley, T. D. *J. Am. Chem. Soc.* **1992**, *114*, 5698. (f) Jiang, Q.; Pestana, D. C.; Carroll, P. J.; Berry, D. H. *Organometallics* **1994**, *13*, 3679. (g) Kreutzer, K. A.; Fisher, R. A.; Davis, W. M.; Spaltenstein, E.; Buchwald, S. L. *Organometallics* **1991**, *10*, 4031. (h) Parkin, G.; Bunel, E.; Burger, B. J.; Trimmer, M. S.; Van Asselt, A.; Bercaw, J.

E. *J. Mol. Catal.* **1987**, *41*, 21. (i) Corey, J. Y.; Zhu, X.–H. *J. Organomet. Chem.* **1992**, *439*, 1. (j) Schubert, U.; Schenkel, A. *Chem. Ber.* **1988**, *121*, 939. (k) Hengge, E.; Weinberger, M. *J. Organomet. Chem.* **1992**, *433*, 21. (l) Takahashi, T.; Hasegawa, M.; Suzuki, N.; Saburi, M.; Rousset, C. J.; Fanwick, P. E.; Negishi, E. *J. Am. Chem. Soc.* **1991**, *113*, 8564.

16. (a) Xue, Z.; Li, L.; Hoyt, L. K.; Diminnie, J. B.; Pollitte, J. L. *J. Am. Chem. Soc.* **1994**, *116*, 2169. (b) Li, L.; Diminnie, J. B.; Liu, X.; Pollitte, J. L.; Xue, Z. *Organometallics* **1996**, *15*, 3520. (c) McAlexander, L. H.; Hung, M.; Li, L.; Diminnie, J. B.; Xue, Z.; Yap, G. P. A.; Rheingold, A. L. *Organometallics* **1996**, *15*, 5231. (d) Wu, Z.; Diminnie, J. B.; Xue, Z. *Organometallics* **1998**, *17*, 2917. (e) Diminnie, J. B.; Hall, H. D.; Xue, Z. *J. Chem. Soc., Chem. Commun.* **1996**, 2383. (f) Diminnie, J. B.; Xue, Z. *J. Am. Chem. Soc.* **1997**, *119*, 12657. (g) Liu, X.; Li, L.; Diminnie, J. B.; Yap, G. P. A.; Rheingold, A. L.; Xue, Z. *Organometallics* **1998**, *17*, 4597. (h) Diminnie, J. B.; Blanton, J. R.; Cai, H.; Quisenberry, K. T.; Xue, Z. *Organometallics* **2001**, *20*, 1504.

17. (a) Hua, F.; Mowat, W.; Skapski, A. C.; Wilkinson, G. *J. Chem. Soc. Chem. Commun.* **1971**, 1477. (b) Mowat, W.; Wilkinson, G. *J. Chem. Soc. Dalton Trans.* **1973**, 1120. (c) Kim, H. P.; Angelici, R. J. *Adv. Organomet. Chem.* **1987**, *27*, 51.

18. (a) Li, L.; Hung, M.; Xue, Z. *J. Am. Chem. Soc.* **1995**, *117*, 12746. (b) Schrock, R. R. *Acc. Chem. Res.* **1979**, *12*, 98. (c) Schrock, R. R. in *Reactions of Coordinated Ligands*, P. S. Braterman, Ed.; Plenum: New York, 1986. (d) Schrock, R. R. *J. Organomet. Chem.* **1986**, *300*, 249. (e) *Advances in Metal*

Carbene Chemistry, Schubert, U. Ed.; *NATO ASI Series*, Series C, Vol. *269*, 1989. (f) Aguero, A.; Osborn, J. A. *New J. Chem.* **1988**, *12*, 111. (g) Schrock, R. R. *Acc. Chem. Res.* **1990**, *23*, 158. (h) Warren, T. H.; Schrock, R. R.; Davis, W. M. *J. Organomet. Chem.* **1998**, *569*, 125.

19. (a) Rothwell, I. P. *Polyhedron* **1985**, *4*, 177. (b) *Comprehensive Organometallic Chemistry* G. Wilkinson, F. G. A. Stone, and E. W. Abel, Eds.; Pergamon: New York, 1982, Vol. 3, Ch. 25 by J. A. Labinger; Vol. 8, Ch. 54 by R. H. Grubbs. (c) *Comprehensive Organometallic Chemistry II*, E. W. Abel, F. G. A. Stone, and G. Wilkinson Eds.; Pergamon: New York, 1982, Vol. 5, Ch. 2 by D. E. Wigley and S. D. Gray; Ch. 5 by M. J. Winter and S. Woodward.
20. (a) Caulton, K. G.; Chisholm, M. H.; Streib, W. E.; Xue, Z. *J. Am. Chem. Soc.* **1991**, *113*, 6082. (b) Xue, Z.; Caulton, K. G.; Chisholm, M. H. *Chem. Mater.* **1991**, *3*, 384. (c) Xue, Z.; Chuang, S.–H.; Caulton, K. G.; Chisholm, M. H. *Chem. Mater* **1998**, *10*, 2365. (d) LaPointe, A. M.; Schrock, R. R.; Davis, W. M. *J. Am. Chem. Soc.* **1995**, *117*, 4802. (e) There is no H/D scrambling among the neopentyl and neopentylidene ligands in $Re(\equiv CBu^t)(=CHBu^t)(CD_2Bu^t)_2$ at 80 °C in toluene-d_8. LaPointe, A. M.; Schrock, R. R. *Organometallics* **1995**, *14*, 1875. (f) Schrock, R. R. *Chem. Rev.* **2002**, *102*, 145.
21. (a) Fellmann, J. D.; Schrock, R. R.; Rupprecht, G. A. *J. Am. Chem. Soc.* **1981**, *103*, 5752. (b) Fellmann, J. D.; Rupprecht, G. A.; Wood, C. D.; Schrock, R. R. *J. Am. Chem. Soc.* **1978**, *100*, 5964.
22. Xue, Z. *Comments Inorg. Chem.* **1996**, *18*, 223.
23. Schrock, R. R.; Sancho, J.; Pederson, S. F. *Inorg. Synth.* **1989**, *26*, 44.

24. (a) Gutekunst, G.; Brook, A. G. *J. Organomet. Chem.* **1982**, *225*, 1. (b) Campion, B. K.; Heyn, R. H.; Tilley, T. D. *Organometallics* **1993**, *12*, 2584.

25. Levine, I. N. *Physical Chemistry* 3rd Ed.; McGraw-Hill: New York, 1988, pp. 307-309.

26. Beck, S.; Lieber, S.; Schaper, F.; Geyer, A.; Brintzinger, H. *J. Am. Chem. Soc.* **2001**, *123*, 1483

27. Carpentier, J.; Maryin, V. P.; Luci, J.; Jordan, R. F. *J. Am. Chem. Soc.* **2001**, *123*, 898.

28. Perrin, C. L.; Dwyer, T. J. *Chem. Rev.* **1990**, *90*, 935.

29. Orrell, K. G.; Šik, V. *Annu. Rep. on NMR Spectrosc.* **1993**, *27*, 103.

30. (a) Koloski, T. S.; Pestana, D. C.; Carrol, P. J.; Berry, D. H. *Organometallics* **1994**, *13*, 489. (b) Figge, L. K.; Carrol, P. J.; Berry, D. H. *Organometallics* **1996**, *15*, 209. (c) Palitzsch, W.; Beyer, C.; Böhme, U.; Rittmeister, B.; Roewer, G. *Eur. J. Inorg. Chem.* **1999**, 1813. (d) Ueno, K.; Sakai, M.; Ogino, H. *Organometallics* **1998**, *17*, 2138.

31. Choi, S.; Lin, Z.; Xue, Z. *Organometallics* **1999**, *18*, 5488.

32. Anderson, R. A.; Chisholm, M. H.; Gibson, J. F.; Reichert, W. W.; Rothwell, I. P.; Wilkinson, G. *Inorg. Chem.* **1981**, *20*, 3934.

33. More, P. M.; Spencer, M. D.; Wilson, S. R.; Girolami, G. S. *Organometallics* **1994**, *13*, 1646.

34. Taylor, J. R. *An Introduction to Error Analysis. The Study of Uncertainties in Physical Measurements*; University Science Books: Mill Valley, CA 1982; Ch. 4, p. 93.

35. (a) Sheldrick, G. M. *SADABS, A Program for Empirical Absorption Correction of Area Detector Data*; University of Göttingen, Göttingen, Germany, 1996. (b) Sheldrick, G. M. *SHELXL-97, A Program for the Refinement of Crystal Structures*, University of Göttingen, Göttingen, Germany, 1997.

36. (a) Mimoun, H. *Comprehensive Coordination Chemistry*; Wilkinson, G.; Gillard, R. D.; McCleverty, J. A.; Eds.; Pergamon Press: Oxford, 1987, Vol. 6, 317. (b) Grasselli, R. K.; Burrington, J. D. *Adv. Catal.* **1981**, *30*, 133. (c) Martell, A. E. *Pure Appl. Chem.* **1983**, *55*, 125. (d) Malmstrom, B. G. *Annu. Rev. Biochem.* **1982**, *51*, 21. (e) Jones, R. D.; Summerville, D. A.; Basolo, F. *Chem. Rev.* **1979**, *79*, 139. (f) Guengerich, F. P.; Macdonald, T. L. *Acc. Chem. Res.* **1984**, *17*, 9.

37. Amato, G.; Arcoria, A.; Ballistreri, F. P.; Tomaselli, G. A.; Bortolini, O.; Conte, V.; Difuria, F.; Modena, G.; Valle, G. *J. Mol. Catal.* **1986**, *37*, 165.

38. (a) Bradley, D. C.; Mehrotra, R. C.; Rothwell, I. P.; Singh A. *Alkoxo and Aryloxo Derivatives of Metals*; Academic Press: SanDiego, 2001. (b) Panek, E. J.; Whitesides, G. M. *J. Am. Chem. Soc.* **1972**, *94*, 8768. (c) Schwartz, J.; Labinger, J. A. *Angew. Chem., Int. Ed. Engl.* **1976**, *15*, 333. (d) Jensen, F. R.; Kiskis, R. C. *J. Am. Chem. Soc.* **1975**, *97*, 5825. (e) Nishinaga, A.; Tomita, H. *J. Mol. Catal.* **1980**, *7*, 179. (f) Constantini, M.; Dromard, A.; Joffret, M. ; Brossard, B.; Varagnat, J. *J. Mol. Catal.* **1980**, *7*, 89. (g) Yasuda, H.; Nagasuna, K.; Asami, K.; Nakamura, A. *Chem. Lett.* **1983**, 955. (h) Lubben, T. V.; Wolczanski, P. T. *J. Am. Chem. Soc.* **1985**, *107*, 701. (i) Han, R.; Parkin, G. *J. Am. Chem. Soc.* **1990**, *112*, 3662. (j) Parkin, G.; Bercaw, J. E. *J. Am. Chem.*

Soc. **1989**, *111*, 391. (k) Barron, A. R. *Chem. Soc., Rev.* **1993**, *22*, 93. (l) Mandimutsira, B.; Yamarik, J. L.; Brunold, T. C.; Gu, W.; Cramer, S. P.; Riordan, C. G. *J. Am. Chem. Soc.* **2001**, *123*, 9194.

39. (a) Labinger, J. A.; Hart, D. W.; Seibert, W. E.; Schwartz, J. *J. Am. Chem. Soc.* **1975**, *97*, 3851. (b) Blackburn, T. F.; Labinger, J. A.; Schwartz, J. *Tetrahedron Lett.* **1975**, *35*, 3041. (c) Gibson, T. *Organometallics* **1987**, *6*, 918. (d) Brindley, P. B.; Scotton, M. J. *J. Chem. Soc. Perkin Trans. II* **1981**, 419. (e) Van Asselt, A.; Santarsiero, B. D.; Bercaw, J. E. *J. Am. Chem. Soc.* **1986**, *108*, 8291. (f) Coughlin, E. B.; Bercaw, J. E. *Organometallics* **1992**, *11*, 465. (g) Lubben, T. V.; Wolczanski, P. T. *J. Am. Chem. Soc.* **1987**, *109*, 424. (h) Wang, R.-J.; Folting, K.; Huffman, J. C.; Chamberlain, L. R.; Rothwell, I. P. *Inorg. Chim. Acta* **1986**, *120*, 81. (i) Gibson, V. C.; Redshaw, C.; Walker, G. L. P.; Howard, J. A. K.; Hoy, V. J.; Cole, J. M.; Kuzmina, L. G.; De Silva, D. S. *J. Chem. Soc., Dalton Trans.* **1999**, 161. (j) Brindley, P. B.; Hodgson, J. C. *J. Organomet. Chem.* **1974**, *65*, 57. (k) Kim, S.-J.; Jung, I. N.; Yoo, B. R.; Cho, S.; Ko, J.; Kim, S. H.; Kang, S. O. *Organometallics* **2001**, *20*, 1501. (l) Schaverien, C. J.; Orpen, A. G. *Inorg. Chem.* **1991**, *30*, 4968. (m) Schaverien, C. J. *J. Chem. Soc., Chem. Comm.* **1991**, 458. (n) Adam, W.; Metz, M.; Prechtl, F.; Renz, M. *Synthesis* **1994**, 563. (o) Adam, W.; Putterlik, J.; Schuhmann, R. M.; Sundermeyer, J. *Organometallics* **1996**, *15*, 4586. (p) Vetter, W. M.; Sen, A. *Organometallics* **1991**, *10*, 244. (q) Van Asselt, A.; Trimmer, M. S.; Henling, L. M.; Bercaw, J. E. *J. Am. Chem. Soc.* **1988**, *110*, 8254. (r) Wu, Z.; Diminnie, J. B.; Xue, Z. *Organometallics*, in revision.

40. Hubert-Pfalzgrag, L. G. *New J. Chem.* **1987**, *11*, 663.

41. (a) Ahn, S.; Mayr, A. *J. Am.Chem. Soc.* **1996**, *118*, 7408. (b) Feher, F. J.; Budzichowski, T. A. *Polyhedron* **1995**, *14*, 3239.

42. (a) Nugent, W. A.; Mayer, J. M. *Metal-Ligand Multiple Bonds*; Wiley: New York, 1988. (b) Churchill, M. R.; Youngs, W. J. *Inorg. Chem.* **1979**, *18*, 2454. (c) VanderLende, D. D.; Abboud, K. A.; Boncella, J. M. *Organometallics* **1994**, *13*, 3378. (d) Schrock, R. R.; DePue, R. T.; Feldman, J.; Yap, K. B.; Yang, D. C.; Davis, W. M.; Park, L.; DiMare, M.; Schofield, M.; Anhaus, J.; Walborsky, E.; Evitt, E.; Krüger, C.; Betz, P. *Organometallics* **1990**, *9*, 2262.

43. (a) Sieburth, S. M.; Mu, W. *J. Org. Chem.* **1993**, *58*, 7584. For Si-O-M complexes, see (b) Marciniec, B.; Maciejewski, H. *Coord. Chem. Rev.* **2001**, *223*, 301. (c) Murugavel, R.; Voigt, A.; Walawalker, M. G.; Roesky, H. W. *Chem. Rev.* **1996**, *96*, 2205. (d) King, L.; Sullivan, A. C. *Coord. Chem. Rev.* **1999**, *189*, 19.

44. Wu, Y.-D, *et al.* unpublished results.

45. Lockwood, M. A.; Fanwick, P. E.; Eisenstein, O.; Rothwell, I. P. *J. Am. Chem. Soc.* **1996**, *118*, 2762.

46. Cheon, J.; Rogers, D. M.; Girolami, G. S. *J. Am. Chem. Soc.* **1997**, *119*, 6804.

47. Clark, D. N.; Schrock, R. R. *J. Am. Chem. Soc.* **1978**, *100*, 6774. See also reference 42b.

48. (a) Searchers were conducted of the Cambridge Structural Database (http://www.ccdc.cam.ac.uk/), and no such linear structure was found. (b)

Feinstein-Jaffe, I.; Gibson, D.; Lippard, S. J.; Schrock, R. R.; Spool, A. *J. Am. Chem. Soc.* **1984**, *106*, 6305.

49. (a) Brock, S. L.; Mayer, J. M. *Inorg. Chem.* **1991**, *30*, 2138. (b) De Wet, J. F.; Caira, M. R.; Gellatly, B. J. *Acta Crystallogr., Sect. B* **1978**, B*34*, 762. (c) Ball, J. M.; Boorman, P. M.; Richardson, J. F. *Inorg. Chem.* **1986**, *25*, 3325.
50. (a) Dori, Z. *Prog. Inorg. Chem.* **1981**, *28*, 239. (b) Che, T. M.; Day, V. W.; Francesconi, L. C.; Klemperer, W. G.; Main, D. J.; Yagasaki, A.; Yaghi, O. M. *Inorg. Chem.* **1992**, *31*, 2920. (c) Errington, R. J.; Wingad, R. L.; Clegg, W.; Elsegood, M. R. J. *Angew. Chem. Int. Ed.* **2000**, *39*, 3884.
51. (a) Cotton, F. A.; Schwotzer, W.; Shamshoun, E. S. *Organometallics* **1984**, *3*, 1770. (b) Huttner, G.; Frank, A.; Fischer, E. O. *Isr. J. Chem.* **1977**, *15*, 133. (c) Cotton, F. A.; Schwotzer, W. *Inorg. Chem.* **1983**, *22*, 387. (d) Rocklage, S. M.; Schrock, R. R.; Churchill, M. R.; Wassermann, R. *J. Organometallics* **1982**, *1*, 1332. (e) Chisholm, M. H.; Hoffman, D. M.; Huffman, J. C. *Inorg. Chem.* **1983**, *22*, 2903. (f) Latesky, S. L.; Selegue, J. P. *J. Am. Chem. Soc.* **1987**, *109*, 4731. (g) Caulton, K. G.; Cayton, R. H.; Chisholm, M. H.; Huffman, J. C.; Lobkovsky, E. B.; Xue, Z. *Organometallics* **1992**, *11*, 321.
52. Campion, B. K.; Falk, J.; Tilley, T. D. *J. Am. Chem. Soc.* **1987**, *109*, 2049.
53. (a) Schmidt, D. D.; Yoke, J. T. *J. Am. Chem. Soc.* **1971**, *93*, 637. (b) Herrmann, W. A.; Serrano, R.; Küsthardt, U.; Ziegler, M. L.; Guggolz, E.; Zahn, T. *Angew. Chem., Int. Ed. Engl.* **1984**, *23*, 515. (c) Gable, K. P.; Juliette, J. J. J.; Li, C. B.; Nolan, S. P. *Organometallics* **1996**, *15*, 5250.

54. (a) Wigley, D. E. *Prog. Inorg. Chem.* **1994**, *42*, 239. (b) Nugent, W. A.; Haymore, B. L. *Coord. Chem. Rev.* **1980**, *31*, 123. (c) Chisholm, M. H.; Rothwell, I. P. in *Comprehensive Coordination Chemistry*; Wilkinson, G, Gillard, R. D., McCleverty, J. A. Ed.; Pergamon: New York, Vol. 2, 1987, p. 161. (d) Barrier, P.; Coffey, T. A.; Forster, G. D.; Hogarth, G. *J. Chem. Soc., Dalton Trans.* **1999**, 4519. (e) Collman, J. P.; Hegedus, L. S.; Norton, J. R.; Finke, R. G. *Principles and Applications of Organotransition Metal Chemistry*; University Science Books: Mill Valley, CA, 1987. (f) Kempe, R. *Angew. Chem. Int. Ed. Engl.* **2000**, *39*, 468. (g) Gade, L. H.; Mountford, P. *Coord. Chem. Rev.* **2001**, *216*, 65.

55. (a) Hoveyda, A. H.; Schrock, R. R. *Chem. Eur. J.* **2001**, *7*, 945. (b) Baumann, R.; Stumpf, R.; Davis, W. M.; Liang, L.; Schrock, R. R. *J. Am. Chem. Soc.* **1999**, *121*, 7822. (c) Schrock, R. R. *Tetrahedron* **1999**, *55*, 8141. (d) Grubbs, R. H.; Chang, S. *Tetrahedron* **1998**, *54*, 4413. (e) Rocklage, S. M.; Schrock, R. R. *J. Am. Chem. Soc.* **1980**, *102*, 7808. (f) Rocklage, S. M.; Schrock, R. R. *J. Am. Chem. Soc.* **1982**, *104*, 3077. (g) Meyer, K. E.; Walsh, P. J.; Bergman, R. G. *J. Am. Chem. Soc.* **1995**, *117*, 974. (h) Meyer, K. E.; Walsh, P. J.; Bergman, R. G. *J. Am. Chem. Soc.* **1994**, *116*, 2669. (i) Krska, S. W.; Zuckerman, R. L.; Bergman, R. G. *J. Am. Chem. Soc.* **1998**, *120*, 11828. (j) Zuckerman, R. L.; Krska, S. W.; Bergman, R. G. *J. Am. Chem. Soc.* **2000**, *122*, 751. (k) McInnes, J. M.; Blake, A. J.; Mountford, P. *J. Chem. Soc., Dalton Trans.* **1998**, 3623. (l) Birdwhistell, K. R.; Boucher, T.; Ensminger, M.; Harris, S.; Johnson, M.; Toporek, S. *Organometallics* **1993**, *12*, 1023. (m) Birdwhistell, K. R.; Lanza, J.;

Pasos, J. *J. Organomet. Chem.* **1999**, *584*, 200. (n) Cantrell, G. K.; Geib, S. J.; Meyer, T. Y. *Organometallics* **2000**, *19*, 3562. (o) Cantrell, G. K.; Meyer, T. Y. *J. Am. Chem. Soc.* **1998**, *120*, 8035.

56. (a) Bennett, J. L.; Wolczanski, P. T. *J. Am. Chem. Soc.* **1997**, *119*, 10696. (b) Walsh, P. J.; Hollander, F. J.; Bergman, R. G. *Organometallics* **1993**, *12*, 3705 and references therein.

57. (a) Burrington, J. D.; Kartisek, C. T.; Grasselli, R. K. *J. Catal.* **1983**, *81*, 489. (b) Fjare, D. E.; Gladfelter, W. L. *J. Am. Chem. Soc.* **1981**, *103*, 1572. (c) Andrews, M. A.; Kaesz, H. D. *J. Am. Chem. Soc.* **1979**, *101*, 7255. (d) Nugent, W. A.; Harlow, R. L. *J. Am. Chem. Soc.* **1980**, *102*, 1759. (e) Chatt, J.; Dilworth, J. R.; Richards, R. L. *Chem. Rev.* **1978**, *78*, 589.

58. (a) Fix, R. M.; Gordon, R. G.; Hoffman, D. M. *Chem. Mater.* **1990**, *2*, 235. (b) Ossola, F.; Maury, F.; *Chem. Vap. Deposition* **1997**, *3*, 137. (c) Lewkebandara, T. S.; Sheridan, P. H.; Heeg, M. J.; Rheingold, A. L.; Winter, C. H. *Inorg. Chem.* **1994**, *33*, 5879. (d) Sun, S.; Chiu, H. U.S. Patent No 6114242, 2000. (e) Zhang, M.; Tu, K. N. *Proc. – Int. Conf. Solid-State Integr. Circuit Technol (5th)*, Institute of Electrical and Electronics Engineers: New York, 1998, 243. (f) Hansen, N. A. K.; Herrmann, W. A. *Chem. Mater.* **1998**, *10*, 1677. (g) Roberson, S. L.; Finello, D.; Davis, R. F. *Thin Solid Films* **1998**, *324*, 30. (h) Nakajima, T.; Shirasaki, T. *J. Electrochem. Soc.* **1997**, *144*, 2096. (i) Baxter, D. V.; Chisholm, M. H.; Gama, G. J.; DiStasi, V. F.; Hector, A. L.; Parkin, I. P. *Chem. Mater.* **1996**, *8*, 1222.

59. (a) Liu, X.; Wu, Z.; Peng, Z.; Wu, Y.; Xue, Z. *J. Am. Chem. Soc.* **1999**, *121*, 5350. (b) Diminnie, J. B.; Liu, X.; Cai, H.; Wu, Z.; Blanton, J. R.; Chen, T.; Tuinman, A. A.; Quisenberry, K. T.; Vallet, C. E.; Zuhr, R. A.; Bearch, D. B.; Peng, Z.; Wu, Y.; Concolino, T. E.; Rheingold, A. L.; Xue, Z. *Pure Appl. Chem.*, **2001**, *73*, 331 (c) Liu, X.; Wu, Z.; Cai, H.; Yang, Y.; Chen, T.; Vallet, C. E.; Zuhr, R. A.; Beach, D. B.; Peng, Z.; Wu, Y.; Concolino, T. E.; Rheingold, A. L.; Xue, Z. *J. Am. Chem. Soc.*, **2001**, *123*, 8011. (d) Cai, H.; Chen, T.; Wang, X.; Schultz, A. J.; Koetzle, T. F.; Xue, Z. *Chem. Comm.* **2002**, 230.

60. (a) Wu, Z.; Xue, Z. *Organometallics* **2000**, *19*, 4191. For related Group 4 amide silyl complexes, see (b) Wu, Z.; Diminnie, J. B.; Xue, Z. *Inorg. Chem.* **1998**, *37*, 6366.

61. (a) Bryson, N.; Youinou, M. T.; Osborn, J. A. *Organometallics* **1991**, *10*, 3389. (b) Morrison, D. L.; Wigley, D. E. *J. Chem. Soc., Chem. Commun.* **1995**, 79. (c) Ortiz, C. G.; Abboud, K. A.; Boncella, J. M. *Organometallics* **1999**, *18*, 4253. (d) Casty, G. L.; Tilley, T. D.; Yap, G. P.; Rheingold, A. L. *Organometallics* **1997**, *16*, 4746.

62. Hao, H.; Cui, C.; Bai, G.; Roesky, H. W.; Noltemeyer, M.; Schmidt, H.; Ding, Y. *Z. Anorg. Allg. Chem.* **2000**, *626*, 1660.

63. Chan, D. M. T.; Fultz, W. C.; Nugent, W. A.; Roe, D. C.; Tulip, T. H. *J. Am. Chem. Soc.* **1985**, *107*, 251.

64. (a) Cameron, P. A.; Britorsek, G. J. P.; Gibson, V. C.; Williams, D. J.; White, J. P. *Chem. Comm.* **1998**, 737. (b) Bell, A.; Clegg, W.; Dyer, P. W.; Elsegood, M. R. J.; Gibson, V. C.; Marshall, E. C. *J. Chem. Soc., Chem. Commun.* **1994**, 2547.

(c) Brandts, J. A.; Leur, M. V.; Gossage, P. A.; Boersma, J.; Spek, A. L.; Koten, G. V. *Organometallics* **1999**, *18*, 2633. (d) Gibson, V. C.; Marshall, E. L.; Redshaw, C.; Clegg, W.; Elsegood, M. R. J. *J. Chem. Soc., Dalton Trans.* **1996**, 4197.

65. Chisholm, M. H.; Chiu, H. T.; Folting, K.; Huffman, J. C. *Inorg. Chem.* **1984**, *23*, 4097.

66. (a) Green, M. L. H.; Konidaris, P. C.; Mountford, P.; Simpson, S. J. *J. Chem. Soc. Chem. Commun.* **1992**, 2516. (b) King, L.; Motevalli, M.; Sullivan, A. C. *J. Chem. Soc., Dalton Trans.* **2000**, *8*, 1357.

67. (a) Chao, Y.; Rodgers, P. M.; Wigley, D. E. Alexander, S. J.; Rheingold, A. L. *J. Am. Chem. Soc.* **1991**, *113*, 6326. (b) Danopoulos, A. A.; Hankin, D. M.; Wilkinson, G.; Cafferkey, K. M.; Sweet, T. K. N.; Hursthous, M. B. *Polyhedron*, **1997**, *16*, 3879. (c) Morrison, D. L.; Rodgers, P. M.; Chao, Y.; Bruck, M. A.; Grittini, C.; Tajima, T. L.; Alexander, S. J.; Rheingold, A. L.; Wigley, D. E. *Organometallics* **1995**, *14*, 2435. (d) Morrison, D. L.; Wigley, D. E. *Inorg. Chem.* **1995**, *34*, 2610.

68. (a) Gibson, V. C.; Redshaw, C.; Walker, G. L. P.; Howard, J. A. K.; Hoy, V. J.; Cole, J. M.; Kuzmina, L. G.; Desilva, D. S.; *J. Chem. Soc., Dalton Trans.* **1999**, 161. (b) Danopoulos, A. A.; Wilkinson, G.; Hussain-Bates, B.; Hursthouse, M. B. *J. Chem. Soc., Dalton Trans.* **1990**, 2753. (c) Chiu, H.-T.; Chang, G.-B.; Ho, W.-Y.; Chuang, S.-H.; Lee, G.-H.; Peng, S.-M. *J. Chin. Chem. Soc.* (Taipei) **1994**, *41*, 755. (d) Nugent, W. A.; Harlow, R. L. *Inorg. Chem.* **1980**, *19*, 777.

(e) Lam, H. W.; Wilkinson, G.; Hussain-Bates, B.; Hursthouse, M. B. *J. Chem. Soc., Dalton Trans.* **1993**, 781.

69. (a) Aullón, G.; Bellamy, D.; Brammer, L.; Bruton, E. A.; Orpen, A. G. *Chem. Comm.* **1998**, 653. (b) Thallapally, P. K.; Nangia, A. *CrystEngComm.* **2001**, paper No. 27.

70. (a) Schultz, A. J.; Stearley, K. L.; Williams, J. M.; Mink, R.; Stucky, G. D. *Inorg. Chem.* **1977**, *16*, 3303. (b) Poole, A. D.; Williams, D. N.; Kenwright, A. M.; Gibson, V. C.; Clegg, W.; Hockless, D. C. R.; O'Neil, P. A. *Organometallics* **1993**, *12*, 2549.

71. Fox, H. H.; Yap, K. B.; Robbins, J.; Cai, S.; Schrock, R. R. *Inorg. Chem.* **1992**, *31*, 2287.

72. (a) Musher, J. N.; Gordon, R. G. *J. Electrochem. Soc.* **1996**, *143*, 736. (b) Hoffman, D. M. *Polyhedron* **1994**, *13*, 1169. (c) Kaloyeros, A. E.; Eisenbraun, E. *Annu. Rev. Mater. Sci.* **2000**, *30,* 363.

73. Lappert, M. F.; Sanger, A. R.; Srivastava, R. C.; Power, P. P. *Metal and Metalloid Amides*; Wiley: New York, 1980.

74. Chisholm, M. H.; Tan, L.-S.; Huffman, J. C. *J. Am. Chem. Soc.* **1982**, *104*, 4879.

75. Chisholm, M. H.; Huffman, J. C.; Tan, L.-S. *Inorg. Chem.* **1981**, *20*, 1859.

76. Bradley, D. C.; Hursthouse, M. B.; Malik, K. M. A.; Vuru, G. B. C. *Inorg. Chim. Acta* **1980**, *44*, L5.

77. (a) Curtis, M. D.; Bell, L. G.; Butler, W. M. *Organometallics* **1985**, *4*, 701. (b) Arnold, J.; Shina, D. N.; Tilley, T. D.; Arif, A. M. *Organometallics* **1986**, *5*, 2037. (c) Jiang, Q.; Carroll, P. J.; Berry, D. H. *Organometallics* **1991**, *10*, 3648.

(d) Nikonov, G. I.; Mountford P.; Green, J. C.; Cooke, P. A.; Leech, M. A.; Blake, A. J.; Howard, J. A. K.; Lemenovskii, D. A. *Eur. J. Inorg. Chem.* **2000**, 1917.

78. Wu, Z.; Diminnie, J. B.; Xue, Z. *J. Am. Chem. Soc.* **1999**, *121*, 4300.

79. (a) Schmidt, D. D.; Yoke, J. T. *J. Am. Chem. Soc.* **1971**, *93*, 637. (b) Herrmann, W. A.; Serrano, R.; Küsthardt, U.; Ziegler, M. L.; Guggolz, E.; Zahn, T. *Angew. Chem., Int. Ed. Engl.* **1984**, *23*, 515. (c) Gable, K. P.; Juliette, J.; Li, C. B.; Nolan, S. P. *Organometallics* **1996**, *15*, 5250.

VITA

Tianniu Chen was born in 1973 in Guichi, Anhui Province, P. R. China. He grew up and attended school in Guichi. After graduating from the Guichi High School in July 1990, and received the second highest score in the college entrance exams in his county, he enrolled at Nanjing University at Nanjing, Jiangsu Province, in the following September. He studied chemistry at Nanjing University and conducted his undergraduate research on formulation process of high purity potassium carbonate via ion exchange unit under the direction of Professor Baoyuan Yu. He graduated in July 1994 with a B.S. degree in chemistry, and began his M.S. studies in the following September at State Key Laboratory of Coordination Chemistry, Institute of Coordination Chemistry, Nanjing University, under the direction of Professor Xinquan Xin. In the M. S. studies, he investigated the factors affecting solid-state reactions at room temperature. It was during this time that he met his future wife, colleague, and soulmate, Dongxiang Zeng. After receiving his M.S. degree in Chemistry in July 1997, he joined the Department of Chemistry, University of Tennessee, in August 1997, and began his Ph. D studies on the synthesis and characterization of early transition metal imido, amido, and silyl complexes under the direction of Professor Ziling (Ben) Xue. He synthesized more than 20 novel complexes and characterized these complexes with X-ray diffraction. He also investigated the reactions of alkylidyne complexes with O_2.

His next position will be a research chemist at Advanced Technology Materials Incorporated (ATMI) in Danbury, Connecticut.